The LIM protein complex establishes a retinal circuitry of visual adaptation by regulating Pax6 α-enhancer activity

Yeha Kim[1], Soyeon Lim[1,8], Taejeong Ha[1,8], You-Hyang Song[1], Young-In Sohn[1], Dae-Jin Park[2], Sun-Sook Paik[3], Joo-ri Kim-Kaneyama[4], Mi-Ryoung Song[5], Amanda Leung[6], Edward M. Levine[6], In-Beom Kim[3], Yong Sook Goo[2], Seung-Hee Lee[1], Kyung Hwa Kang[7], and Jin Woo Kim[1,9]

[1] Department of Biological Sciences, Korea Advanced Institute of Science and Technology (KAIST), Daejeon 305-701, South Korea;

[2] Department of Physiology, Chungbuk National University School of Medicine, Cheongju 361-763, South Korea;

[3] Department of Anatomy, College of Medicine, The Catholic University of Korea, Seoul 137-701, South Korea;

[4] Department of Biochemistry, Showa University School of Medicine, Tokyo 142-8555, Japan;

[5] Department of Life Sciences, Gwangju Institute of Science and Technology (GIST), Gwangju 500-712, South Korea;

[6] Department of Ophthalmology and Visual Sciences, Vanderbilt University, Nashville, TN 37232, United States of America;

[7] KAIST Institute of BioCentury, Daejeon 305-701, South Korea;

[8] These authors contributed equally to this work;

[9] Correspondence: jinwookim@kaist.ac.kr

Key words: Pax6, LIM domain protein, retina, cell fate determination, visual adaptation

Abstract

The visual responses of vertebrates are sensitive to the overall composition of retinal interneurons including amacrine cells, which tune the activity of the retinal circuitry. The expression of *Paired-homeobox 6* (*PAX6*) is regulated by multiple *cis*-DNA elements including the intronic α-enhancer, which is active in GABAergic amacrine cell subsets. Here, we report that the LIM domain transcription factor complex containing transforming growth factor ß1-induced transcript 1 protein (Tgfb1i1) interacts with the LIM domain transcription factors Lhx3 and Isl1 to inhibit the α-enhancer in the post-natal mouse retina. *Tgfb1i1*$^{-/-}$ mice show elevated α-enhancer activity leading to overproduction of Pax6ΔPD isoform that supports the GABAergic amacrine cell fate maintenance. Consequently, the *Tgfb1i1*$^{-/-}$ mouse retinas show a sustained light response, which becomes more transient in mice with the auto-stimulation-defective *Pax6*$^{\Delta PBS/\Delta PBS}$ mutation. Together, we show the antagonistic regulation of the α-enhancer activity by Pax6 and the LIM protein complex is necessary for the establishment of an inner retinal circuitry, which controls visual adaptation.

Introduction

The retina is a primary sensory tissue that receives light stimulus and converts it into electrical signals, which are then sent to the brain for further processing. After light detection by rod and cone photoreceptors, the first step in visual processing occurs in bipolar cells that are either stimulated or inhibited by light-absorbed photoreceptors (Masland, 2012). The activities of bipolar cells are then tuned by horizontal cells while they receive visual input from the photoreceptors and by amacrine cells while they deliver the signals to retinal ganglion cells (RGCs) (Hoon et al., 2014; Masland, 2012). The amacrine cells do not simply convey the signals from bipolar cells, but they also invert the signals by releasing inhibitory neurotransmitters such as **γ**-aminobutyric acid (GABA) and glycine. Therefore, even subtle changes in the composition and connectivity of amacrine cell subsets might alter the output of the retina, modifying the visual information sent to the brain.

The neurons of the vertebrate retina develop in an ordered fashion from multipotent retinal progenitor cells (RPCs) (Cepko, 2014). A number of transcription factors with precise temporal and spatial expression patterns control the composition of retinal neurons via the hierarchical and reciprocal regulation of other transcription factor expression (Zagozewski et al., 2014). Thus, the alterations of transcription factors that specify retinal neuron subtypes should modify visual output of mature retina. Those transcription factors include Pax6 in amacrine cells (Marquardt et al., 2001), Vsx2 in bipolar cells (Liu et al., 1994), Otx2 in bipolar cells and photoreceptors (Koike et al., 2007; Nishida et al., 2003), and Lhx2 and Sox2 in Müller glia and certain amacrine subtypes (de Melo et al., 2012; Gordon et al., 2013; Lin et al., 2009). These transcription factors are not only expressed in the earlier optic structures to play critical roles in the eye and brain development (Danno et al., 2008; Glaser et al., 1994; Yun et al., 2009), but also in the mature retinal neurons to support the survival and functions of the

neurons (de Melo et al., 2012; Kim et al., 2015). However, the mechanisms underlying the recurrent expression of transcription factors in the retinal lineage are still largely unknown.

Pax6 is one of the earliest transcription factors expressed in the eye field, and as such, it is considered as a master regulator of eye development (Ashery-Padan and Gruss, 2001; Hanson and Van Heyningen, 1995). Pax6 contains two DNA-binding domains—a paired domain (PD) and a homeodomain (HD)—linked via a glycine-rich domain, and activates target gene transcription through its C-terminal proline-, serine-, and threonine-rich (PST) domain (Epstein et al., 1994; Xu et al., 1999a). Multiple *cis*-regulatory elements govern *Pax6* expression in various mouse tissues (Kammandel et al., 1999; Xu et al., 1999b). The "α-enhancer", located within intron 4 of the *Pax6* gene, is active in the retina from embryo to adult (Kammandel et al., 1999; Marquardt et al., 2001; Plaza et al., 1995). This retina-specific enhancer activity sustains in RPCs in the peripheral retina of the embryos and regulates neuronal differentiation in a context-dependent manner (Marquardt et al., 2001). In the mature eye, the α-enhancer is active in cells of the ciliary body and amacrine cells of the retina citation needed.

The α-enhancer contains multiple binding sites for transcription factors, including the auto-stimulatory Pax6 (Kammandel et al., 1999), the stimulatory Msx1 (Kammandel et al., 1999) and Pou4f2 (Plaza et al., 1999), and the inhibitory Pax2 (Kammandel et al., 1999; Schwarz et al., 2000) and Vax1 and 2 (Mui et al., 2005). Although the inhibition of α-enhancer activity by Vax1&2 has been shown to be crucial for the development of the retina-optic stalk border (Mui et al., 2005), the roles the other transcription factors that bind the α-enhancer in the retina play in retinal development and function remain unclear. In this study, we show that regulation of *Pax6* expression through the α-enhancer fine tunes amacrine cell subtype composition, and consequently, the visual output of the retina.

90

Results

Identification of Lhx3 and Tgfb1i1 as Pax6 α-enhancer binding proteins in mouse retina

According to DNase footprinting (DF) results, the *Pax6* α-enhancer contains four retina-specific transcription factor-binding sites called DF1–4 (Plaza et al., 1995). It also contains an auto-regulatory Pax6 binding sequence (PBS; Figure 1A). The AT-rich region designated DF4 recruits both positive and negative regulators expressed in the optic vesicle and embryonic retina (Lakowski et al., 2007; Mui et al., 2005; Plaza et al., 1999; Schwarz et al., 2000). Still, the transcription factors responsible for regulating α-enhancer activity in the post-natal retina are not yet known.

In a proteomic screen for DF4-binding proteins in R28 rat RPCs, we identified Lhx3 (LIM domain homeobox 3) and Hic-5 (hydrogen peroxide induced clone 5)/Tgfb1i1 (tumor growth factor-β1 induced transcript 1 protein)/Ara55 (androgen receptor-associated protein 55) as potential candidates (Figure 1B; see Materials and Methods for details). These proteins share the LIM (LIN-11, Isl1, or MEC-3) protein-protein interaction domain (Karlsson et al., 1990; Way and Chalfie, 1988). In addition, Lhx3 contains a homeodomain and acts as a transcription factor (Bridwell et al., 2001; Roberson et al., 1994). Tgfb1i1 has four leucine-rich domains (LDs), which mediate interactions with other LD-containing protein, and four LIM domains, which mediate both self-oligomerization and interactions with other LIM domain-containing proteins (Mori et al., 2006; Nishiya et al., 1999).

Lhx3 is absent from the embryonic mouse retina, but is expressed in bipolar cells beginning around the first post-natal week (Figure 1C, top; Figure 1 – figure supplement 1A) (Balasubramanian et al., 2014). Tgfb1i1 is expressed in most of post-natal retina, but is absent from the embryonic and adult mouse retinas (Figure 1C, bottom; Figure 1 – figure supplement 1B). We also noticed Lhx3- and Tgfb1i1-expressing cells in P8 retinas show no

116 *Pax6* α-enhancer activity (Figure 1C), as visualized by an GFP reporter in *Pax6 α-*
117 *enhancer::Cre-IRES-GFP* (*P6α-CreiGFP*) mice (Marquardt et al., 2001). This suggests a
118 potential negative relationship between these LIM domain proteins and the α-enhancer
119 activity.

120 To validate our screening results, we further examined the binding of those LIM-
121 domain containing proteins in P7 retinal nuclear extracts to DF4 sequence, and found Lhx3
122 and Tgfb1i1 in these extracts bind wild-type DF4 dsDNA (DF4-WT) but not mutant DF4
123 dsDNA (DF4-MUT) in which the 5'-ATTA-3' homeodomain target sequence is replaced with 5'-
124 CGGC-3' (Figure 1 – figure supplement 2A). Not only the endogenous Lhx3 but also *in vitro*-
125 translated Lhx3 specifically binds the DF4 oligomer (Figure 1 – figure supplement 2B). *In*
126 *vitro*-translated Tgfb1i1, however, lacks a DNA-binding motif, and so does not bind the DF4
127 oligomer (Figure 1 – figure supplement 2B). This suggests Tgfb1i1 binds the α-enhancer
128 indirectly, possibly via an interaction with another DF4-binding protein like Lhx3.

129 To determine whether Lhx3 and Tgfb1i1 bind the α-enhancer *in vivo*, we performed a
130 chromatin immunoprecipitation (ChIP) analysis using rabbit polyclonal antibodies raised
131 against Lhx3 or Tgfb1i1. We checked the ChIP DNA fragments isolated from P7 retinas for
132 two mouse *Pax6* gene sequences located in the ectodermal enhancer of the 5'-UTR and the
133 α-enhancer of intron 4 using PCR (Figure 1D) and quantitative PCR (qPCR; Figure 1E). Since
134 both of these enhancer elements include auto-regulatory Pax6 binding sequences (Aota et al.,
135 2003; Kammandel et al., 1999), we used ChIP DNA fragments obtained with anti-Pax6 rabbit
136 IgG (α-Pax6) as a positive control and those obtained with pre-immune rabbit IgG (RbIgG) as
137 a negative control. We found that, in the mouse retina, Lhx3 and Tgfb1i1 interact specifically
138 with the α-enhancer but not the ectodermal enhancer (Figure 1D,E).

139 As other LIM domain-containing transcription factors can target the same DNA
140 sequences as Lhx3 (Gehring et al., 1994), we also determined whether other LIM domain

transcription factors expressed in the post-natal retina, such as Islet-1 (Isl1) and Lhx2 (Balasubramanian et al., 2014) (Figure 1 – figure supplement 3A), also can bind the Pax6 α-enhancer DF4 sequence. We found Lhx2, but not Isl1, shows specific binding to the DF4 sequence (Figure 1 – figure supplement 3C). Isl1 instead binds DF3, which contains the predicted Isl1 binding sequence 5'-CATTAG-3' (Lee et al., 2008; Leonard et al., 1992) (Figure 1 – figure supplement 3D). Conversely, the DF4-recognizing LIM transcription factors Lhx2 and Lhx3 do not bind the DF3 sequence (Figure 1 – figure supplement 3D). Collectively, these results suggest Tgfb1i1 binds the α-enhancer indirectly, possibly via an interaction with these LIM domain transcription factors.

Lhx3 and Isl1 inhibit Pax6 α-enhancer activity in a Tgfb1i1-dependent manner

Lhx3 is expressed in cone bipolar cells but not in amacrine cells, including the Pax6 α-GFP-positive subpopulation (Figure 1C; Figure 1 – figure supplement 3A,B) (Balasubramanian et al., 2014). On the contrary, Lhx2 is expressed primarily in Müller glia (Balasubramanian et al., 2014) but also in amacrine cells, including those with α-enhancer activity (Figure 1 – figure supplement 3A,B). Lhx9 is also expressed in amacrine cells (Balasubramanian et al., 2014), about 60% of which show *Pax6* α-enhancer activity (Figure 1 – figure supplement 3A,B). Both Lhx2 and Lhx9 activate the *Pax6 α*-luciferase reporter in a dose-dependent manner (Figure 2A,B). In contrast, Lhx3 and Lhx4 do not affect α-enhancer activity alone (Figure 2A), but they antagonize Pax6-induced activation of the α-enhancer (Figure 2B). Isl1 is expressed in ON bipolar cells and cholinergic amacrine cells (Elshatory et al., 2007; Galli-Resta et al., 1997; Haverkamp et al., 2003), but not in *Pax6* α-enhancer-active amacrine cells (Figure 1 – figure supplement 3A,B). Isl1 does not affect *Pax6* α-enhancer activity alone, but it does activate the enhancer in the presence of Pax6 (Figure 2A,B). Together, these results suggest LIM domain transcription factors in the mouse retina can be categorized based on how they affect *Pax6* α-

enhancer—some are stimulatory (i.e., Lhx2 and Lhx9), some are inhibitory (i.e., Lhx3 and Lhx4), and some are context-sensitive (i.e., Isl1).

Tgfb1i1, although it is unable to bind the α-enhancer directly (Figure 1 – figure supplement 2B), inhibits Pax6-induced α-enhancer activity upon overexpression (Figure 2C). This inhibition of the α-enhancer is even more significant when Tgfb1i1 is co-expressed with both Lhx3 and Isl1 (Figure 2D,E). We hypothesized that multiple LIM domains of Tgfb1i1 allow it to form a multi-protein complex that blocks α-enhancer-dependent gene expression. To assess this, we co-expressed these LIM domain transcription factors with Lmo4 (LIM-domain-only 4), which prevents Isl1 and Lhx3 from interacting with one another or with other LIM domain-containing proteins (Thaler et al., 2002). Lmo4 alone caused a dose-dependent increase in α-enhancer activity and potentiated Pax6-induced activation of the α-enhancer (Figure 2C). In the presence of Lmo4, Lhx3 and Isl1 cannot inhibit the α-enhancer (Figure 2D). Thus, Tgfb1i1 and Lmo4 appear to oppositely regulate α-enhancer activity by antagonistically modulating the formation of the LIM domain transcription factor complex.

Pax6 and Tgfb1i1 competitively bind Isl1 to antagonistically regulate the α-enhancer

We next used co-immunoprecipitation to determine whether Isl1, Lhx3, and Tgfb1i1 form a LIM protein complex in P7 mouse retina. We were able to detect Isl1 in complexes recovered using Lhx3 and Tgfb1i1, which are also capable of precipitating one another (Figure 3A). This suggests these three proteins may exist as a complex in the retina. To further examine the molecular nature of this LIM protein complex, we used combinatorial transfections of constructs encoding Lhx3, Isl1, and Tgfb1i1 into human embryonic kidney 293T (HEK293T) cells. The results of these transfections are summarized in Figure 3 – source data 1.

In the co-immunoprecipitation experiments, we found that Isl1 binds to Lhx3 with its homeodomain (HD) and/or LIM binding domain (LBD), as reported previously (Thaler et al.,

2002), whereas it interacts with Tgfb1i1 with its LIM domain(s) (Figure 3B [left column]; Figure 3 – figure supplement 1B,C). Lhx3 binds to Tgfb1i1 and Isl1 via its LIM domain(s) (Figure 3B [center column]; Figure 3 – figure supplement 1E,F). Tgfb1i1 also uses LIM domain(s) to interact with Isl1 and Lhx3 (Figure 3B [right columns]; Figure 3 – figure supplement 1H,I). We further tested whether Tgfb1i1 binds Lhx3 and Isl1 separately or whether they form a complex of Lhx3-Tgfb1i1-Isl1. We found overexpressed Tgfb1i1 further enhanced the association between Lhx3 and Isl1 (Figure 3C). Lmo4, in contrast, induces a dose-dependent decrease in the association between Isl1 and Lhx3 (Figure 3D). Collectively, these results suggest Tgfb1i1 links Isl1 and Lhx3 to form a hetero-tetrameric (or larger) complex while Lmo4 interferes with the complex formation.

It is possible Pax6 interacts with the homeodomains of Isl1 and Lhx3 to form a Pax6-LIM protein complex, since Pax6 reportedly interacts with various homeodomain-containing proteins (Granger et al., 2006; Mikkola et al., 2001). We also found Pax6 interacts only with Isl1, but not Lhx3, via its paired domain (PD) (Figure 3E; Figure 3 – figure supplement 1G). Both the HD and LIM domains of Isl1 participated to interact with Pax6, thus Pax6 might compete with Tgfb1i1 and Lhx3 to bind Isl1 (Figure 3H, top; Figure 3 – figure supplement 1D).

The DF3 and DF4, which are separated by an auto-regulatory PBS, are respective targets of Isl1 and Lhx3 (Figure 1A; Figure 1 – figure supplement 3C,D). Thus, Pax6 binding to the PBS may hinder the binding of Isl1-Tgfb1i1-Lhx3 complex to the DF3 and DF4 sequences, and vice versa. Using ChIP analyses in the cultured cells, we found Isl1, Lhx3, and Tgfb1i1 reduce the binding of Pax6 to the α-enhancer when all three are co-expressed but not when expressed individually (Figure 3G, three right graphs). Conversely, Pax6 expression interferes with the access of Tgfb1i1 to the α-enhancer (Figure 3G, rightmost graph). Pax6 does not affect Lhx3 binding to the α-enhancer, but it promotes Isl1 binding (Figure 3H, two center graphs). Together, these molecular interaction results suggest two

different transcription factor complexes occupying the α-enhancer region. The Isl1-Pax6 complex binds to the DF3 and PBS and activates the α-enhancer (Figure 3H, top), whereas the Isl1-Tgfb1i1-Lhx3 complex binds to DF3 and DF4 to cover the area between those two sequences and inhibit the access of Pax6 to DF3 (Figure 3H, bottom).

***Tgfb1i1*$^{-/-}$ retinas have excessive *Pax6* α-enhancer-active GABAergic amacrine cells**

We, next, examined the *Pax6* α-enhancer activity by detecting Pax6 α-GFP-positive cells in P14 *Tgfb1i1*$^{-/-}$ mice in comparison to *Tgfb1i1*$^{+/+}$ (wild-type, WT) littermates to validate the molecular mechanism proposed by our *in vitro* data *in vivo*. In support of the idea that Tgfb1i1 plays an important role in the inhibition of *Pax6* α-enhancer, the *Tgfb1i1*$^{-/-}$ mouse retinas show more cells positive for the Pax6 α-GFP reporter than the retinas of their *Tgfb1i1*$^{+/+}$ littermates (Figure 4A,B). We also examined the retinal composition of those littermate mice, and we only observed differences in the amacrine and bipolar cell populations among the major retinal cell types (Figure 4C – F; other retinal cell types are not shown). *Tgfb1i1*$^{-/-}$ mouse retinas have more Pax6-positive amacrine cells and fewer Vsx2-positive bipolar cells than *Tgfb1i1*$^{+/+}$ littermates (Figure 4C – F).

We classified amacrine cells positive for Gad67 (glutamate decarboxylase 67 kDa), GABA, and Bhlhb5 (basic helix-loop-helix domain containing, class B, 5) as GABAergic; cells positive for ChAT (choline acetyl transferase) as cholinergic; and cells positive for GlyT1 (glycine transporter 1) as glycinergic. Among those amacrine cell subtypes, only GABAergic amacrine cells showed a significant increase, while the numbers of cholinergic and glycinergic amacrine cells remain unchanged (Figure 4C,D). Moreover, the Pax6 α-GFP-positive cells are mainly GABAergic amacrine cells (Figure 4C,D; Figure 4 – figure supplement 1), suggesting a positive relationship between *Pax6* α-enhancer activity and GABAergic amacrine cell fate and a negative role of Tgfb1i1 in this.

Among bipolar cell subtypes, the *Tgfb1i1*$^{-/-}$ mouse retinas show fewer Vsx1-positive OFF bipolar cells without significant changes in G0α-positive ON bipolar cells, including PKCα-positive rod bipolar cells (Figure 4E,F). However, the numbers of type-2 OFF bipolar cells, which are positive to Bhlhb5 and Recoverin, are not greatly different between *Tgfb1i1*$^{+/+}$ and *Tgfb1i1*$^{-/-}$ mouse retinas (Figure 4C – F; Figure 4 – figure supplement 1), whereas Bhlhb5-positive GABAergic amacrine cell subsets, which include Pax6 α-GFP-positive population, were significantly increased in *Tgfb1i1*$^{-/-}$ mouse retinas (Figure 4C – F; Figure 4 – figure supplement 1). The results therefore suggest that Tgfb1i1 is necessary for the development of Vsx1-positive OFF bipolar cells, except for type-2 subset, in mouse retina.

We also tried to investigate the roles of Lhx3 in the post-natal mouse retina, which cannot develop in *Lhx3*-deficient mice that die perinatally (Sheng et al., 1996). We, thus, electroporated DNA constructs encoding Cas9 endonuclease and single guide RNA (sgRNA) targets to mouse *Lhx3* sequence, together with the pCAGIG DNA construct expressing EGFP (enhanced green fluorescent protein), into P0 mouse retinas (Figure 4 – figure supplement 2A; see Materials and Methods for details). We then examined the fates of EGFP-positive cells, which supposedly co-express Cas9 and the Lhx3 sgRNA, in the mouse retinas at P14. We found GABAergic amacrine cell identities of the retinal cells expressing the constructs were significantly enhanced, whereas OFF bipolar cell identities of the cells were remarkably diminished (Figure 4 – figure supplement 2B – D). Collectively, our results suggest that Tgfb1i1 supports the development of OFF bipolar cell subsets, while it antagonizes the development of GABAergic amacrine cell subset, by forming Lhx3-containing protein complex that inhibits *Pax6* α-enhancer activity in post-natal mouse retina.

Positive correlation between Pax6 α-enhancer-driven Pax6ΔPD expression and GABAergic amacrine cell fate

In P14 mouse retinas, Lhx3-positive bipolar cells co-expressing Isl1 comprise only 20% of total Lhx3-positive cells (Figure 5 – figure supplement 1B,C). In contrast, 82% of Lhx3-positive retinal cells co-express Isl1 at P7, which is when Tgfb1i1 is expressed in most retinal cell types apart from amacrine cells (Figure 5 – figure supplement 1A,C). This suggests the Isl1-Tgfb1i1-Lhx3 complex may form in the retinal cells around the first post-natal week at the peak of bipolar cell development (Morrow et al., 2008; Rapaport et al., 2004). Supporting this, the interaction between Isl1 and Lhx3 is significantly reduced in P7 *Tgfb1i1*$^{-/-}$ retinas (Figure 5A, top). This might trigger an over-activation of *Pax6* transcription, driven by the α-enhancer.

However, Pax6 levels did not differ in *Tgfb1i1*$^{-/-}$ and *Tgfb1i1*$^{+/+}$ mouse retinas (Figure 5B, larger Pax6 bands), despite the increase of Pax6-positive cells in *Tgfb1i1*$^{-/-}$ mouse retina (Figure 4C,D). We did, instead, observe a specific increase in the level of Pax6ΔPD isoform, which is an alternative transcript produced at downstream of the α-enhancer sequence (Lakowski et al., 2007; Plaza et al., 1995), in the *Tgfb1i1*$^{-/-}$ mouse retina (Figure 5B, smaller Pax6 bands). This Pax6ΔPD isoform is selectively enriched in Pax6 α-GFP-positive cells purified from P7 *P6α-CreiGFP* retinas by fluorescence activated cell sorting (FACS) (Figure 5C). Our results, thus, suggest hyperactivation of the *Pax6* α-enhancer in *Tgfb1i1*$^{-/-}$ retinas triggers ectopic expression of Pax6ΔPD isoform, but not the canonical Pax6.

We, next, investigated the role of α-enhancer-driven Pax6ΔPD expression in retinal cell fate determination by overexpressing Pax6ΔPD, which is connected with EGFP by internal ribosome entry site (IRES), in post-natal mouse retina (Figure 5D–G; Figure 5 – figure supplement 2). About 54% of EGFP-positive INL cells in P14 mouse retinas, which were electroporated with the pCAGIG-Pax6ΔPD DNA at P0, are identified as Syntaxin-positive amacrine cells, whereas only 26% of EGFP-positive INL cells are amacrine cells in the retinas electroporated with control pCAGIG DNA (Figure 5 – figure supplement 2A [top row], D). This is also contrary to the results of pCAGIG-Pax6-electroporated mouse retinas, in which about

85% of EGFP-positive INL cells are identified as amacrine cells (Figure 5 – figure supplement 2A [top row, middle], D). Moreover, by showing insignificantly different marker positivity with EGFP;Syntaxin double-positive INL cells (54%±7.56%(Syntaxin) vs. 46%±7.33%(Gad67)), majority of EGFP-positive amacrine cells in the pCAGIG-Pax6ΔPD-electroporated retinas are predicted as GABAergic amacrine cells, which are approximately half of the EGFP;Syntaxin double-positive amacrine cell population in pCAGIG-Pax6-electroporated mouse retinas (85%±7.2%(Syntaxin) vs. 44%±9.17%(Gad67)) (Figure 5F,G; Figure 5 – figure supplement 2A [second row], D). The populations of EGFP-positive cholinergic and glycinergic amacrine cells in pCAGIG-Pax6ΔPD-electroporated mouse retinas are not greatly different from those in pCAGIG-electroporated mouse retinas, but are lower than those in pCAGIG-Pax6-electroporated mouse retinas (Figure 5 – figure supplement 2A [bottom two rows], D). Together, these results suggest that Pax6ΔPD preferentially supports GABAergic amacrine cell fate, while full-length Pax6 induces all amacrine cell types in a similar ratio observed in normal mouse retina (Voinescu et al., 2009).

Mouse retinas expressing ectopic Pax6ΔPD show almost no EGFP-positive cells co-expressing OFF bipolar cell markers including Vsx1, Recoverin, and Bhlhb5 (Figure 5F [bottom row], G; Figure 5 – figure supplement 2B,D). On the contrary, significant numbers of EGFP-positive cells co-expressed ON bipolar cell marker G0α in pCAGIG-Pax6ΔPD-electroporated mouse retinas, and the numbers are not significantly different from those in pCAGIG-electroporated samples (Figure 5 – figure supplement 2B,D). EGFP-positive cells in pCAGIG-Pax6-electroporated mouse retinas, however, are almost absent of both ON and OFF bipolar cell marker co-expression (Figure 5 – figure supplement 2B,D). The results therefore suggest that Pax6ΔPD inhibits only OFF bipolar cell fate, while full-length Pax6 suppress both ON and OFF bipolar cell fates.

316 ***Pax6-dependent Pax6 α-enhancer activation is important for GABAergic amacrine cell***
317 ***fate maintenance***

318 Next, to inactivate the α-enhancer, we generated *Pax6*$^{\Delta PBS/\Delta PBS}$ mice by deleting the auto-
319 stimulatory PBS in the α-enhancer using the CRISPR/Cas9 system (Figure 6A; see Materials
320 and Methods for details). Despite the *Pax6* α-enhancer being active in the mouse retina from
321 embryo to adult, the gross morphologies of *Pax6*$^{\Delta PBS/\Delta PBS}$ mouse eyes are indistinguishable
322 from *Pax6*$^{+/+}$ WT eyes (Figure 6B), implicating dispensable roles of *Pax6* α-enhancer-induced
323 Pax6ΔPD expression in the eye and retinal development. However, in P14 *Pax6*$^{\Delta PBS/\Delta PBS}$
324 retinas, the α-enhancer-driven GFP and Pax6ΔPD expression are reduced significantly, but
325 not entirely abolished (Figure 6B – D). Since Pax6 does not bind and activate the *Pax6*$^{\Delta PBS}$ α-
326 enhancer (Figure 6 – figure supplement 1), this suggests the presence of positive regulator(s)
327 of the α-enhancer in the mouse retina other than Pax6.

328 P14 *Pax6*$^{\Delta PBS/\Delta PBS}$ retinas show significantly fewer GABAergic amacrine cells than the
329 retinas of *Pax6*$^{+/+}$ WT littermates, despite similar total numbers of Pax6-positive amacrine
330 cells (Figure 6E [left two columns], F; Figure 6 – figure supplement 2). Conversely,
331 *Pax6*$^{\Delta PBS/\Delta PBS}$ retinas show more OFF bipolar cells (i.e., Vsx1-positive), despite similar total
332 numbers of Vsx2-positive bipolar cells (Figure 6E [right two columns], F; Figure 6 – figure
333 supplement 2). However, the numbers of GABAergic amacrine cells, which start to develop in
334 the embryonic retina (Voinescu et al., 2009), were not significantly different between *Pax6*$^{+/+}$
335 and *Pax6*$^{\Delta PBS/\Delta PBS}$ retinas until P4 when the bipolar cells start to develop (Figure 6 – figure
336 supplement 3A [bottom three rows], B). The results therefore suggest that Pax6-dependent
337 activation of *Pax6* α-enhancer is not essential for the embryonic development of GABAergic
338 amacrine cells but it might be necessary for the development and/or maintenance of those
339 cells in the post-natal retina.

340 To test a possibility of antagonistic fate determination of newborn retinal neurons

between GABAergic amacrine and OFF bipolar cell subsets in the post-natal mouse retinas, we repeatedly injected bromodeoxyuridine (BrdU) to WT, *Tgfb1i1*$^{-/-}$, and *Pax6*$^{\Delta PBS/\Delta PBS}$ mice to label GABAergic amacrine and OFF bipolar cells, which are born between post-natal day 4 and 7. We failed to find BrdU;Bhlhb5 double-positive GABAergic amacrine cells in P14 WT, *Tgfb1i1*$^{-/-}$, and *Pax6*$^{\Delta PBS/\Delta PBS}$ mouse retinas, suggesting the lack of newborn GABAergic amacrine cells in the post-natal mouse retinas (Figure 6 – figure supplement 3C,E). Furthermore, the number of BrdU;Vsx1 double-positive OFF bipolar cells in those mouse retinas were not significantly different each other (Figure 6 – figure supplement 3C [bottom row], D), despite the remarkable decrease and increase of total Vsx1-positive cell numbers in P14 *Tgfb1i1*$^{-/-}$ and *Pax6*$^{\Delta PBS/\Delta PBS}$ in mouse retinas, respectively (Figure 4E,F; Figure 6E,F). The results therefore suggest that the alteration of OFF bipolar cells in those two mutant mouse retinas was not caused by neurogenic fate changes of newborn retinal cells but may have resulted from transdifferentiation of preexisting retinal cells.

We, thus, traced the fates of retinal cells born in the embryonic retina by injecting BrdU to pregnant female mice at 15 dpc (days post coitum). The numbers of Bhlhb5;BrdU-labeled GABAergic amacrine cells are significantly decreased in P7 *Pax6*$^{\Delta PBS/\Delta PBS}$ mouse retinas in comparison to their WT littermate mouse retinas (Figure 6 – figure supplement 3D [top row], F). Conversely, Vsx1;BrdU-labeled OFF bipolar cell numbers are significantly increased in the *Pax6*$^{\Delta PBS/\Delta PBS}$ mouse retinas (Figure 6 – figure supplement 3D [bottom row], F). Taken together, these results suggest Pax6 and the Isl1-Tgfb1i1-Lhx3 complex in the post-natal mouse retina competitively regulate the *Pax6* α-enhancer-driven expression of Pax6ΔPD, which maintains GABAergic amacrine cell fate against the transdifferentiation into OFF bipolar cells.

Visual adaptation of the retina is sensitive to Pax6 α-enhancer-active GABAergic

amacrine cell number

We next determined whether these changes in the *Pax6* α-enhancer-active (P6α) GABAergic amacrine cell and OFF bipolar cell numbers influence visual responses in *Tgfb1i1*$^{-/-}$ and *Pax6*$^{\Delta PBS/\Delta PBS}$ mice. Using the OptoMotry system (Prusky et al., 2004), we observed a significant reduction in visual acuity of P60 *Tgfb1i1*$^{-/-}$ mice compared to age-matched WT and *Pax6*$^{\Delta PBS/\Delta PBS}$ mice (Figure 7A, graph). Upon the measurement of light response of a whole retina by electroretinogram (ERG), the amplitudes for the a- and b-waves in dark-adapted (scotopic) and light-adapted (photopic) ERG responses of P60 *Tgfb1i1*$^{-/-}$ and *Pax6*$^{\Delta PBS/\Delta PBS}$ mouse eyes were, however, unaltered in comparison to those of WT littermate controls (Figure 7 – figure supplement 1). The results suggest that the functions of photoreceptors (determined by ERG a-waves) and ON bipolar cells (determined by ERG b-waves) are intact in those mutant mice. In support of this, the numbers of photoreceptors and ON bipolar cells in P60 *Tgfb1i1*$^{-/-}$ and *Pax6*$^{\Delta PBS/\Delta PBS}$ mouse retinas were not significantly different from those in their littermate WT mice (Figure 7 – figure supplement 2). Therefore, the reduced visual acuity of *Tgfb1i1*$^{-/-}$ mice might be caused by either the changes of visual pathway components in the brain or the alterations of amacrine cells and RGCs at downstream of bipolar cells.

We, therefore, measured the light-evoked activity of individual retinal circuits by performing multi-electrode array (MEA) recordings of RGCs, which represent the final circuit component in the retina. We found an increase in basal firing rate and mean spike number, but no change in maximum spike rate for the light-ON responses of P60 *Tgfb1i1*$^{-/-}$ retinas when compared to WT littermate controls (Figure 7B [top], C). Conversely, we observed a reduction in the basal firing rate, maximum spike rate, and mean spike number for the ON responses of P60 *Pax6*$^{\Delta PBS/\Delta PBS}$ retinas (Figure 7B [bottom], D). Interestingly, a significant number of RGCs in P60 *Tgfb1i1*$^{-/-}$ retinas do not return to the resting state after a transient light response (Figure 7B, arrowhead). Considering the GABAergic identity of P6α amacrine

391 cells and the increase of the cells in the *Tgfb1i1*$^{-/-}$ retinas (Figure 4C,D; Figure 4 – figure
392 supplement 1), it suggests this specific amacrine cell subset might disinhibit ON response by
393 acting to other inhibitory retinal neurons in light-ON pathway (Chavez et al., 2010; Demb and
394 Singer, 2012; Eggers et al., 2013).

395 The low visual acuity and sustained light response of *Tgfb1i1*$^{-/-}$ mouse retinas suggest
396 that the hypersensitivity of the mice to light interferes with their detection of dark objects on
397 brighter backgrounds (Figure 7A, predicted views). To test this hypothesis, we presented the
398 mice with two different types of visual stimuli. First, we trained dark-adapted mice to associate
399 a water reward with a flashing light stimulus. Then, we counted correct water-licking events in
400 response to various intensities of flash light (Figure 7 – figure supplement 3A). *Tgfb1i1*$^{-/-}$ mice
401 not only learn this task faster than WT mice (Figure 7 – figure supplement 3B), but they also
402 show more sensitive detection of the light stimuli (Figure 7E). However, in a second visual
403 task requiring mice to detect a drifting grate stimulus after a light stimulus, *Tgfb1i1*$^{-/-}$ mice
404 perform worse than WT mice (Figure 7F; Figure 7 – figure supplement 3C,D). This suggests
405 *Tgfb1i1*$^{-/-}$ retinas are more slowly re-sensitized after light exposure than WT retinas.
406 Conversely, the re-sensitization of *Pax6*$^{\Delta PBS/\Delta PBS}$ retinas is significantly faster than WT retinas,
407 despite being less sensitive to light (Figure 7F,G; Figure 7 – figure supplement 3). These
408 results are consistent with our MEA recordings, which showed sustained and transient light
409 responses in *Tgfb1i1*$^{-/-}$ and *Pax6*$^{\Delta PBS/\Delta PBS}$ RGCs, respectively (Figure 7B–D).

410 Collectively, the results suggest that P6α amacrine cells control the tone of light-ON
411 retinal pathway. Overall tone of light-ON pathway was increased in *Tgfb1i1*$^{-/-}$ mouse retinas,
412 which have extra P6α amacrine cells, whereas it is decreased in *Pax6*$^{\Delta PBS/\Delta PBS}$ mouse retinas
413 having reduced P6α amacrine cell number. Consequently, the light-ON pathway is augmented
414 in *Tgfb1i1*$^{-/-}$ mouse retinas and attenuated in *Pax6*$^{\Delta PBS/\Delta PBS}$ mouse retinas to make the retinas
415 hypersensitive and hyposensitive to light stimulus, respectively (Figure 7B – E). On the other

hand, the *Tgfb1i1*$^{-/-}$ mouse retinas cannot be re-sensitized as fast as WT retinas, while the *Pax6*$^{\Delta PBS/\Delta PBS}$ mouse retinas can be re-sensitized more quickly than WT retinas after a light stimulus. Given the GABAergic identity of the cells, the P6α amacrine cells may inhibit the activity of post-synaptic partners, which are not identified yet but can be predicted as an inhibitory neuron in light-ON pathway (Figure 7F). Therefore, the results indicate that proper number of P6α amacrine cells should be present in the retina to respond to light efficiently and adequately.

Discussion

Transcription factors frequently act in combination, allowing relatively few to generate the tremendous cellular diversity of the nervous system (Jessell, 2000). Especially, the “LIM code” mixes and matches LIM domain-containing transcription factors to direct tissue- and cell-specific gene expression (Gill, 2003; Shirasaki and Pfaff, 2002). Lhx3, for example, specifies motor neuron cell fate in the spinal cord by forming a hetero-hexameric complex with Isl1 and nuclear LIM interactor (NLI) for the binding to the promoter of the *Mnx1/Hb9* gene, whereas it specifies V2 interneuron cell fate by forming a hetero-tetrameric complex with NLI at the promoter of the *Chx10/Vsx2* gene (Thaler et al., 2002). Given that the various LIM homeodomain transcription factors, including Lhx2, Lhx3, Lhx4, and Lhx9, share a consensus target sequence (Gehring et al., 1994), we speculate Isl1 partners with different LIM homeodomain transcription factors in a cell-context-dependent manner. In contrast to its relationship with Lhx3, Isl1 cooperates with Lhx2 to activate the α-enhancer in cultured cell lines (data not shown). However, this is unlikely to occur *in vivo*, because Lhx2 and Isl1 are expressed mutually exclusively in RPCs (Lhx2) and post-mitotic RGCs (Isl1) of the embryonic mouse retina, in GABAergic (Lhx2) and cholinergic amacrine cells (Isl1) in the mature retina,

as well as in Müller glia (Lhx2) and ON bipolar cells (Isl1) (Balasubramanian et al., 2014; Elshatory et al., 2007; Gordon et al., 2013; Pan et al., 2008). Moreover, *Lhx2$^{flox/flox}$;P6α-Cre* retinas, which lack Lhx2 expression in the Cre-active lineages (Gordon et al., 2013), show no change in the number of *Pax6* α-enhancer-active cells (data not shown). This suggests Lhx2 may be dispensable for the activation of the *Pax6* α-enhancer in the mouse retina.

We propose that a Tgfb1i1 dimer links Isl1 and Lhx3 to form a hetero-tetrameric complex that represses the *Pax6* α-enhancer (Figure 2,3). The effects of Tgfb1i1 on the α-enhancer could be achieved by blocking Pax6's access the PBS sequence (Figure 3G,H). Alternatively, Tgfb1i1 may also recruit transcriptional co-repressors, such as NCoR (nuclear receptor co-repressor) (Heitzer and DeFranco, 2006), to the *Pax6* α-enhancer. These negative effects of Tgfb1i1 on the *Pax6* α-enhancer can be antagonized by Lmo4, which is persistently co-expressed with Pax6 in the retina and interferes with the interactions between Tgfb1i1 and Lhx3 and/or Isl1 (Duquette et al., 2010) (Figure 2D,3D). Retinas lacking *Lmo4* have fewer GABAergic amacrine cells than controls (Duquette et al., 2010), which suggests Lmo4 may positively affect *Pax6* α-enhancer-dependent GABAergic amacrine cell fate determination by inhibiting the formation of the LIM complex. However, the antagonistic regulation of the LIM complex by Tgfb1i1 and Lmo4 could not be applied to OFF bipolar cell fate determination, since OFF bipolar cells numbers are decreased commonly in *Tgfb1i1$^{-/-}$* and Lmo4-cko mouse retinas. Our results suggest that Tgfb1i1 and Lmo4 might involve in the development of different OFF bipolar cell subsets. The numbers of Bhlhb5-positive OFF bipolar cell subsets were not altered significantly in *Tgfb1i1$^{-/-}$* mouse retinas (Figure 4E,F), in contrast to a significant decrease in Lmo4-cko mouse retinas.

In addition to its canonical form, two alternative forms of Pax6, Pax6(5a) and Pax6ΔPD, are produced by alternative splicing and internal transcription initiation, respectively (Epstein et al., 1994; Mishra et al., 2002). Pax6ΔPD does not affect Pax6 target

gene expression via the conserved PBS (data not shown). Instead, as previously reported (Mikkola et al., 2001), Pax6ΔPD may potentiate the expression of Pax6 target genes by interacting with full-length Pax6. This facilitation of Pax6-induced gene transcription by Pax6ΔPD may also occur with the *Pax6* α-enhancer, resulting in a feed-forward activation of the α-enhancer. Alternatively, it may bind another promoter element containing the Pax6 homeodomain target DNA sequence (TAATT(/C)NA(/C)ATTA). Therefore, future studies will be needed to identify the targets of Pax6ΔPD in RPCs and post-mitotic retinal neurons. This will provide a full understanding of the distinctive roles Pax6 and Pax6ΔPD play in the retina.

Although the mechanisms of light adaptation and re-sensitization in the photoreceptors are fairly well-understood, how the inner retina contributes to these mechanisms is less clear. Acting downstream of rod bipolar cells that deliver visual signals from rod photoreceptors, A17 GABAergic amacrine cells provide a direct feedback inhibition to the rod bipolar cells (Chavez et al., 2010). In parallel, unidentified subset of GABAergic amacrine cells is also proposed to inhibit rod bipolar cells at downstream of ON-cone bipolar cells, which can be activated by AII amacrine cells in the rod pathway as well as by daylight (Demb and Singer, 2012; Eggers et al., 2013). GABAergic inhibition to the rod bipolar cells could be reduced in *Tgfb1i1*$^{-/-}$ mouse retinas, leading to sustained ON responses (Figure 7A). Conversely, the ON pathway in *Pax6*$^{\Delta PBS/\Delta PBS}$ mouse retinas is activated more transiently and is also more readily re-activated by subsequent visual stimuli (Figure 7D). Therefore, the P6α amacrine cells might attenuate those GABAergic inhibitions to rod bipolar cells and prevent premature inactivation of rod pathway. However, future studies should identify molecular and electrophysiological identities of the P6α amacrine cells and their pre- and post-synaptic partners to fully understand this visual adaptive circuits in the inner retina.

Materials and Methods

DNA constructs and mouse lines

cDNA clones were generous gifts from Dr. Motoko Shibanuma (Hic-5/Tgfb1i1) and Dr. Seth Blackshaw (Lhx2 and Lhx9). The full-length and fragment DNAs used in this study were isolated by PCR amplification from these cDNAs. *Tgfb1i1*$^{-/-}$ mice were generated as previously described (Kim-Kaneyama et al., 2011). *Pax6*$^{\Delta PBS/\Delta PBS}$ mice were generated using the CRISPR/Cas9 system (Cong et al., 2013). The pX330 vector was obtained from Addgene and digested with BbsI for insertion of a pair of phosphorylated dsDNA oligos (5'-CACCGAAGTCGCTCCGGATCATGCA-3', 5-AAACTGCATGATCCGGAGCGACTTC-3') that target the *PBS* in the *Pax6* α-enhancer. A T7 promoter was added to the 5' end of the sgRNA sequence in the pX330-sgRNA construct. This construct was then used as a template for *in vitro* transcription using the MEGAshortscript T7 kit (Life Technologies). The *in vitro* transcribed sgRNAs (50 ng/ml) were injected into C57BL6/J mouse embryos (2 cell-stage) together with Cas9 mRNA (100 ng/μl; purchased from Toolgen Inc.). Then, these embryos were injected into the inner cell mass of ICR embryos. Four resulting F1 chimeric male mice were crossed to C57BL6/J female mice to obtain an F2 generation with the potential to carry deletions in the PBS. Then, tail DNA from each F2 mouse (n=51) was prepared and used as a template for the PCR-amplification of the *Pax6* α-enhancer sequence. Each resulting PCR product was cloned into the pGEM-T vector for sequencing. Four F2 mice carry different heterozygous deletions in the PBS sequence were obtained. Before breeding with littermate *Pax6*$^{+/\Delta PBS}$ female mice, *Pax6*$^{+/\Delta PBS}$ male mice were crossed with C57BL6/J females for more than 6 generations to dilute any potentially OFF target mutations. All experiments using mice were performed according to the regulations of the KAIST-IACUC (KA2012-38).

Cell culture and luciferase assay

HEK293T (RRID: CVCL_0063) and R28 retinal progenitor cells (RRID: CVCL_5I35) were obtained from ATCC and a gift from Dr. Gail Seigel (University of Rochester School of Medicine and Dentistry), respectively. These cell-lines are not in the list of commonly

misidentified cell lines (by the International Cell Line Authentication Committee). These cells were regularly checked for mycoplasma contamination. The cells were maintained in DMEM supplemented with 10% fetal bovine serum (GIBCO). Cells were combinatorially transfected with DNA constructs via the PEI (polyethylenimine) method (Polyscience). The PCR-amplified mouse *Pax6* α-enhancer sequence was fused to the pGL3-luciferase vector (Promega) and co-transfected with DNA constructs of interest and pSV-β-gal plasmids. Transfected cells were harvested 24 hrs after transfection, and cell extracts were assessed for luciferase activity followed by normalization using β-galactosidase activity.

DNA affinity-capture assay

The $(CA)_5$ or $(TG)_5$ ssDNA oligonucleotides were coupled to CNBr-preactivated Sepharose 4B (GE Healthcare) according to the manufacturer's protocol. R28 cells (~10^8) were incubated in a low salt buffer (10 mM HEPES, 10 mM KCl, 0.1 mM EDTA, 1 mM DTT, and 0.5 mM PMSF) on ice for 10 mins to rupture the plasma membranes. Then, the nuclei were collected by centrifugation. After treating the isolated nuclei with 10% (final v/v) NP-40 for 20 mins, a solution containing 20 mM HEPES, 0.4 M NaCl, 1 mM EDTA, 1 mM DTT, and 1 mM PMSF was added to extract nuclear protein complexes. These nuclear extracts were then pre-cleared with a 5% (final v/v) slurry of protein A agarose beads (Invitrogen) in a binding buffer (10 mM Tris-Cl pH 7.5, 0.4 M NaCl, 1 mM EDTA, 1 mM DTT, and 5% glycerol) at 4ºC for 30 min.

Double-stranded DF4 dsDNA oligonucleotides with 5'-$(GT)_5$ single-strand overhangs were synthesized with a 5' terminal amine modification and incubated with the R28 nuclear extracts overnight at 4ºC with agitation. The protein-DF4 dsDNA complexes were then incubated with the ssDNA-coupled Sepharose 4B for 6 hrs at 4ºC, centrifuged, washed twice in binding buffer, washed twice in wash buffer (10 mM Tris-Cl pH 7.5, 1.2 mM NaCl, 1 mM EDTA, 1 mM DTT, 0.1% Nonidet P-40), and washed twice in PBS. Protein-DF4 complexes bound to the column were then eluted in SDS sample buffer for SDS-PAGE and subsequent silver staining. The silver-stained protein bands, which were enriched in $(CA)_5$-coupled Sepharose 4B relative to $(TG)_5$-coupled Sepharose 4B, were isolated for trypsin digestion

549 before being subjected to MALDI-TOF MS/MS analysis at the Korean Basic Science Institute
550 (KBSI) proteomics core facility.
551
552 **Electrophoretic mobility shift assay (EMSA)**
553 Biotin-labeled and unlabeled dsDNA probes in binding buffer (75 mM NaCl, 1 mM EDTA, 1
554 mM DTT, 10 mM Tris-HCl (pH 7.5), 6% glycerol, 2 mg BSA, and 500 ng poly (dI-dC)) were
555 incubated on ice for 30 min with LIM proteins produced using the TNT® Quick Coupled
556 Transcription/Translation kit (Promega). The EMSA was carried out on a 6% polyacrylamide
557 gel in 0.5X TBE buffer. The DNA-protein complexes were then transferred to a nylon
558 membrane (GE Healthcare), and the biotin-labeled probes were detected using the Phototop-
559 Star Detection Kit (New England BioLabs) according to the manufacturer's recommendations.
560
561 **Co-immunoprecipitation**
562 P7 mouse retinas and transfected HEK293T cells were lysed in a buffer consisting of 10 mM
563 Tris-HCl (pH 7.4), 200 mM NaCl, 1% Triton X-100, 1% NP-40, and a protease inhibitor
564 cocktail (Invitrogen). Cell lysates were centrifuged at 12,000 g for 10 min. The resulting
565 supernatants were incubated with appropriate antibodies at 4ºC for 16 h, and then pre-
566 washed protein A/G-sepharose (GE Healthcare) was added to the samples. The protein A/G-
567 sepharose immune complexes were washed five times with cell lysis buffer and subjected to
568 SDS-PAGE and Western blotting (WB) for detection of co-immunoprecipitated proteins.
569
570 **Chromatin immunoprecipitation (ChIP)**
571 P7 mouse retinas were isolated, chopped, and cross-linked with 1% formaldehyde in PBS for
572 10 min at room temperature. After a 5 min incubation in 125 mM glycine, the tissues were
573 homogenized and the nuclei were isolated. These nuclei were then subjected to sonication to
574 break their chromatin into ~600 bp fragments in a lysis buffer containing 50 mM Tris-HCl (pH
575 7.5), 150 mM NaCl, 5 mM EDTA, 0.5% NP-40, 1% Triton X-100, and a protease inhibitor
576 cocktail (Invitrogen). After pre-clearing with protein A agarose beads for 1 h, the nuclear
577 extracts were incubated for 16 h with 1 μg of the appropriate antibody followed by incubation

with protein A beads for 45 min at room temperature. The immune complexes were then washed three times with lysis buffer and then three more times with the same wash buffer containing 500 mM LiCl. After adding a Chelex 100 slurry to the washed beads, the DNA fragments were eluted for use as templates for qPCR. We used specific primers to amplify sequences in the ectoderm enhancer (fp1, 5'-CTAAAGTAGACACAGCCTT; rp1, 5'-GGAGACATTAGCTGAATTC) and the α-enhancer (fp2, 5'-GTGACAAGGCTGCCACAAGCGCC, rp2, 5'- CCGTGTCTAGACAGAAGCCCTCTC) of the mouse *Pax6* gene. qPCR was performed using the iTaq fast SYBR Green Master Mix (BioRad) with these same primers and analyzed using the CFX-Manager software (Bio-Rad). Gene expression was normalized to that of a sample containing only protein A beads.

Immunohistochemistry

Frozen sections (12 μm) of embryonic heads and post-natal mouse eyes were incubated for 1 h in a blocking solution containing 5% normal donkey serum and 5% normal goat serum in PBS containing 0.2% Triton X-100. The sections were incubated with the antibodies listed in Table 1 for 16 h at 4ºC. Fluorescent images were obtained with a confocal microscope (Olympus FV100 and Zeiss LSM710) after staining with Cy3, Alexa 647, and Alexa 488-conjugated secondary antibodies at room temperature for 1 h.

Fluorescence activated cell sorting (FACS)

P6α-Cre adult mouse eyes were dissected and placed in Hank's Balanced Salt Solution (HBSS; Life technologies) to remove the lens. Retinas were peeled from the eyes and placed in 1 ml HBSS containing activated 10 mg/ml papain (Sigma-Aldrich) for 5 min at 37ºC. Retinal cells were resuspended in HBSS with 2% FCS followed by centrifugation at 1,600 rpm for 2 min. Cell pellets were then gently triturated in HBSS with 2% FCS, filtered through a 70 μm Filcons membrane prior to FACS analysis. GFP-positive retinal cells were then sorted in an Aria Fusion Cell Sorter (Becton Dickinson) at 495 nm excitation and 519 nm emission. Following FACS analysis, cells were collected by centrifugation at 1,600 rpm for 5 min and

606 the cells were lysed in a buffer containing 10 mM Tris-HCl (pH 8.0), 1 mM EDTA, 1% Triton
607 X-100, 0.1% SDS, and 150 mM NaCl.
608
609 **Subretinal DNA electroporation**

610 Electroporation experiments were performed as previously described (Matsuda and Cepko,
611 2004). Approximately 0.5 µl (total; 5 µg/µl) DNA solution mixed with fast green dye was
612 injected into the subretinal space of P0 mouse retinas, and square electric pulses were
613 applied (100 V; five 50-ms pulses at 950-ms intervals). For CRISPR/Cas9-mediated deletion
614 of *Lhx3* gene, dsDNA oligos (sgRNA-Lhx3-1, 5'-(P)-CACCGGACCCGTCCCGGGAATCCGC-
615 3' and 5'-AAACGCGGATTCCCGGGACGGGTCC-3'; sgRNA-Lhx3-2, 5'-
616 CACCGTGCTGGCGTTGTTGGCGCGA-3' and 5'-AAACTCGCGCCAACAACGCCAGCAC-3')
617 were cloned into the pX330 vector before co-electroporation with the pCAGIG vector (molar
618 ratio of pX330 constructs to pCAGIG is 1:0.5).
619
620 **Multielectrode array (MEA) recordings**
621 Mouse retinas were cut into 3 mm x 3 mm patches in artificial cerebrospinal fluid (ACSF)
622 solution (124 mM NaCl, 10 mM glucose, 1.15 mM KH_2PO_4, 25 mM $NaHCO_3$, 1.15 mM $MgSO_4$,
623 2.5 mM $CaCl_2$, and 5 mM KCl) bubbled with 95% O_2 + 5% CO_2 at pH 7.3–7.4 and 32^{o}C.
624 Retinal patches were then mounted, ganglion cell layer down, on a planar 8 x 8 MEA, and the
625 light-evoked RGC spikes were recorded using the MEA60 system (Multi Channel Systems
626 GmbH, Germany). White light stimuli were applied with a DLP projector (Hewlett Packard, ep-
627 7122) focused onto the photoreceptor layer of the retina through four convex lenses. Light
628 intensity was 170–200 µW/cm^2 (116–136 lux) in 8–10 µW/cm^2 (5.5–6.8 lux) background
629 illumination. Light stimuli were given in 1 sec pulses with 6 sec inter-pulse intervals to a total
630 of 40 pulses per retina. All experiments were performed after sufficient dark adaptation (> 1h).
631
632 **Visual acuity test**
633 Mouse visual acuity was measured with the OptoMotry system (Cerebral Mechanics Inc.) as

previously described (Prusky et al., 2004). Mice, of which genotypes are not determined before the measurement, were adapted to ambient light for 30 mins and then placed on the stimulus platform, which is surrounded by four computer monitors displaying grating patterns randomly presented by the OptoMotry software. Mice that stopped moving and began tracking the gratings with reflexive head movements in concert with their rotation were counted as successful visual detection events. The detection thresholds were then obtained from the OptoMotry software.

Visual performance test

A. Surgery

Adult mice (postnatal days 35–40) were anesthetized with isoflurane (1.5% induction and 1.0% maintenance) and fixed to a stereotaxic frame. Body temperature was maintained at 37°C. Custom-designed head plates were attached to the skull with small screws (Small Parts) and dental cement (Lang Dental).

B. Behavior test

Visual detection task

In this task, head plate-implanted mice (P45-P80) were trained to lick a water nozzle when they detected a visual stimulus (114 Lux). All mice used for this task were water-deprived for 1 day before beginning the training protocol. For the visual stimulus, we presented a full-field flashing light 5 times (10 Hz for 500 ms) through a gamma-corrected LCD monitor placed 10 cm from the left eye. Each stimulus trial began with a visual stimulus (500 ms in duration) and ended with a 2 s inter-trial period. Non-stimulus trials were randomly interleaved with stimulus trials using custom code (Presentation). We detected each lick through a custom-made lickport (4.0 mm ID) using a transistor-based lickometer system. Licks detected during the final 2 s of stimulus trials (i.e., in the response window) were rewarded with 4 μl of water (on). We delivered water rewards by gravity into the lickport under the control of a solenoid valve. Licks detected during the response window of non-stimulus trials were punished with a mild air puff (300 ms) and a longer inter-trial interval (8 s, timeout) (off). We delivered compressed

air puff punishments (10 psi) through a plastic tip (1.0 mm ID) located 2 cm from the face and controlled by a solenoid valve. Mice whose spontaneous lick rate during non-stimulus trials fell below 0.4 were advanced to the next phase. In the next phase, we measured lick rates in response to 9 different intensities of visual stimuli presented randomly with equal probability.

Visual adaptation task

We trained mice to discriminate a continuous light from a drifting grate stimulus presented after continuous light under a simple go/no-go protocol. Training proceeded in two steps: conditioning and discrimination. For conditioning (2–8 days), we trained each mouse to lick in response to continuous light. Each trial began with a continuous light (go stimulus, 2 s duration) and ended with an inter-trial period of 2 s. Licks detected in the final 2 s of the trial (i.e., in the response window) were rewarded with 10 μl of water for 2 s. During the conditioning phase, water rewards were still given after continuous light even if the animal failed to lick during the response window. Mice exceeding 300 licks within 1 hr were advanced to the discrimination phase. For discrimination (15 days), we trained mice to lick only when continuous light (2 s) was presented (go trial) and not to lick when a drifting horizontal grate stimulus (1 s) was presented after a continuous light stimulus (1 s) (no-go trial). All visual stimuli used for training were fixed at 57 Lux. We never presented the same type of stimulus more than three consecutive times. Licks within the response window of go trials were rewarded with water (4 μl) for 2 s, and licks within the response window of no-go trials were punished with mild air puffs (300 ms) and a longer inter-trial interval (8 s, timeout). Mice were neither rewarded nor punished for misses (i.e., no lick in a go trial) or correct rejections (i.e., no lick in a no-go trial). Training ended when the mouse stopped licking for 10 consecutive go trials.

Mice that reached threshold performance (lick rates in no-go trials < 0.4) were advanced to the next phase. In the next phase, we presented five different intensities of a continuous light higher or equal to 57 lux before a drifting grate stimulus fixed at 57 lux. We presented all stimuli randomly with equal probability.

Acknowledgements

We thank Drs. Samuel Pfaff, Motoko Shibanuma, and Seth Blackshaw generous gifts of the research materials used in the study. We also thank Dr. Jong Soon Choi for the help with MALDI-TOF mass spectrometry and Dr. Suk-Jo Kang and Jiyoun Min for their help with FACS. This work was supported by grants from the Global Research Laboratory Program (NRF-2009-00424; JWK), Brain Research Program (NRF-2013-056566; JWK), Basic Science Research Program (NRF-2014R1A2A2A01003069; JWK), and Stem Cell Research Program (NRF-2006-2004289; KHK) funded by the Korean National Research Foundation (NRF); and by National Institute of Health of United States (NIH R01-EY013760; EML).

References

Aota, S.-i., Nakajima, N., Sakamoto, R., Watanabe, S., Ibaraki, N., and Okazaki, K. (2003). Pax6 autoregulation mediated by direct interaction of Pax6 protein with the head surface ectoderm-specific enhancer of the mouse Pax6 gene. Dev. Biol. *257*, 1-13.

Ashery-Padan, R., and Gruss, P. (2001). Pax6 lights-up the way for eye development. Curr. Opion. Cell Biol. *13*, 706-714.

Balasubramanian, R., Bui, A., Ding, Q., and Gan, L. (2014). Expression of LIM-homeodomain transcription factors in the developing and mature mouse retina. Gene Expr. Patterns *14*, 1-8.

Bridwell, J.L., Price, J.R., Parker, G.E., Schiller, A.M., Sloop, K.W., and Rhodes, S.J. (2001). Role of the LIM domains in DNA recognition by the Lhx3 neuroendocrine transcription factor. Gene *277*, 239-250.

Cepko, C. (2014). Intrinsically different retinal progenitor cells produce specific types of progeny. Nat. Rev. Neurosci. *15*, 615-627.

Chavez, A.E., Grimes, W.N., and Diamond, J.S. (2010). Mechanisms underlying lateral GABAergic feedback onto rod bipolar cells in rat retina. J. Neurosci. *30*, 2330-2339.

Cong, L., Ran, F.A., Cox, D., Lin, S., Barretto, R., Habib, N., Hsu, P.D., Wu, X., Jiang, W., Marraffini, L.A.*, et al.* (2013). Multiplex genome engineering using CRISPR/Cas systems. Science *339*, 819-823.

722 Danno, H., Michiue, T., Hitachi, K., Yukita, A., Ishiura, S., and Asashima, M. (2008). Molecular
723 links among the causative genes for ocular malformation: Otx2 and Sox2 coregulate Rax
724 expression. Proc. Natl. Acad. Sci. U. S. A. *105*, 5408-5413.

725 de Melo, J., Miki, K., Rattner, A., Smallwood, P., Zibetti, C., Hirokawa, K., Monuki, E.S.,
726 Campochiaro, P.A., and Blackshaw, S. (2012). Injury-independent induction of reactive gliosis
727 in retina by loss of function of the LIM homeodomain transcription factor Lhx2. Proc. Natl.
728 Acad. Sci. U. S. A. *109*, 4657-4662.

729 Demb, J.B., and Singer, J.H. (2012). Intrinsic properties and functional circuitry of the AII
730 amacrine cell. Visual neuroscience *29*, 51-60.

731 Duquette, P.M., Zhou, X., Yap, N.L., MacLaren, E.J., Lu, J.J., Wallace, V.A., and Chen, H.-H.
732 (2010). Loss of LMO4 in the retina leads to reduction of GABAergic amacrine cells and
733 functional deficits. PLoS One *5*, e13232.

734 Eggers, E.D., Mazade, R.E., and Klein, J.S. (2013). Inhibition to retinal rod bipolar cells is
735 regulated by light levels. J. Neurophysiol. *110*, 153-161.

736 Elshatory, Y., Everhart, D., Deng, M., Xie, X., Barlow, R.B., and Gan, L. (2007). Islet-1 controls
737 the differentiation of retinal bipolar and cholinergic amacrine cells. J. Neurosci. *27*, 12707-
738 12720.

739 Epstein, J.A., Glaser, T., Cai, J., Jepeal, L., Walton, D.S., and Maas, R.L. (1994). Two
740 independent and interactive DNA-binding subdomains of the Pax6 paired domain are
741 regulated by alternative splicing. Genes Dev. *8*, 2022-2034.

742 Galli-Resta, L., Resta, G., Tan, S.-S., and Reese, B.E. (1997). Mosaics of islet-1-expressing
743 amacrine cells assembled by short-range cellular interactions. J. Neurosci. *17*, 7831-7838.

744 Gehring, W.J., Qian, Y.Q., Billeter, M., Furukubo-Tokunaga, K., Schier, A.F., Resendez-Perez,
745 D., Affolter, M., Otting, G., and Wüthrich, K. (1994). Homeodomain-DNA recognition. Cell *78*,
746 211-223.

747 Gill, G.N. (2003). Decoding the LIM development code. Transac. Am. Clin. Climatol. Assoc.
748 *114*, 179.

749 Glaser, T., Jepeal, L., Edwards, J.G., Young, S.R., Favor, J., and Maas, R.L. (1994). PAX6
750 gene dosage effect in a family with congenital cataracts, aniridia, anophthalmia and central
751 nervous system defects. Nat. Genet. *7*, 463-471.

752 Gordon, P.J., Yun, S., Clark, A.M., Monuki, E.S., Murtaugh, L.C., and Levine, E.M. (2013).
753 Lhx2 balances progenitor maintenance with neurogenic output and promotes competence
754 state progression in the developing retina. J. Neurosci. *33*, 12197-12207.

755 Granger, A., Bleux, C., Kottler, M.-L., Rhodes, S.J., Counis, R., and Laverrière, J.-N. (2006).
756 The LIM-homeodomain proteins Isl-1 and Lhx3 act with steroidogenic factor 1 to enhance
757 gonadotrope-specific activity of the gonadotropin-releasing hormone receptor gene promoter.
758 Mol. Endocrinol. *20*, 2093-2108.

759 Hanson, I., and Van Heyningen, V. (1995). Pax6: more than meets the eye. Trends Genet. *11*,

268-272.

Haverkamp, S., Ghosh, K.K., Hirano, A.A., and Wässle, H. (2003). Immunocytochemical description of five bipolar cell types of the mouse retina. J. Comp. Neurol. *455*, 463-476.

Heitzer, M., and DeFranco, D. (2006). Mechanism of action of Hic-5/androgen receptor activator 55, a LIM domain-containing nuclear receptor coactivator. Mol. Endocrinol. *20*, 56-64.

Hoon, M., Okawa, H., Della Santina, L., and Wong, R.O. (2014). Functional architecture of the retina: development and disease. Prog. Ret. Eye Res. *42*, 44-84.

Jessell, T.M. (2000). Neuronal specification in the spinal cord: inductive signals and transcriptional codes. Nat. Rev. Genet. *1*, 20-29.

Kammandel, B., Chowdhury, K., Stoykova, A., Aparicio, S., Brenner, S., and Gruss, P. (1999). Distinctcis-Essential Modules Direct the Time–Space Pattern of thePax6Gene Activity. Dev. Biol. *205*, 79-97.

Karlsson, O., Thor, S., Norberg, T., Ohlsson, H., and Edlund, T. (1990). Insulin gene enhancer binding protein Isl-1 is a member of a novel class of proteins containing both a homeo-and a Cys His domain. Nature *344*, 879-882.

Kim, H.T., Kim, S.J., Sohn, Y.I., Paik, S.S., Caplette, R., Simonutti, M., Moon, K.H., Lee, E.J., Min, K.W., Kim, M.J*., et al.* (2015). Mitochondrial Protection by Exogenous Otx2 in Mouse Retinal Neurons. Cell Rep. *13*, 990-1002.

Kim-Kaneyama, J.-r., Takeda, N., Sasai, A., Miyazaki, A., Sata, M., Hirabayashi, T., Shibanuma, M., Yamada, G., and Nose, K. (2011). Hic-5 deficiency enhances mechanosensitive apoptosis and modulates vascular remodeling. J. Mol. Cell. Cardiol. *50*, 77-86.

Koike, C., Nishida, A., Ueno, S., Saito, H., Sanuki, R., Sato, S., Furukawa, A., Aizawa, S., Matsuo, I., Suzuki, N*., et al.* (2007). Functional roles of Otx2 transcription factor in postnatal mouse retinal development. Mol. Cell. Biol. *27*, 8318-8329.

Lakowski, J., Majumder, A., and Lauderdale, J.D. (2007). Mechanisms controlling Pax6 isoform expression in the retina have been conserved between teleosts and mammals. Dev. Biol. *307*, 498-520.

Lee, S., Lee, B., Joshi, K., Pfaff, S.L., Lee, J.W., and Lee, S.-K. (2008). A regulatory network to segregate the identity of neuronal subtypes. Dev. Cell *14*, 877-889.

Leonard, J., Serup, P., Gonzalez, G., Edlund, T., and Montminy, M. (1992). The LIM family transcription factor Isl-1 requires cAMP response element binding protein to promote somatostatin expression in pancreatic islet cells. Proc. Natl. Acad. Sci. U. S. A. *89*, 6247-6251.

Lin, Y.-p., Ouchi, Y., Satoh, S., and Watanabe, S. (2009). Sox2 plays a role in the induction of amacrine and Müller glial cells in mouse retinal progenitor cells. Invest. Ophthal. Vis. Sci. *50*, 68-74.

Liu, I.S., Ploder, L., Vidgen, D., van der Kooy, D., Kalnins, V.I., and Mclnnes, R.R. (1994). Developmental expression of a novel murine homeobox gene (Chx10): evidence for roles in

798 determination of the neuroretina and inner nuclear layer. Neuron *13*, 377-393.

799 Marquardt, T., Ashery-Padan, R., Andrejewski, N., Scardigli, R., Guillemot, F., and Gruss, P.
800 (2001). Pax6 is required for the multipotent state of retinal progenitor cells. Cell *105*, 43-55.

801 Masland, R.H. (2012). The neuronal organization of the retina. Neuron *76*, 266-280.

802 Matsuda, T., and Cepko, C.L. (2004). Electroporation and RNA interference in the rodent
803 retina in vivo and in vitro. Proc. Natl. Acad. Sci. U. S. A. *101*, 16-22.

804 Mikkola, I., Bruun, J.A., Holm, T., and Johansen, T. (2001). Superactivation of Pax6-mediated
805 transactivation from paired domain-binding sites by dna-independent recruitment of different
806 homeodomain proteins. The Journal of biological chemistry *276*, 4109-4118.

807 Mishra, R., Gorlov, I.P., Chao, L.Y., Singh, S., and Saunders, G.F. (2002). PAX6, paired
808 domain influences sequence recognition by the homeodomain. J. Biol. Chem. *277*, 49488-
809 49494.

810 Mori, K., Asakawa, M., Hayashi, M., Imura, M., Ohki, T., Hirao, E., Kim-Kaneyama, J.-r., Nose,
811 K., and Shibanuma, M. (2006). Oligomerizing potential of a focal adhesion LIM protein Hic-5
812 organizing a nuclear-cytoplasmic shuttling complex. J. Biol. Chem. *281*, 22048-22061.

813 Morrow, E.M., Chen, C., and Cepko, C.L. (2008). Temporal order of bipolar cell genesis in the
814 neural retina. Neural. Dev. *3*.

815 Mui, S.H., Kim, J.W., Lemke, G., and Bertuzzi, S. (2005). Vax genes ventralize the embryonic
816 eye. Genes Dev. *19*, 1249-1259.

817 Nishida, A., Furukawa, A., Koike, C., Tano, Y., Aizawa, S., Matsuo, I., and Furukawa, T. (2003).
818 Otx2 homeobox gene controls retinal photoreceptor cell fate and pineal gland development.
819 Nat. Neurosci. *6*, 1255-1263.

820 Nishiya, N., Iwabuchi, Y., Shibanuma, M., Côté, J.-F., Tremblay, M.L., and Nose, K. (1999).
821 Hic-5, a paxillin homologue, binds to the protein-tyrosine phosphatase PEST (PTP-PEST)
822 through its LIM 3 domain. J. Biol. Chem. *274*, 9847-9853.

823 Pan, L., Deng, M., Xie, X., and Gan, L. (2008). ISL1 and BRN3B co-regulate the
824 differentiation of murine retinal ganglion cells. Development *135*, 1981-1990.

825 Plaza, S., Dozier, C., Langlois, M.-C., and Saule, S. (1995). Identification and characterization
826 of a neuroretina-specific enhancer element in the quail Pax-6 (Pax-QNR) gene. Mol. Cell. Biol.
827 *15*, 892-903.

828 Plaza, S., Hennemann, H., Möröy, T., Saule, S., and Dozier, C. (1999). Evidence that POU
829 factor brn-3B regulates expression of Pax-6 in neuroretina cells. Journal of neurobiology *41*,
830 349-358.

831 Prusky, G.T., Alam, N.M., Beekman, S., and Douglas, R.M. (2004). Rapid quantification of
832 adult and developing mouse spatial vision using a virtual optomotor system. Invest.
833 Ophthalmol. Vis. Sci. *45*, 4611-4616.

834 Rapaport, D.H., Wong, L.L., Wood, E.D., Yasumura, D., and LaVail, M.M. (2004). Timing and

topography of cell genesis in the rat retina. J. Comp. Neurol. *474*, 304-324.

Roberson, M.S., Schoderbek, W.E., Tremml, G., and Maurer, R.A. (1994). Activation of the glycoprotein hormone alpha-subunit promoter by a LIM-homeodomain transcription factor. Mol. Cell. Biol. *14*, 2985-2993.

Schwarz, M., Cecconi, F., Bernier, G., Andrejewski, N., Kammandel, B., Wagner, M., and Gruss, P. (2000). Spatial specification of mammalian eye territories by reciprocal transcriptional repression of Pax2 and Pax6. Development *127*, 4325-4334.

Sheng, H.Z., Zhadanov, A.B., Mosinger, B., Jr., Fujii, T., Bertuzzi, S., Grinberg, A., Lee, E.J., Huang, S.P., Mahon, K.A., and Westphal, H. (1996). Specification of pituitary cell lineages by the LIM homeobox gene Lhx3. Science *272*, 1004-1007.

Shirasaki, R., and Pfaff, S.L. (2002). Transcriptional codes and the control of neuronal identity. Ann. Rev. Neurosci. *25*, 251-281.

Thaler, J.P., Lee, S.-K., Jurata, L.W., Gill, G.N., and Pfaff, S.L. (2002). LIM factor Lhx3 contributes to the specification of motor neuron and interneuron identity through cell-type-specific protein-protein interactions. Cell *110*, 237-249.

Voinescu, P.E., Kay, J.N., and Sanes, J.R. (2009). Birthdays of retinal amacrine cell subtypes are systematically related to their molecular identity and soma position. J. Comp. Neurol. *517*, 737-750.

Way, J.C., and Chalfie, M. (1988). mec-3, a homeobox-containing gene that specifies differentiation of the touch receptor neurons in C. elegans. Cell *54*, 5-16.

Xu, H.E., Rould, M.A., Xu, W., Epstein, J.A., Maas, R.L., and Pabo, C.O. (1999a). Crystal structure of the human Pax6 paired domain-DNA complex reveals specific roles for the linker region and carboxy-terminal subdomain in DNA binding. Genes Dev *13*, 1263-1275.

Xu, P.-X., Zhang, X., Heaney, S., Yoon, A., Michelson, A.M., and Maas, R.L. (1999b). Regulation of Pax6 expression is conserved between mice and flies. Development *126*, 383-395.

Yun, S., Saijoh, Y., Hirokawa, K.E., Kopinke, D., Murtaugh, L.C., Monuki, E.S., and Levine, E.M. (2009). Lhx2 links the intrinsic and extrinsic factors that control optic cup formation. Development *136*, 3895-3906.

Zagozewski, J.L., Zhang, Q., Pinto, V.I., Wigle, J.T., and Eisenstat, D.D. (2014). The role of homeobox genes in retinal development and disease. Dev. Biol. *393*, 195-208.

Figure legends

Figure 1. Identification of Lhx3 and Tgfb1i1 as Pax6 α-enhancer binding proteins.
(A) (Top) The genomic structure of the mouse *Pax6* gene. Exons are shown as boxes, and arrows denote transcription initiation sites. (Bottom) The DF3, PBS, and DF4 sequences in the retina-specific α-enhancer are indicated with their core homeodomain (HD) and paired domain (PD) binding sites colored red. **(B)** Nuclear extracts from R28 rat retinal precursor cells were incubated with DF4 dsDNA oligomers with single-stranded 5'-$(GT)_5$-3' overhangs. DF4 oligomer-protein complexes were then added to Sepharose 6B columns conjugated with single-stranded DNA (ssDNA) of 5'-$(CA)_5$-3', which is complementary to the single-stranded overhang sequence of the oligomer, or 5'-$(TG)_5$-3' non-specific binding control. Proteins bound to the ssDNA column were eluted for SDS-PAGE and detected by silver staining. Protein bands specifically enriched in the $(CA)_5$ column were then eluted from the gel and digested for mass spectrometric identification. This analysis identified the two bands marked by arrows as Lhx3 and Tgfb1i1. **(C)** Lhx3 and Tgfb1i1 expression in post-natal day 8 (P8) *Pax6 α-enhancer::Cre-IRES-GFP* (*P6α-CreiGFP*) mouse retinas stained with rabbit anti-Lhx3 (top) and anti-Tgfb1i1 (bottom) antibodies (red). These were also co-stained with a chick anti-GFP antibody (green). Scale bars, 100 μm. **(D)** DNA fragments bound to Pax6, Lhx3, and Tgfb1i1 in P7 mouse retinas were isolated by chromatin immunoprecipitation (ChIP) using rabbit polyclonal antibodies against each protein. The relative enrichment of each protein on the ectoderm enhancer and the α-enhancer of *Pax6* gene was determined by PCR amplification of each enhancer sequence from the ChIP DNA fragments. **(E)** qPCR threshold cycle (Ct) values for each ChIP sample were compared to those of a protein-A bead only sample to obtain relative expression ($2^{-\Delta Ct}$). The graph shows the ratio of $2^{-\Delta Ct}$ values for each sample to those of a pre-immune rabbit IgG (Rb-IgG) ChIP sample. Error bars indicate standard deviations (STD, n=5).

Figure 2. Lhx3 and Isl1 inhibit Pax6 α-enhancer activity in a Tgfb1i1-sensitive manner.

(A) The effects of LIM domain transcription factors on *Pax6* α-enhancer activity were measured with a *Pax6* α-enhancer luciferase reporter in HEK293T cells. These cells were co-transfected with DNA constructs encoding cDNAs of the indicated genes as well as the *Pax6* *α*-luciferase reporter (0.2 μg). The triangles denote increasing doses of the indicated constructs (0.5 μg, 1 μg, and 2 μg). Relative luciferase activity of each sample was normalized to co-expressed β-galactosidase activity. **(B)** The effects of LIM domain transcription factors on Pax6-induced activation of the α-enhancer were also examined in the cells transfected with same DNA constructs used in (A) plus Pax6 construct (0.5 μg). **(C)** Regulatory effects of Tgfb1i1 and Lmo4 on *Pax6* α-enhancer activity were also examined in the transfected cells as described in (A) and (B). **(D** and **E)** Cooperative effects of Isl1, Lhx3, and Tgfb1i1 on *Pax6* α-enhancer activity were examined with the indicated combinations. (A – E) The blue lines indicated relative luciferase activity in samples expressing only the luciferase reporter, while red lines indicate activity of samples expressing the reporter with Pax6. The values on the Y-axes are averages. Error bars indicate STD (n>5); *p<0.05, **p<0.01, ***p<0.001.

Figure 3. Pax6 and Tgfb1i1 antagonistically regulate Isl1-Lhx3 complex formation.
(A) Interactions between endogenous Isl1, Lhx3, and Tgfb1i1 in P7 mouse retinas measured by reciprocal co-immunoprecipitation (co-IP) and subsequent Western blotting (WB) with the indicated antibodies. P7 mouse retinal cell lysates were divided into two input tubes (1 and 2) in prior to the co-IP with indicated antibodies and subsequent WB detection of co-immunoprecipitated proteins. 5% of input cell lysates were used to compare the relative amount of the proteins in the retinal cell lysates used for co-IP. **(B)** Interactions between epitope-tagged Lhx3 and Isl1, Lhx3 and Tgfb1i1, and Isl1 and Tgfb1i1 in HEK293T cells were determined by co-IP and WB. Successful expression of each transfected cDNA was determined by WB for each protein in cell lysates (50 μg/lane; 5% of the co-IP input) with the corresponding epitope-tag antibodies. Arrows indicate specific WB bands, and asterisks indicate non-specific bands. **(C** and **D)** The effects of Tgfb1i1 and Lmo4 on Isl1-Lhx3 complex formation in HEK293T cells. Triangles denote increasing amounts of each DNA construct (1

μg, 2 μg, and 4 μg). Interaction between Pax6 and LIM domain proteins **(E)** and effect of Pax6 on LIM domain protein complex formation **(F)** in HEK293T cells were also examined by co-IP and WB analyses. **(G)** Reciprocal effects of LIM domain proteins and Pax6 on the binding to human *PAX6* α-enhancer sequence in the transfected HEK293T cells were measured by qPCR amplification of α-enhancer sequences in DNA fragments isolated by ChIP with the indicated epitope tag-specific antibodies. Relative enrichment of each protein on the α-enhancer was determined by comparing the qPCR value of the transfected samples with those produced by antibodies bind non-specifically to the enhancer element in untransfected HEK293T cells. Error bars indicate STD (n>5) ; *p<0.05, **p<0.01, ***p<0.001. **(H)** Schematic model depicting the binding of the Pax6-Isl1 and Isl1-Tgfb1i1-Lhx3 complexes to the *Pax6* α-enhancer element. HD, homeodomain; LBD, LIM-binding domain; LD, leucine-rich domain; PD, paired domain.

Figure 4. Elevated GABAergic amacrine cell number in Tgfb1i1$^{-/-}$ mouse retinas.
(A) *Pax6* α-enhancer-active cells in P14 *Tgfb1i1*$^{+/+}$ and *Tgfb1i1*$^{-/-}$ littermate mouse retinas were visualized by immunodetection of GFP expressed from the *P6α-CreiGFP* transgene. ONL, outer nuclear layer; INL, inner nuclear layer; GCL, ganglion cell layer. **(B)** GFP-positive cell population in 250 μm x 250 μm retinal area. **(C)** P14 *Tgfb1i1*$^{+/+}$ and *Tgfb1i1*$^{-/-}$ littermate mouse retinas stained with antibodies detecting amacrine cell subtype-specific markers. Pax6, pan-amacrine cells; ChAT, cholinergic amacrine cells; GlyT1, glycinergic amacrine cells; GABA, Gad67 and Bhlhb5 (in the bottom half of INL in the images in E), GABAergic amacrine cells. **(D)** Fold-changes of amacrine cell numbers in P14 *Tgfb1i1*$^{-/-}$ retinas compared to *Tgfb1i1*$^{+/+}$ littermate retinas. **(E)** P14 *Tgfb1i1*$^{+/+}$ and *Tgfb1i1*$^{-/-}$ mouse retinas stained for bipolar cell-specific markers. Vsx2, pan-bipolar cell marker; PKCα, rod bipolar cells; G0α, rod and ON-cone bipolar cells; Vsx1, OFF bipolar cells; Recoverin, photoreceptors (in the ONL) and type-2 OFF bipolar cells (in the INL); Bhlhb5 (in the top half of INL), type-2 OFF bipolar cells. **(F)** Fold-changes in marker-positive cell numbers in *Tgfb1i1*$^{-/-}$ retinas compared to *Tgfb1i1*$^{+/+}$ littermate retinas. Values on the Y-axes of B, D, and F are averages. Error bars indicate STD (n=4, 3 litters); *, p<0.05; **, p<0.01; ***, p<0.001. Scale bars in the pictures, 100 μm.

954

955 ***Figure 5. Pax6 α-enhancer-induced Pax6ΔPD isoform supports GABAergic amacrine***
956 ***cell fate.***
957 **(A)** Reciprocal co-IP and WB analyses with the indicated antibodies reveal a reduced
958 interaction between Isl1 and Lhx3 in P7 *Tgfb1i1*$^{-/-}$ mouse retinas compared with littermate
959 *Tgfb1i1*$^{+/+}$ retinas (top two WB images). *Tgfb1i1*$^{-/-}$ retinal lysates show 1.6-fold higher Isl1 level
960 than *Tgfb1i1*$^{+/+}$ retinal lysates and no significant change in the levels of Lhx3 and Actinβ1
961 (bottom four WB images). **(B)** No significant difference in the assembly of Isl1 and Pax6 was
962 observed in P7 *Tgfb1i1*$^{+/+}$ and *Tgfb1i1*$^{-/-}$ littermate mouse retinas (top two WB images).
963 *Tgfb1i1*$^{-/-}$ retinas show higher expression of the Pax6ΔPD isoform than *Tgfb1i1*$^{+/+}$ retinas and
964 no change in full-length Pax6 (bottom two WB images). **(C)** Pax6 α-enhancer-active cells
965 were isolated from P14 *P6α-CreiGFP* retinas by repeated FACS (see the Materials and
966 Methods). Lysates of GFP(+) and GFP(-) retinal cells were then analyzed by 10% SDS-PAGE
967 and WB with a rabbit anti-Pax6 antibody. Successful purification of the cells was confirmed by
968 WB detection of GFP in each fraction. **(D)** Diagram of pCAGIG DNA constructs encoding V5-
969 tagged Pax6 (pCAGIG-V5-Pax6) and Pax6ΔPD (pCAGIG-V5-Pax6ΔPD). These constructs
970 express EGFP from an IRES linked to the V5-Pax6 or V5-Pax6ΔPD cDNAs. This allowed for
971 the confirmation of successful expression of the cDNAs in in P7 mouse retinas electroporated
972 with the indicated pCAGIG DNA constructs at P0 by WB detection of EGFP and V5. **(E)** Co-
973 expression of V5-Pax6ΔPD and EGFP in P7 mouse retinas was also determined by
974 immunostaining with mouse anti-V5 (red) and chick anti-GFP (green) antibodies. **(F)** The
975 identities of EGFP-positive retinal cells co-expressing Pax6 or Pax6ΔPD in P14 mouse
976 retinas were determined by staining with antibodies against various amacrine and bipolar cell-
977 specific proteins. The images are mouse retinal sections stained with anti-GABA (top) and
978 anti-Vsx1 (bottom) antibodies. Arrowheads indicate cells positive to both of EGFP and the
979 markers. Additional immunostaining images are provided in Figure 5 – figure supplement 2.
980 **(G)** EGFP-positive cells co-expressing each cell type-specific marker are shown as a
981 percentage of total EGFP-positive INL cells. Values on the Y-axis are averages. Error bars
982 indicate STD (n=5); **, $p<0.01$; ***, $p<0.001$.

983

984 ***Figure 6. Pax6-dependent Pax6 α-enhancer activation is positively correlated with***
985 ***GABAergic amacrine cell number.***
986 **(A)** Genomic DNA was isolated from the tails of *Pax6*$^{+/+}$ (left) and *Pax6*$^{\Delta PBS/\Delta PBS}$ (right) mice
987 for sequencing the Pax6 α-enhancer region. The Pax6 binding sequence (PBS) in the α-
988 enhancer is colored red. The *Pax6*$^{\Delta PBS}$ allele is missing 6 nucleotides (5'-TGCATG-3') in the
989 PBS. **(B)** Whole eye images of P30 *Pax6*$^{+/+}$*;P6α-CreiGFP* and *Pax6*$^{\Delta PBS/\Delta PBS}$*;P6α-CreiGFP*
990 littermate mice (left) and the mouse eye sections stained with H&E (center) or an anti-GFP
991 antibody (right). Scale bar in the rightmost column is 100 μm. **(C)** Pax6 α-GFP-positive cells in
992 P30 *Pax6*$^{+/+}$ and *Pax6*$^{\Delta PBS/\Delta PBS}$ retinas (250 μm x 250 μm). Error bars indicate STD (n=4, 2
993 independent litters). **(D)** Full-length Pax6 and Pax6ΔPD in P14 *Pax6*$^{+/+}$ and *Pax6*$^{\Delta PBS/\Delta PBS}$
994 retinal cell lysates were detected by WB with anti-Pax6 antibody and WB band intensities
995 were compared to show the relative values below the WB image. **(E)** Distributions of pan-
996 amacrine cell marker Pax6, GABAergic amacrine cell subset marker GABA, pan-bipolar cell
997 marker Vsx2, and OFF bipolar cell marker Vsx1 in P14 *Pax6*$^{+/+}$ and *Pax6*$^{\Delta PBS/\Delta PBS}$ littermate
998 retinas were visualized with immunostaining with antibodies recognizing respective markers.
999 Scale bars, 100 μm. Additional images of amacrine and bipolar cell subtypes are shown in
1000 Figure 6 – figure supplement 2. **(F)** Quantification of relative numbers of amacrine and bipolar
1001 cell subsets in mouse retinas. Error bars indicate STD (n=5, 3 independent litters). *, p<0.05;
1002 **, p<0.01.
1003
1004 ***Figure 7. Pax6 α-enhancer-active amacrine cells are important for visual adaptation.***
1005 **(A)** Visual acuity was measured in P60 mice using the OptoMotry system as previously
1006 described (Prusky et al., 2004) (for details, see the Materials and Methods). Error bars
1007 indicate STD (n=6). **, p<0.01. **(B)** Peristimulus time histograms (PSTHs) for RGCs in P60
1008 *Tgfb1i1*$^{+/+}$ and *Tgfb1i1*$^{-/-}$ littermate and P60 *Pax6*$^{+/+}$ and *Pax6*$^{\Delta PBS/\Delta PBS}$ littermate mouse
1009 retinas were obtained by multielectrode array (MEA) recordings. Maximum and mean
1010 numbers of spike were counted from each PSTH. Insets are representative PSTH patterns.
1011 Arrowhead indicates the sustained light-ON responses of RGCs. Maximum (max, **C**) and

mean (**D**) numbers of spikes were counted from each PSTH. The numbers on the Y-axis are averages (WT, n=526 (in 4 mice); *Tgfb1i1*$^{-/-}$, n=534 (in 6 mice); *Pax6*$^{+/+}$, n=175; *Pax6*$^{\Delta PBS/\Delta PBS}$, n=276). Error bars indicate STD. Statistical significance was determined using the D'Agostino & Pearson omnibus normality test followed by one-way ANOVAs and Sidak's test for multiple comparisons. *, p<0.05; ***, p<0.001. **(E)** Visual detection in P60 *Tgfb1i1*$^{-/-}$, *Pax6*$^{\Delta PBS/\Delta PBS}$, and their WT littermate mice trained to lick water in response to light stimuli. The experimental scheme and task learning curves are provided in Figures 7 – figure supplement 3A and 3B (for details, see the Materials and Methods). **(F)** The mice were also given water in association with a continuous light stimulus (2 s) but not with a continuous light stimulus (1 s) followed by a drifting grate stimulus (1 s) (see the experimental scheme and task learning curves in Figures 7 – figure supplement 3C and 3D). Visual responses were quantified as ratios of hit rates (HitR, Go) to false alarm rates (FAR, Nogo). Error bars in (E) and (F) indicate STD. *, p<0.05; **, p<0.01; ***, p<0.001 (Unpaired t-test). **(G)** Diagram depicting the modulation of retinal circuitry important for visual adaptation by *Pax6* α-enhancer-active (P6α) GABAergic amacrine cells.

Figure supplements

Figure 1 – figure supplement 1. Lhx3 and Tgfb1i1 expression in embryonic and mature mouse retinas. E14.5 and P30 *P6α-CreiGFP* mouse retinas stained with anti-Lhx3 (**A**) and anti-Tgfb1i1 (**B**) antibodies. Lhx3 is absent in E14.5 mouse retinas but expressed in bipolar cell subsets in post-natal (P8, Figure 1C) and adult (P30) mouse retinas. Tgfb1i1 is absent in E14.5 and P30 mouse retinas, but is expressed in P8 mouse retina (Figure 1C). The specificity of anti-Tgfb1i1 antibody was confirmed by staining P30 *Tgfb1i1-ko* mouse retinas (bottom). Scale bars, 50 μm.

Figure 1 – figure supplement 2. Binding abilities of Lhx3 and Tgfb1i1 to *Pax6 α*-enhancer sequence. (A) P7 retinal nuclear extracts were incubated with either the wild-type DF4 (DF4-WT) dsDNA oligomers used in Figure 1B or mutant DF4 dsDNA oligomers (DF4-Mut) in which the homeobox core binding sequence ATTA was replaced with CGGC. Proteins captured by the $(CA)_5$ ssDNA column were eluted for SDS-PAGE and Western blot (WB) analyses detecting Lhx3 and Tgfb1i1. Arrows indicate specific bands and the asterisk marks a non-specific band. **(B)** To evaluate direct binding of Lhx3 and Tgfb1i1 to DF4 sequence in the *Pax6 α*-enhancer, we performed an EMSA with biotin-labeled DF4 dsDNA oligomers (Bio-DF4) pre-incubated with *in vitro* translated Lhx3 and Tgfb1i1. **(C)** Lhx3 binding to the conserved homeodomain binding sequence in DF4 was measured by adding unlabeled competitor DNA (DF4 (WT-Comp) or mutated DF4 (Mut-Comp, ATTA to CGGC)) at 1-, 10-, 100-, and 200-fold the concentration of the Bio-DF4 probe. The asterisk marks non-specific bands.

Figure 1 – figure supplement 3. Relationship between LIM domain transcription factor expression and *Pax6 α*-enhancer activity in mouse retina. (A) P14 *P6α-CreiGFP* mouse retinas stained with rabbit antibodies recognizing LIM domain transcription factors (LIM-TF), Isl1, Lhx2, Lhx3, and Lhx9, and a mouse antibody recognizing GFP, which represents *Pax6 α*-enhancer activity. Images in the bottom row are magnified versions of the dotted areas in

the top row. Scale bars, 100 μm. **(B)** Population of Pax6 α-GFP-positive cells co-expressing each LIM domain transcription factor in total LIM-TF-expressing cells (red bars) or in total GFP-expressing cells (green bars) were obtained and shown in a graph. Error bars represent standard deviations (STD; n=4, 3 litters). **(C** and **D)** EMSA performed with biotin-labeled dsDNA probes for the *Pax6 α*-enhancer *DF4* (Bio-DF4; **C**) or *DF3* (Bio-DF3; **D**) sequences. Unbound free DNA probes and LIM domain protein-bound DNA probes are indicated by arrows. An asterisk indicates a non-specific protein-bound probe band.

Figure 3 – figure supplement 1. Pax6 and Tgfb1i1 antagonistically regulate Isl1-Lhx3 complex formation. (A) Schematics for the full-length and deletion mutants of Isl1, Lhx3, Pax6, and Tgfb1i1 used in these experiments. HD, homeodomain; LIM, LIM domain; LBD, LIM binding domain; LD, leucin-rich domain; PD, paired domain; PST, transactivation domain enriched in proline, sereine, and threonine. **(B – I)** 293T cells (~10^6) were transfected with DNA constructs (10 μg total) encoding the indicated protein fragments. Cell lysates collected at 48h post-transfection were incubated with antibodies against the epitope tags to immunoprecipitate each protein and its binding partners. Co-immunoprecipitated proteins were then analyzed by SDS-PAGE and subsequent WB with the indicated antibodies. In parallel, the cell lysates (containing 50 μg protein) were also analyzed by SDS-PAGE and WB with the indicated antibodies to examine relative levels of the overexpressed proteins in the transfected cells.

Figure 3 – source data 1

Figure 4 – figure supplement 1. Elevation of *Pax6 α*-enhancer-active GABAergic amacrine cells in *Tgfb1i1*$^{-/-}$ mouse retinas. (A) P14 *Tgfb1i1*$^{+/+}$*;P6α-CreiGFP* and *Tgfb1i1*$^{-/-}$*;P6α-CreiGFP* littermate mouse retinas co-stained with antibodies against amacrine cell subtype markers and GFP. Pax6, pan-amacrine cell marker; ChAT, cholinergic; GlyT1, glycinergic; Gad67, GABAergic; GABA, GABAergic subsets; Bhlhb5, GABAergic subsets (bottom of the INL). Outset images in the bottom row are magnified versions of the dotted box

areas in the top row. Scale bar, 100 μm. ONL, outer nuclear layer; INL, inner nuclear layer; GCL, ganglion cell layer. (**B**) Populations of GFP-positive cells co-expressing amacrine cell subset markers are shown in a graph. Values on the Y-axis are averages. Error bars indicate STD (n=4, 3 litters). *, p<0.05; **, p<0.01.

Figure 4 – figure supplement 2. Deletion of *Lhx3* in the post-natal mouse retina. (A) To delete *Lhx3* in the post-natal mouse retina, we designed two independent sgRNAs complementary to the sequences near the translation initiation site in the exon2 (highlighted in red), following the suggestion of the CRISPR Design server (http://crispr.mit.edu). The sequences were cloned into pX330 (pX330-U6-Chimeric_BB-CBh-hSpCas9) DNA construct, which express the cloned sgRNA and Cas9 endonuclease. **(B)** P14 mouse retinas, which were electroporated with the indicated pX330 DNA constructs at P0, were stained for the detection of various amacrine cell markers, including Pax6 (pan-amacrine), Gad67 (GABAergic), GABA (GABAergic subsets), Bhlhb5 (GABAergic subsets, bottom half of the INL), and GlyT1 (glycinergic), and bipolar cell markers, including Vsx2 (pan-bipolar), G0α (ON bipolar), Vsx1 (OFF bipolar), and Bhlhb5 (type-2 OFF bipolar, top half of the INL), as well as for EGFP, which is expressed from co-electroporated pCAGIG DNA construct. Thus, EGFP-positive retinal cells are expected to express sgRNA and Cas9 from the indicated pX330 DNA constructs. Successful loss of *Lhx3* in the mouse retinas was examined by immunostaing of Lhx3. Scale bar, 100 μm. **(C)** Ratio of marker-positive cells to total INL cells of each sample was then compared with that of pX330+pCAGIG (Mock) sample. **(D)** Population of EGFP-positive cells co-expressing each amacrine or bipolar cell type-specific marker in total EGFP-positive INL cells were obtained and shown in a graph. Scores on the Y-axis of the graphs in C and D are averages (n=6, 2 independent batches). Error bars indicate STD (n=6, 2 independent batches); *, p<0.05; **, p<0.01; ***, p<0.001.

Figure 5 – figure supplement 1. Distribution of Isl1- and Lhx3-expressing cells in *Tgfb1i1*$^{+/+}$ and *Tgfb1i1*$^{-/-}$ mouse retinas. P7 (**A**) and P14 (**B**) *Tgfb1i1*$^{+/+}$ and *Tgfb1i1*$^{-/-}$ littermate mouse retinas stained with a guinea pig anti-Isl1 antibody (green) and a rabbit anti-

Lhx3 antibody (red). Images in the right columns are magnified versions of the dotted areas in the left columns. Scale bars, 100 μm. Isl1(-) (red) and Isl1(+) (yellow) cells among Lhx3(+) cells are shown in the graph in **(C)** and populations expressing each marker in total INL cells are shown in the graph in **(D)**. Y-axis values in the graphs are averages and error bars indicate STD (n=4, 3 independent litters). *, $p<0.05$; **, $p<0.01$.

Figure 5 – figure supplement 2. Ectopic expression of Pax6 isoforms in the post-natal mouse retinas. (A) P14 mouse retinas, which had been electroporated with the indicated DNA constructs at P0, were stained for the detection of various amacrine cell markers, including Syntaxin (pan-amacrine), Gad67 (GABAergic), GABA (GABAergic subsets; results are in Figure 5G), Bhlhb5 (GABAergic subsets, bottom half of the INL), ChAT (cholinergic), and GlyT1 (glycinergic). EGFP cDNA is linked to the *Pax6* cDNAs via IRES, thus those two cDNAs are transcribed in a single mRNA. Thus, the cells expressing EGFP together with the amacrine cell markers can be counted to investigate the effects of overexpressed Pax6 isoforms on retinal cell fate determination. Scale bar, 100 μm. **(B)** The retinas were also stained for the detection of bipolar cell markers Vsx2 (pan-bipolar), G0α (ON bipolar), Vsx1 (OFF bipolar; results are in Figure 5G), Recoverin (type-2 OFF bipolar), and Bhlhb5 (type-2 OFF bipolar, top half of the INL). Scale bar, 100 μm. **(C)** Retinal layer distribution of EGFP-positive cells in the indicated electroporated mouse retinas. **(D)** EGFP-positive cells co-expressing each amacrine or bipolar cell type-specific marker are shown as a percentage of total EGFP-positive INL cells. Scores on the Y-axis in the graphs in (C) and (D) are averages. Error bars indicate STD (n=6, 4 independent batches); *, $p<0.05$; **, $p<0.01$; ***, $p<0.001$.

Figure 6 – figure supplement 1. Impaired response of the *Pax6$^{\Delta PBS}$* *α*-enhancer to Pax6. **(A)** Luciferase expression at downstream of a *Pax6 α*-enhancer mutant lacking its *PBS* (*Pax6-αΔPBS*) was measured by detecting chemiluminescence emitted from the lysates of HEK293T cells combinatorially expressing Pax6, Lhx3, Isl1, and Tgfb1i1 (n=4). Bindings of Pax6, Isl1, Lhx3, and Tgfb1i1 to the *Pax6 α*-enhancer sequence in P30 *Pax6$^{+/+}$* and *Pax6$^{\Delta PBS/\Delta PBS}$* mouse retinas were assessed by qPCR **(B**, n=4**)** and PCR **(C)** amplification of

DNA fragments isolated by ChIP with a rabbit IgG recognizing each respective protein. Error bars indicate STD; ***, p<0.001.

Figure 6 – figure supplement 2. Distribution of amacrine and bipolar cell subsets in *Pax6*$^{+/+}$ and *Pax6*$^{\Delta PBS/\Delta PBS}$ mouse retina. P14 *Pax6*$^{+/+}$ and *Pax6*$^{\Delta PBS/\Delta PBS}$ littermate retinas co-stained with amacrine cell and bipolar cell subtype marker-specific antibodies. Gad67, GABAergic amacrine cells; ChAT, cholinergic amacrine cells; GlyT1, glycinergic amacrine cells; PKCα, rod bipolar cells; Bhlhb5, OFF bipolar cells and GABAergic amacrine cells. Scale bar, 100 μm. Quantification results are shown in Figure 6F.

Figure 6 – figure supplement 3. Fate determination of GABAergic amacrine cells and OFF bipolar cells in the post-natal mouse retinas. (A) The effects of deletions of *Tgfb1i1* (*Tgfb1i1*$^{-/-}$) and *PBS* sequence of *Pax6 α*-enhancer (*Pax6*$^{\Delta PBS/\Delta PBS}$) on GABAergic amacrine cell development were investigated by immunostaining of various GABAergic amacrine cell markers, including Gad67, GABA, and Bhlhb5. Distribution of entire amacrine cells was examined by immunostaining of pan-amacrine cell marker Syntaxin. The effects of the gene deletions on *Pax6 α*-enhancer activity was also determined by detecting cells expressing Pax6 α-GFP. Scale bars, 100 μm (top) and 50 μm (rest). **(B)** Relative numbers of marker-positive cells in P4 *Tgfb1i1*$^{-/-}$ and *Pax6*$^{\Delta PBS/\Delta PBS}$ mouse retinas are determined by comparing with those in their WT littermate mice. Error bars denote STD (n=4, 2 independent litters). *, p < 0.05. **(C)** To identify the fate of cells were born in WT, *Tgfb1i1*$^{-/-}$, and *Pax6*$^{\Delta PBS/\Delta PBS}$ between post-natal day 4 and 7 (P4 and P7) when bipolar cells and Müller glia are predominantly generated, the mice were repeatedly injected with BrdU (5 mg/kg) at P4, P5, and P6. Eye sections of the BrdU-injected mice were obtained at P14 for the immunodetection of Bhlhb5-positive GABAergic amacrine cells and Vsx1-positive OFF bipolar cells, which had exited cell cycle after incorporating BrdU between P4 and P7. Scale bar, 50 μm. **(D)** To trace the fates of cells produced in the embryonic retina when amacrine cells are generated, pregnant mice were injected with BrdU (5 mg/kg) at 15 dpc (E15) and the identities of cells had exited cell cycle after incorporating BrdU were examined at P7. Scale bar, 50 μm. **(E** and **F)** BrdU-

labeled cell population in Bhlhb5-positive GABAergic amacrine cells, which locate the bottom half of INL, and that in Vsx1-positive OFF bipolar cell population in P14 mouse retinas as (C) and P7 mouse retina as (D) are quantified. Values in the Y-axis are average and error bars denote STD (n=4, 2 independent litters). *, $p < 0.05$.

Figure 7 – figure supplement 1. ERGs of mouse retinas. P60 WT, *Tgfb1i1*$^{-/-}$, and *Pax6*$^{\Delta PBS/\Delta PBS}$ mice were dark-adapted for 16 hours. Then, their scotopic ERG responses were assessed at a light intensity of 2.5 cds (left). Average amplitudes of scotopic ERG a-waves and b-waves measured from WT (white bars, n=8), *Tgfb1i1*$^{-/-}$ (gray bars, n=6), and *Pax6*$^{\Delta PBS/\Delta PBS}$ (black bars, n=4) eyes. Photopic (center) and flicker (right) ERG responses of these mice were also measured after adaptation under room light (30 cd/m^2).

Figure 7 – figure supplement 2. Cell composition of P60 WT, *Tgfb1i1*$^{-/-}$, and *Pax6*$^{\Delta PBS/\Delta PBS}$ mouse retinas. (A) Composition of P60 WT, *Tgfb1i1*$^{-/-}$, and *Pax6*$^{\Delta PBS/\Delta PBS}$ mouse retinas were determined by examining cell type-specific markers. Rhodopsin, rod photoreceptors; M-opsin, M-cone photoreceptors; Calbindin, horizontal cells (HZ; arrowheads); Vsx2, bipolar cells (BP); Sox2, Müller glia (MG; arrowheads); Pax6, amacrine cells (AC); Brn3b, retinal ganglion cells (RGCs); glial fibrillary acidic protein (Gfap), astrocytes (AS). Scale bar, 100 μm. **(B)** Relative numbers of marker-positive cells in P60 *Tgfb1i1*$^{-/-}$ and *Pax6*$^{\Delta PBS/\Delta PBS}$ mouse retinas were determined by comparing with those in their WT littermate mice. Error bars denote STD (n=4, 2 independent litters). *, $p<0.05$; **, $p<0.01$. **(C)** Distribution of amacrine cell subtypes in P60 WT, *Tgfb1i1*$^{-/-}$, and *Pax6*$^{\Delta PBS/\Delta PBS}$ mice were determined by examining cell type-specific markers. ChAT, cholinergic; GlyT1, glycinergic; Gad67 and Bhlhb5 (AC in the bottom half of INL), GABAergic. Scale bar, 100 μm. **(D)** Relative numbers of marker-positive cells in P60 *Tgfb1i1*$^{-/-}$ and *Pax6*$^{\Delta PBS/\Delta PBS}$ mouse retinas were determined by comparing with those in their WT littermate mice. Error bars denote STD (n=4, 2 independent litters). **, $p<0.01$; ***, $p<0.001$. **(E)** Distribution of bipolar cell subtypes in P60 WT, *Tgfb1i1*$^{-/-}$, and *Pax6*$^{\Delta PBS/\Delta PBS}$ mice were determined by examining cell type-specific markers. PKCα, rod bipolar cell; Vsx1 and Bhlhb5 (BP in the top of INL in (C)), OFF

bipolar cells. Scale bar, 100 μm. **(F)** Relative numbers of marker-positive cells in P60 *Tgfb1i1*$^{-/-}$ and *Pax6*$^{\Delta PBS/\Delta PBS}$ mouse retinas were determined by comparing with those in their WT littermate mice. Error bars denote STD (n=4, 2 independent litters). *, $p<0.05$; **, $p<0.01$; ***, $p<0.001$.

Figure 7 – figure supplement 3. Experimental scheme assessing mouse visual responses. (A) P60 mice were trained to associate water rewards with flashing light stimuli. Correct and incorrect lick rates were used to measure visual detection. **(B)** Lick rates during the learning period for mice responding to various intensity of light as shown in Figure 4E. **(C)** P60 mice were trained to associate water rewards only with a continuous (2 s) light stimulus and not a continuous (1 s) light followed by a drifting grate image (1 s). Correct and incorrect lick rates were used to measure visual discrimination of the drifting grate from various intensities of light stimulus. **(D)** Lick rates during the learning period.

Kim et al._Table 1

Table 1. Antibody used in this study

Antigen	Species	Producer	Dilution
Bhlhb5	Goat	Santa Cruz	1:100
Brn3b	Goat	Santa Cruz	1:200
Calbindin	Mouse	Sigma	1:200
Calretinin	Mouse	Millipore	1:1,000
ChAT	Goat	Millipore	1:200
Isl1	Rabbit	gift from Dr. Mi-Ryoung Song	1:500
Isl1	Guinea Pig	gift from Dr. Mi-Ryoung Song	1:10,000
Gad67	Mouse	Millipore	1:500
GABA	Guinea Pig	Millipore	1:300
GFAP	Rabbit	Abcam	1:500
GFP	Chick	Abcam	1:200
GFP	Rabbit	Santa Cruz	1:500
GlyT1	Rabbit	Abcam	1:200
G0alpha	Mouse	Millipore	1:300
G/R opsin	Rabbit	Millipore	1:200
Lhx2	Goat	Santa Cruz	1:200
Lhx3	Rabbit	Abcam	1:1000
Lhx9	Rabbit	Santa Cruz	1:500
Pax6	Rabbit	Abcam	1:200
Pax6	Rabbit	Covance	1:300
PKCalpha	Mouse	Sigma	1:200
Recoverin	Rabbit	Chemicon	1:200
Rhodopsin	Mouse	Millipore	1:500
Sox2	Goat	Santa Cruz	1:100
Sox9	Rabbit	Santa Cruz	1:200
Tgfb1i1(Hic-5)	Mouse	BD	1:100
Tgfb1i1(Hic-5)	Rabbit	Abcam	1:100
Vsx1	Goat	Santa Cruz	1:50
Vsx2(Chx10)	Mouse	Santa Cruz	1:200
V5	Mouse	Genway Biotech	1:1,000

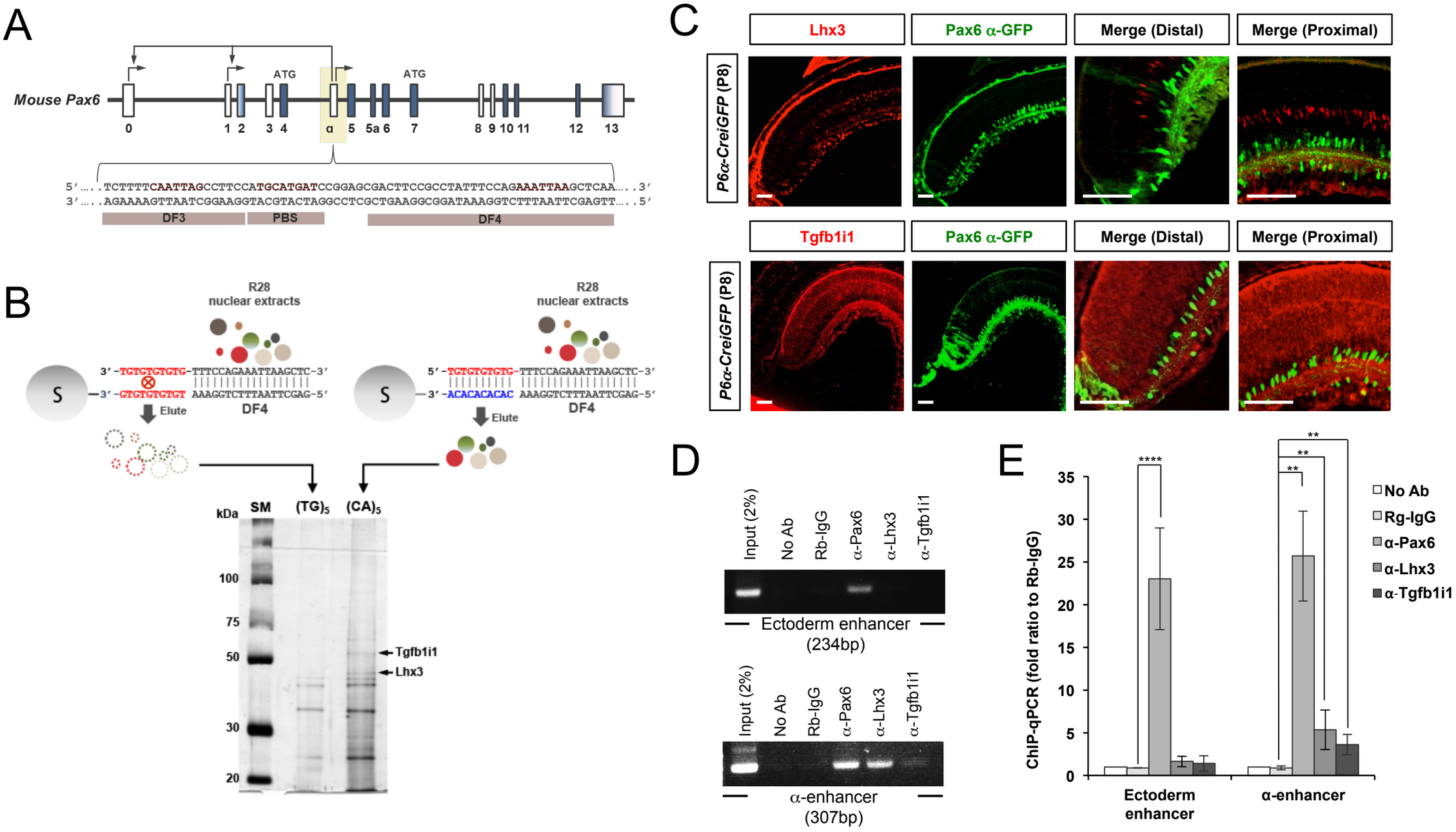
A
Mouse Pax6
ATG
ATG
0
1 2
3 4
α
5
5a 6
7
8 9 10 11
12
13
5′…..TCTTTTCAATTAGCCTTCCATGCATGATCCGGAGCGACTTCCGCCTATTTCCAGAAATTAAGCTCAA…..3′
3′…..AGAAAAGTTAATCGGAAGGTACGTACTAGGCCTCGCTGAAGGCGGATAAAGGTCTTTAATTCGAGTT…..5′
DF3
PBS
DF4
B
R28
nuclear extracts
S
3′-TGTGTGTGTG-TTTCCAGAAATTAAGCTC-3′
3′-GTGTGTGTGT AAAGGTCTTTAATTCGAG-5′
Elute
DF4
R28
nuclear extracts
S
5′-TGTGTGTGTG-TTTCCAGAAATTAAGCTC-3′
3′-ACACACACAC AAAGGTCTTTAATTCGAG-5′
Elute
DF4
kDa
SM
(TG)5
(CA)5
100
75
50
30
20
Tgfb1i1
Lhx3
C
Lhx3
Pax6 α-GFP
Merge (Distal)
Merge (Proximal)
P6α-CreiGFP (P8)
Tgfb1i1
Pax6 α-GFP
Merge (Distal)
Merge (Proximal)
P6α-CreiGFP (P8)
D
Input (2%)
No Ab
Rb-IgG
α-Pax6
α-Lhx3
α-Tgfb1i1
Ectoderm enhancer
(234bp)
Input (2%)
No Ab
Rb-IgG
α-Pax6
α-Lhx3
α-Tgfb1i1
α-enhancer
(307bp)
E
ChIP-qPCR (fold ratio to Rb-IgG)
35
30
25
20
15
10
5
0
****
**
**
**
No Ab
Rg-IgG
α-Pax6
α-Lhx3
α-Tgfb1i1
Ectoderm enhancer
α-enhancer

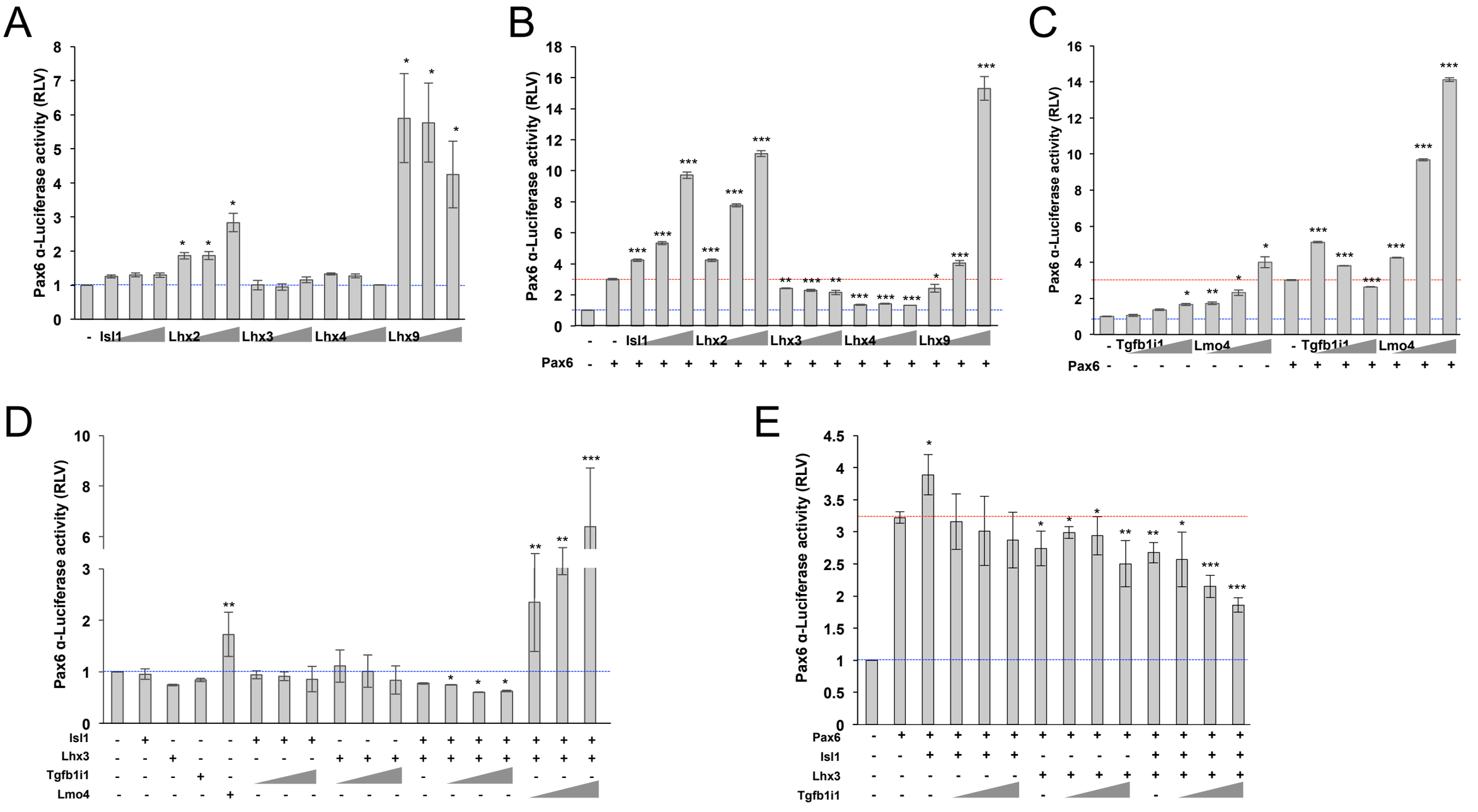
A
Pax6 α-Luciferase activity (RLV)
- Isl1 Lhx2 Lhx3 Lhx4 Lhx9
B
Pax6 α-Luciferase activity (RLV)
- - Isl1 Lhx2 Lhx3 Lhx4 Lhx9
Pax6
C
Pax6 α-Luciferase activity (RLV)
- Tgfb1i1 Lmo4 - Tgfb1i1 Lmo4
Pax6
D
Pax6 α-Luciferase activity (RLV)
Isl1
Lhx3
Tgfb1i1
Lmo4
E
Pax6 α-Luciferase activity (RLV)
Pax6
Isl1
Lhx3
Tgfb1i1

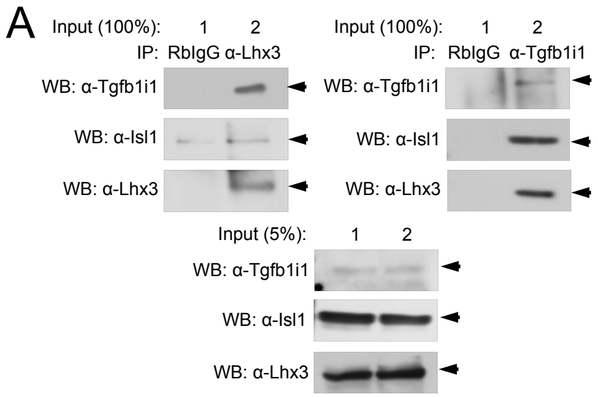
A
Input (100%): 1 2
IP: RbIgG α-Lhx3
WB: α-Tgfb1i1
WB: α-Isl1
WB: α-Lhx3
Input (100%): 1 2
IP: RbIgG α-Tgfb1i1
WB: α-Tgfb1i1
WB: α-Isl1
WB: α-Lhx3
Input (5%): 1 2
WB: α-Tgfb1i1
WB: α-Isl1
WB: α-Lhx3

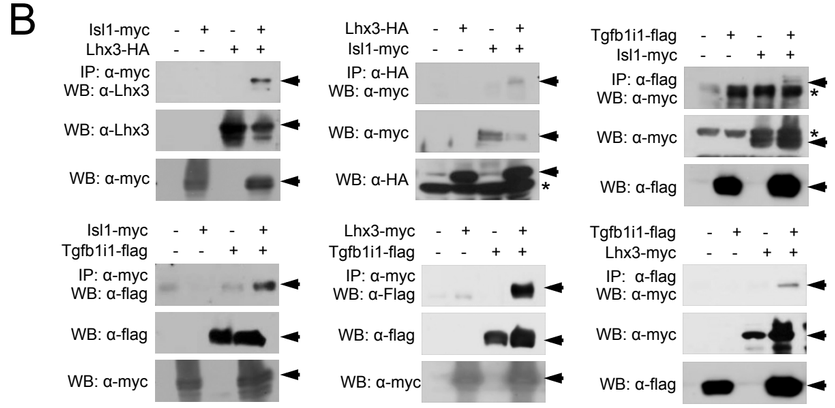
B
Isl1-myc
Lhx3-HA
IP: α-myc
WB: α-Lhx3
WB: α-Lhx3
WB: α-myc
Lhx3-HA
Isl1-myc
IP: α-HA
WB: α-myc
WB: α-myc
WB: α-HA
Tgfb1i1-flag
Isl1-myc
IP: α-flag
WB: α-myc
WB: α-myc
WB: α-flag
Isl1-myc
Tgfb1i1-flag
IP: α-myc
WB: α-flag
WB: α-flag
WB: α-myc
Lhx3-myc
Tgfb1i1-flag
IP: α-myc
WB: α-Flag
WB: α-flag
WB: α-myc
Tgfb1i1-flag
Lhx3-myc
IP: α-flag
WB: α-myc
WB: α-myc
WB: α-flag

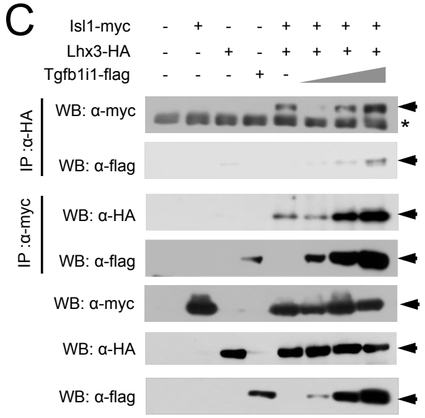
C
Isl1-myc
Lhx3-HA
Tgfb1i1-flag
IP :α-HA
WB: α-myc
WB: α-flag
IP :α-myc
WB: α-HA
WB: α-flag
WB: α-myc
WB: α-HA
WB: α-flag

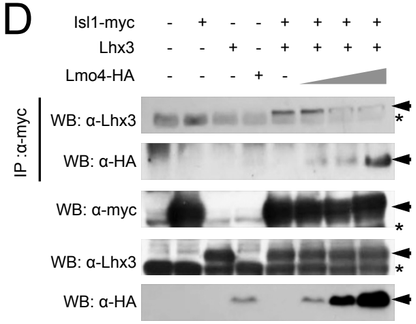
D
Isl1-myc
Lhx3
Lmo4-HA
IP :α-myc
WB: α-Lhx3
WB: α-HA
WB: α-myc
WB: α-Lhx3
WB: α-HA

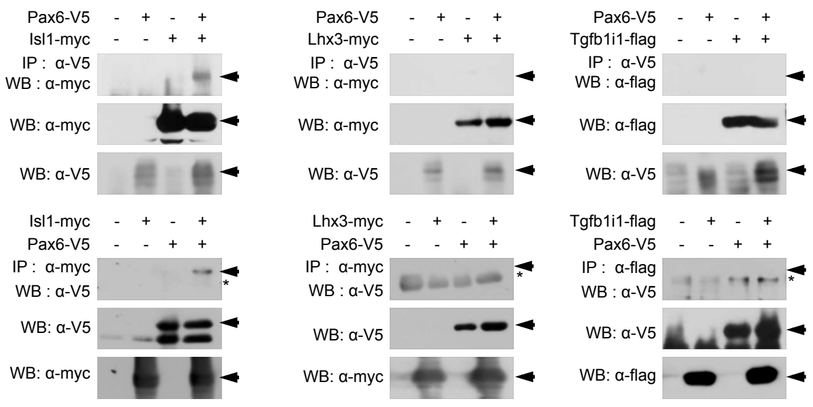
E
Pax6-V5
Isl1-myc
IP : α-V5
WB : α-myc
WB: α-myc
WB: α-V5
Isl1-myc
Pax6-V5
IP : α-myc
WB : α-V5
WB: α-V5
WB: α-myc
Pax6-V5
Lhx3-myc
IP : α-V5
WB : α-myc
WB: α-myc
WB: α-V5
Lhx3-myc
Pax6-V5
IP : α-myc
WB : α-V5
WB: α-V5
WB: α-myc
Pax6-V5
Tgfb1i1-flag
IP : α-V5
WB : α-flag
WB: α-flag
WB: α-V5
Tgfb1i1-flag
Pax6-V5
IP : α-flag
WB : α-V5
WB: α-V5
WB: α-flag

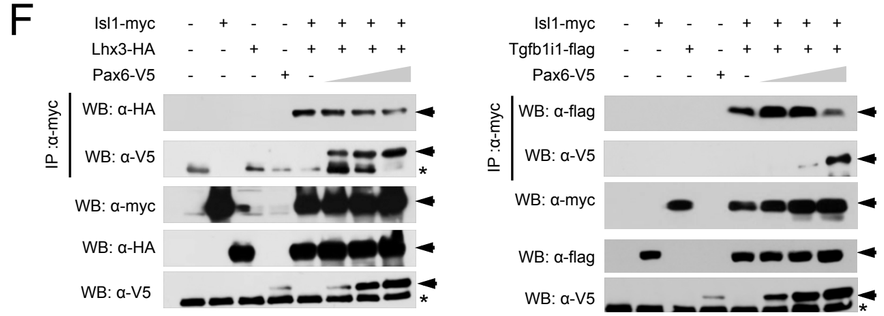
F
Isl1-myc
Lhx3-HA
Pax6-V5
IP :α-myc
WB: α-HA
WB: α-V5
WB: α-myc
WB: α-HA
WB: α-V5
Isl1-myc
Tgfb1i1-flag
Pax6-V5
IP :α-myc
WB: α-flag
WB: α-V5
WB: α-myc
WB: α-flag
WB: α-V5

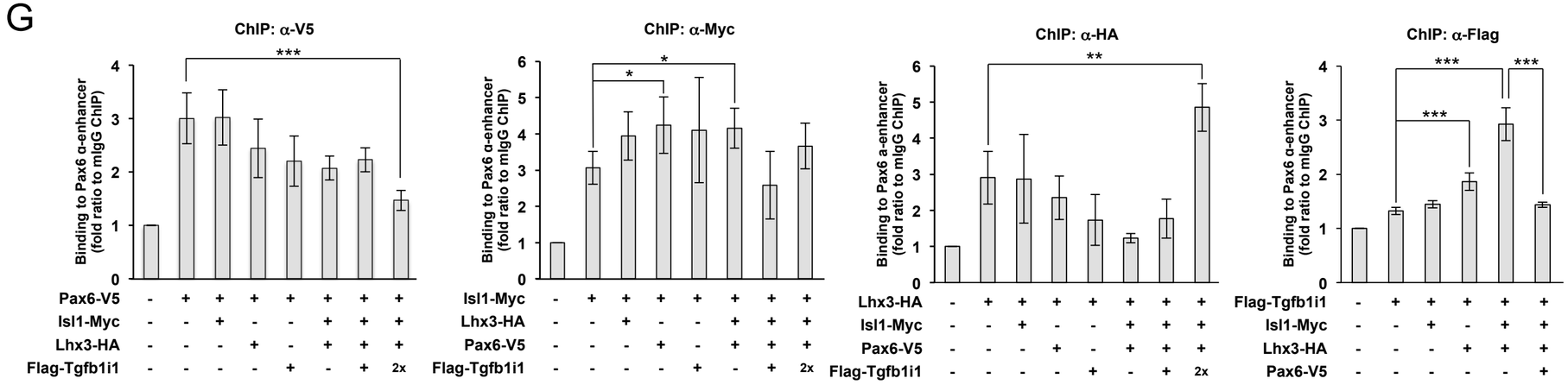
G
ChIP: α-V5
Binding to Pax6 α-enhancer (fold ratio to migG ChIP)
***
Pax6-V5
Isl1-Myc
Lhx3-HA
Flag-Tgfb1i1
ChIP: α-Myc
*
*
Isl1-Myc
Lhx3-HA
Pax6-V5
Flag-Tgfb1i1
ChIP: α-HA
**
Lhx3-HA
Isl1-Myc
Pax6-V5
Flag-Tgfb1i1
ChIP: α-Flag
***
***
***
Flag-Tgfb1i1
Isl1-Myc
Lhx3-HA
Pax6-V5

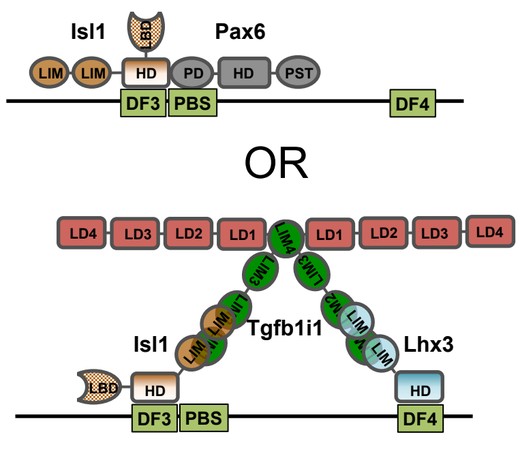
H
Isl1
Pax6
LIM
LIM
HD
PD
HD
PST
DF3
PBS
DF4
OR
LD4
LD3
LD2
LD1
LIM4
LD1
LD2
LD3
LD4
Isl1
Tgfb1i1
Lhx3
LBD
HD
DF3
PBS
HD
DF4

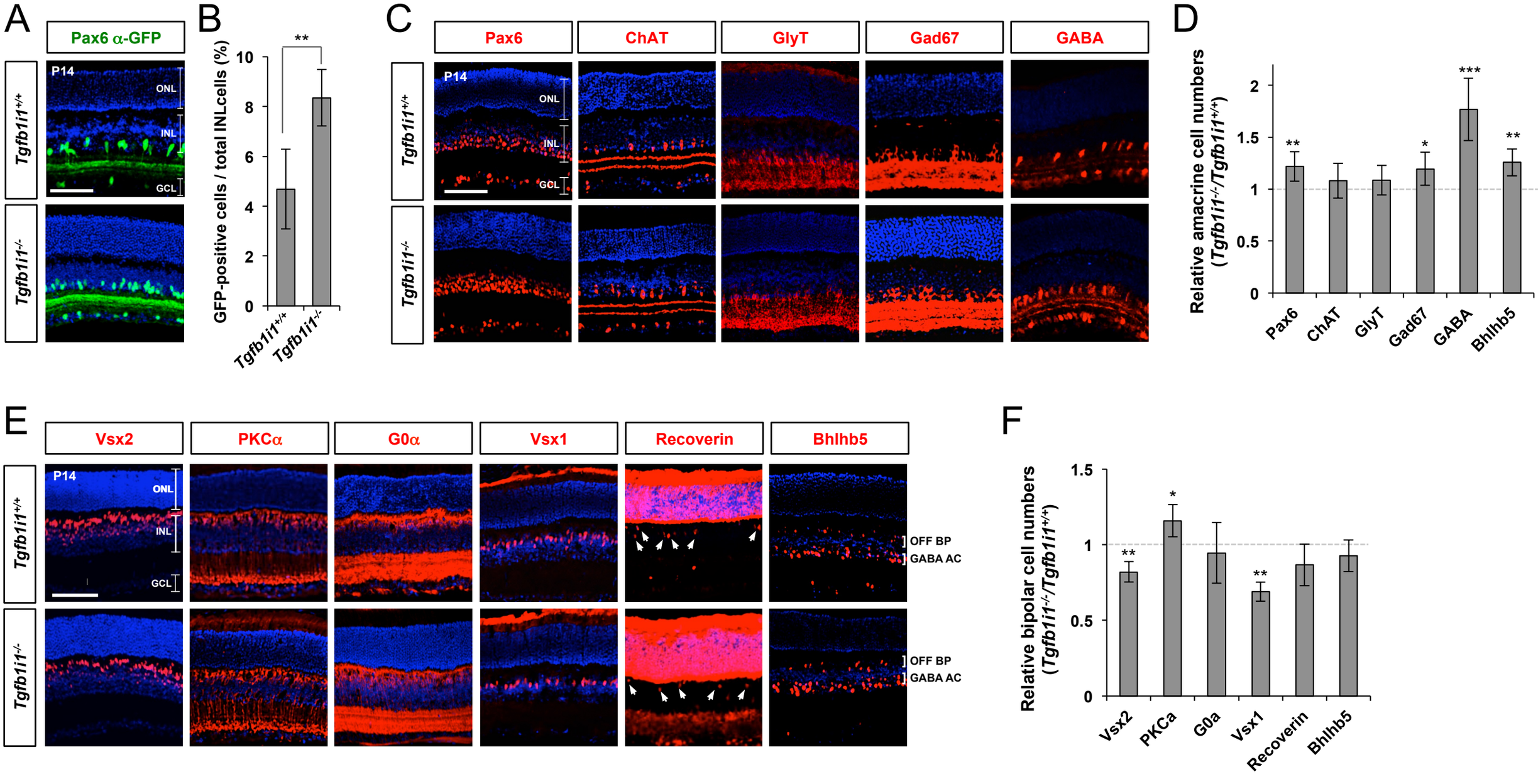
A
Pax6 α-GFP
Tgfb1i1+/+
Tgfb1i1-/-
P14
ONL
INL
GCL
B
GFP-positive cells / total INLcells (%)
**
Tgfb1i1+/+
Tgfb1i1-/-
C
Pax6
ChAT
GlyT
Gad67
GABA
D
Relative amacrine cell numbers
(Tgfb1i1-/-/Tgfb1i1+/+)
Pax6
ChAT
GlyT
Gad67
GABA
Bhlhb5
E
Vsx2
PKCα
G0α
Vsx1
Recoverin
Bhlhb5
OFF BP
GABA AC
F
Relative bipolar cell numbers
(Tgfb1i1-/-/Tgfb1i1+/+)
Vsx2
PKCa
G0a
Vsx1
Recoverin
Bhlhb5

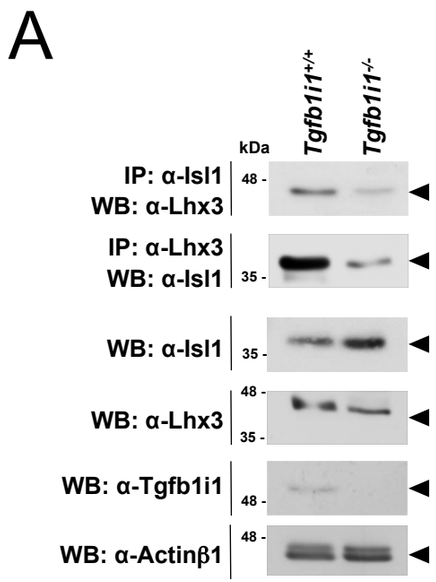
A
Tgfb1i1+/+
Tgfb1i1-/-
kDa
IP: α-Isl1
WB: α-Lhx3
IP: α-Lhx3
WB: α-Isl1
WB: α-Isl1
WB: α-Lhx3
WB: α-Tgfb1i1
WB: α-Actinβ1
48
35

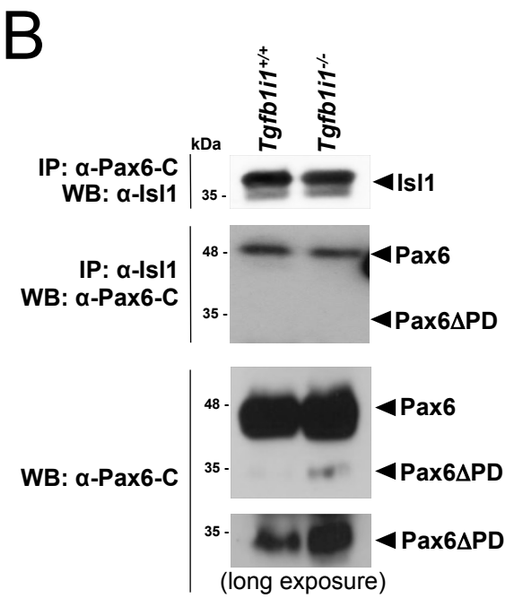
B
Tgfb1i1+/+
Tgfb1i1-/-
kDa
IP: α-Pax6-C
WB: α-Isl1
Isl1
IP: α-Isl1
WB: α-Pax6-C
Pax6
Pax6ΔPD
WB: α-Pax6-C
Pax6
Pax6ΔPD
Pax6ΔPD
(long exposure)

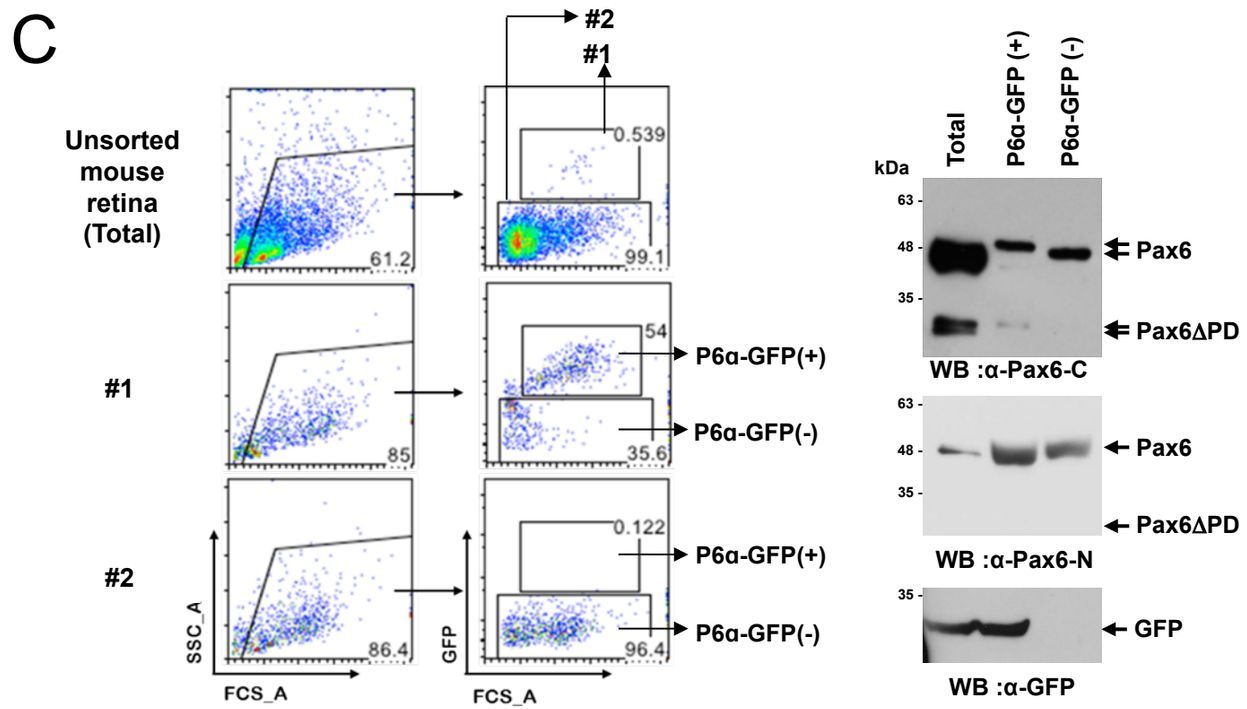
C
Unsorted mouse retina (Total)
#1
#2
61.2
0.539
99.1
85
54
35.6
86.4
0.122
96.4
P6α-GFP(+)
P6α-GFP(-)
SSC_A
FCS_A
GFP
Total
P6α-GFP (+)
P6α-GFP (-)
kDa
63
48
35
Pax6
Pax6ΔPD
WB :α-Pax6-C
WB :α-Pax6-N
GFP
WB :α-GFP

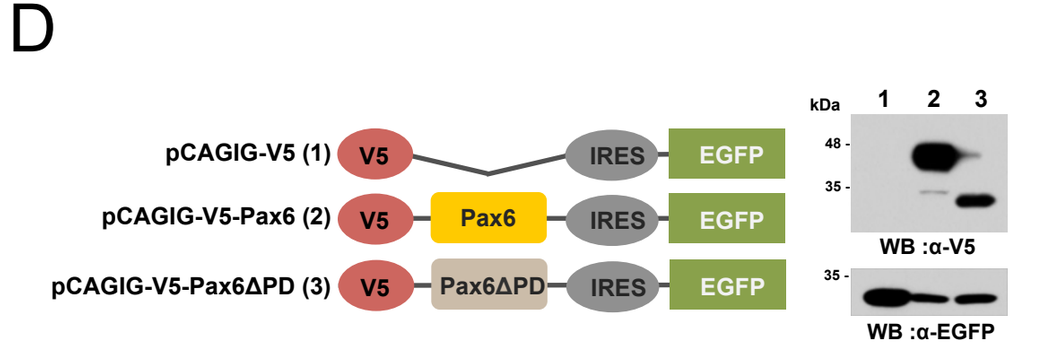
D
pCAGIG-V5 (1)
pCAGIG-V5-Pax6 (2)
pCAGIG-V5-Pax6ΔPD (3)
V5
Pax6
Pax6ΔPD
IRES
EGFP
kDa
1
2
3
48
35
WB :α-V5
WB :α-EGFP

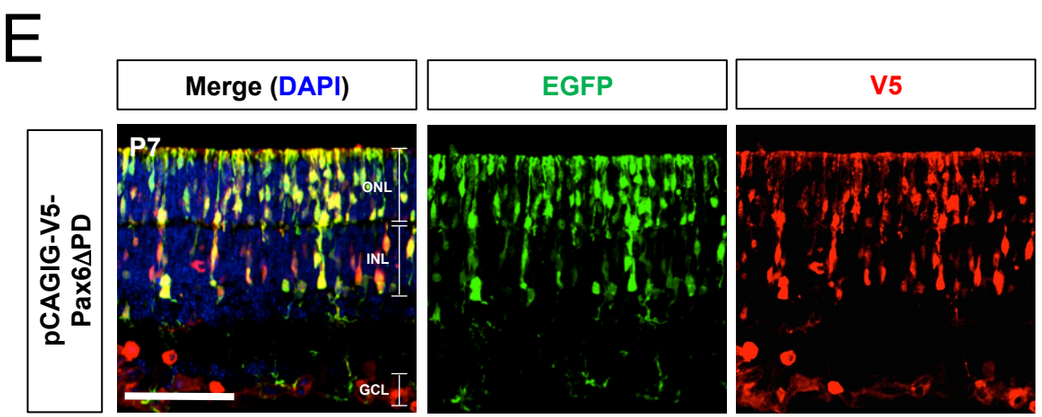
E
Merge (DAPI)
EGFP
V5
pCAGIG-V5-Pax6ΔPD
P7
ONL
INL
GCL

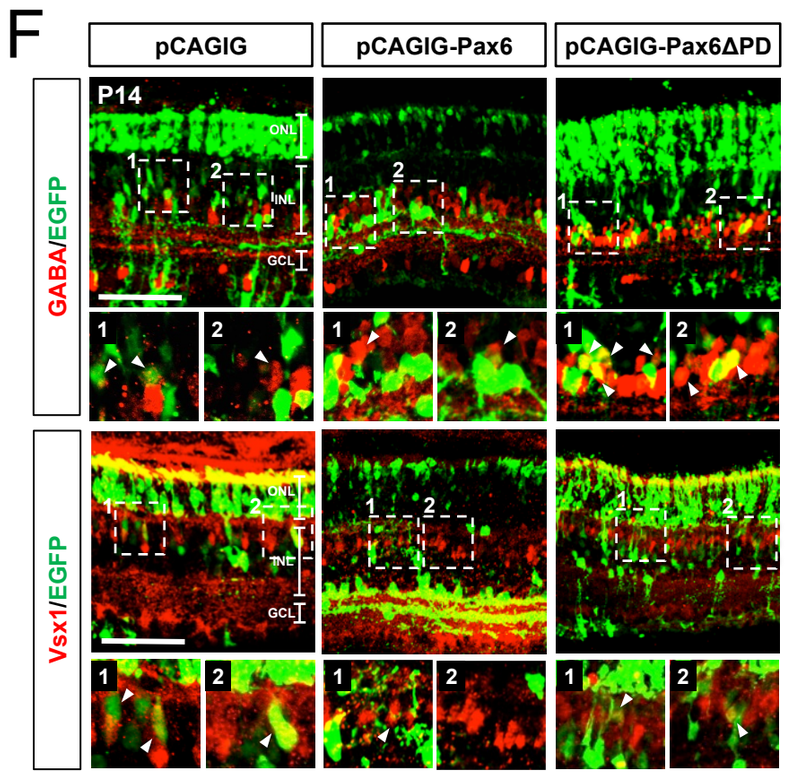
F
pCAGIG
pCAGIG-Pax6
pCAGIG-Pax6ΔPD
GABA/EGFP
Vsx1/EGFP
P14
ONL
INL
GCL
1
2

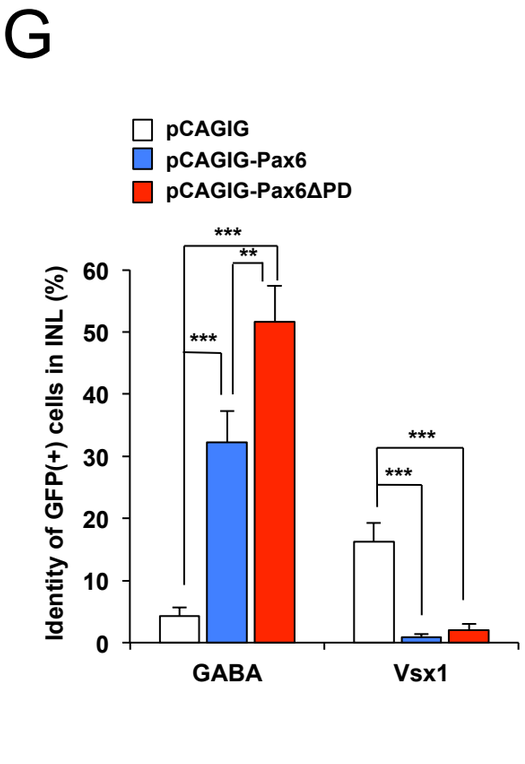
G
pCAGIG
pCAGIG-Pax6
pCAGIG-Pax6ΔPD
Identity of GFP(+) cells in INL (%)
60
50
40
30
20
10
0
***
**
GABA
Vsx1

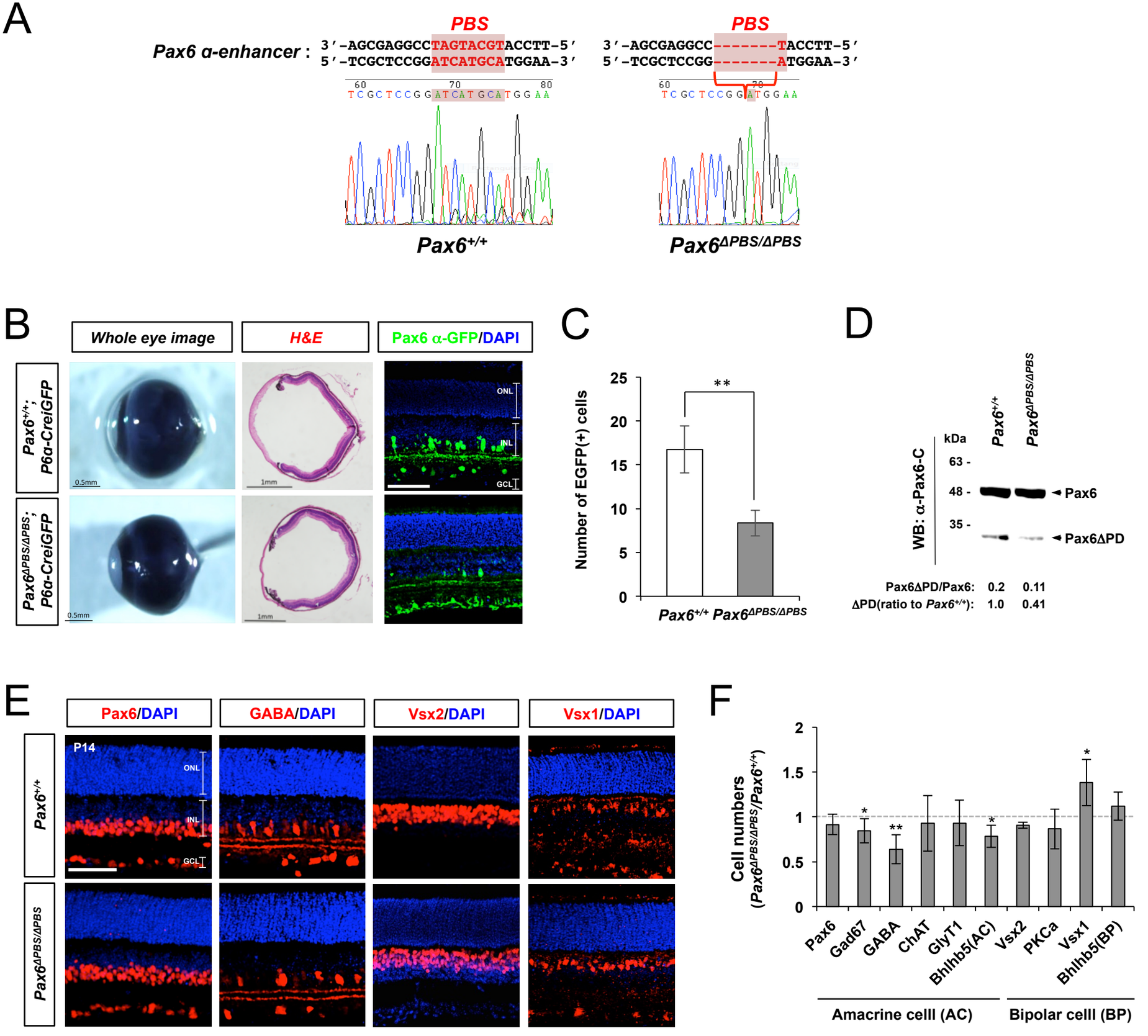
A
PBS
Pax6 α-enhancer :
3′-AGCGAGGCCTAGTACGTACCTT-5′
5′-TCGCTCCGGATCATGCATGGAA-3′
3′-AGCGAGGCC-------TACCTT-5′
5′-TCGCTCCGG-------ATGGAA-3′
Pax6+/+
Pax6ΔPBS/ΔPBS
B
Whole eye image
H&E
Pax6 α-GFP/DAPI
Pax6+/+; P6α-CreiGFP
Pax6ΔPBS/ΔPBS; P6α-CreiGFP
ONL
INL
GCL
C
Number of EGFP(+) cells
Pax6+/+ Pax6ΔPBS/ΔPBS
D
WB: α-Pax6-C
kDa
Pax6
Pax6ΔPD
Pax6ΔPD/Pax6: 0.2 0.11
ΔPD(ratio to Pax6+/+): 1.0 0.41
E
Pax6/DAPI
GABA/DAPI
Vsx2/DAPI
Vsx1/DAPI
P14
F
Cell numbers (Pax6ΔPBS/ΔPBS/Pax6+/+)
Pax6
Gad67
GABA
ChAT
GlyT1
Bhlhb5(AC)
Vsx2
PKCa
Vsx1
Bhlhb5(BP)
Amacrine cellI (AC)
Bipolar cellI (BP)

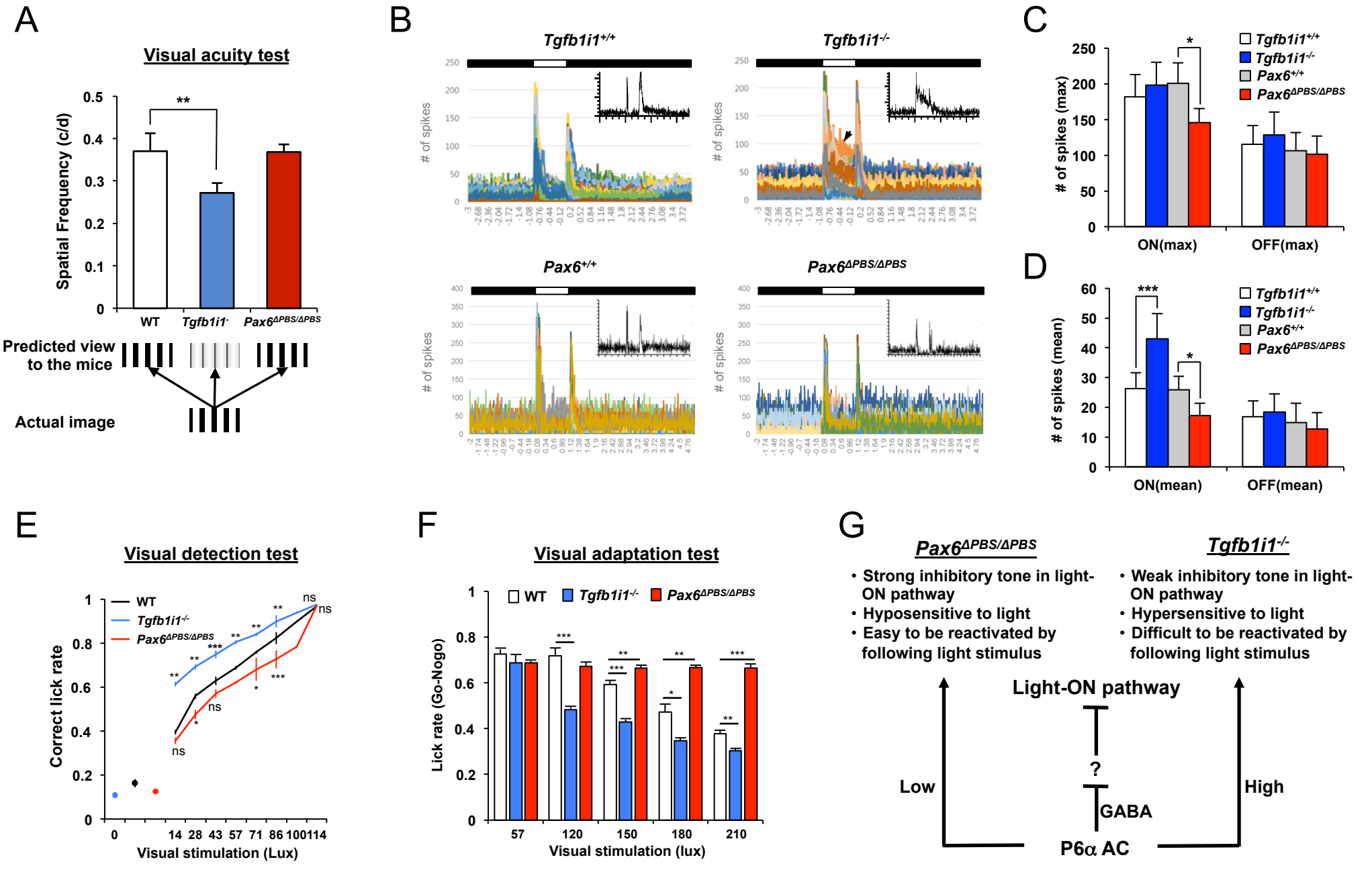
A
Visual acuity test
Spatial Frequency (c/d)
WT
Tgfb1i1-
Pax6ΔPBS/ΔPBS
Predicted view to the mice
Actual image
B
Tgfb1i1+/+
Tgfb1i1-/-
Pax6+/+
Pax6ΔPBS/ΔPBS
# of spikes
C
# of spikes (max)
ON(max)
OFF(max)
D
# of spikes (mean)
ON(mean)
OFF(mean)
E
Visual detection test
Correct lick rate
Visual stimulation (Lux)
F
Visual adaptation test
Lick rate (Go-Nogo)
Visual stimulation (lux)
G
Pax6ΔPBS/ΔPBS
• Strong inhibitory tone in light-ON pathway
• Hyposensitive to light
• Easy to be reactivated by following light stimulus
Tgfb1i1-/-
• Weak inhibitory tone in light-ON pathway
• Hypersensitive to light
• Difficult to be reactivated by following light stimulus
Light-ON pathway
Low
High
?
GABA
P6α AC

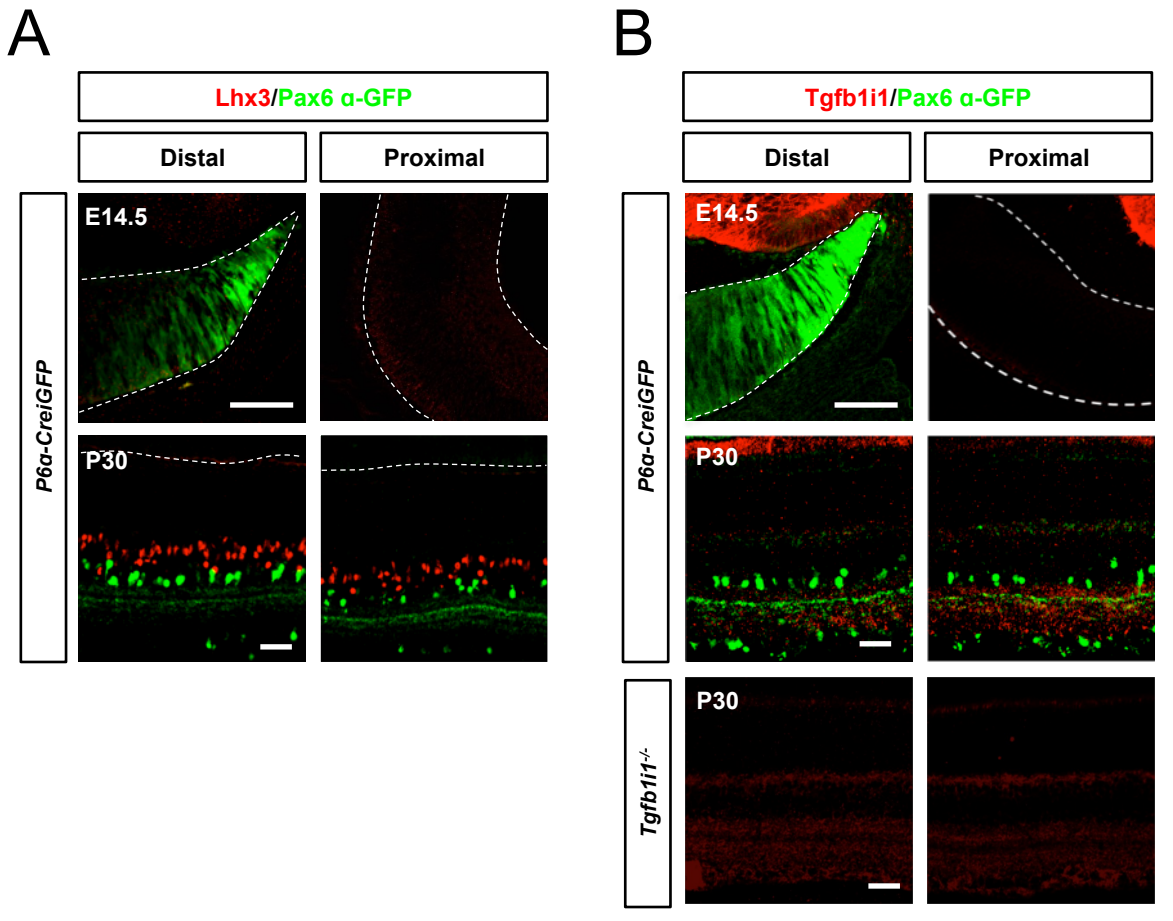
A
Lhx3/Pax6 α-GFP
Distal
Proximal
E14.5
P30
P6α-CreiGFP
B
Tgfb1i1/Pax6 α-GFP
Distal
Proximal
E14.5
P30
P6α-CreiGFP
P30
Tgfb1i1-/-

Kim et al._Fig1_figure supplement 2

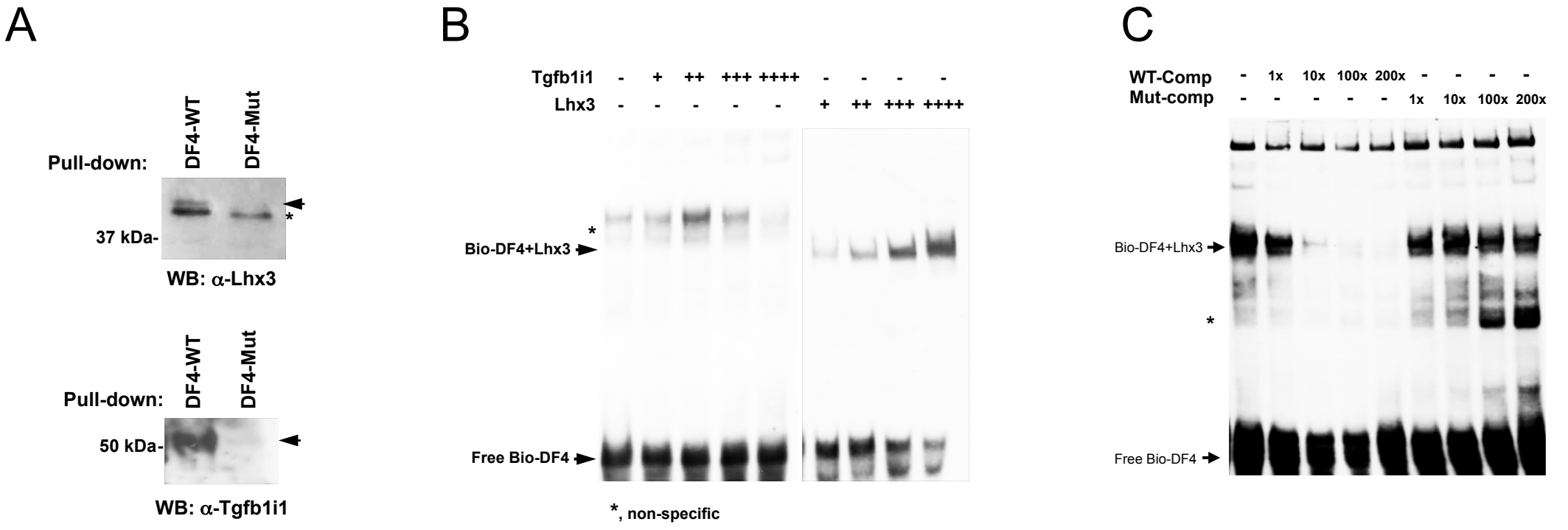

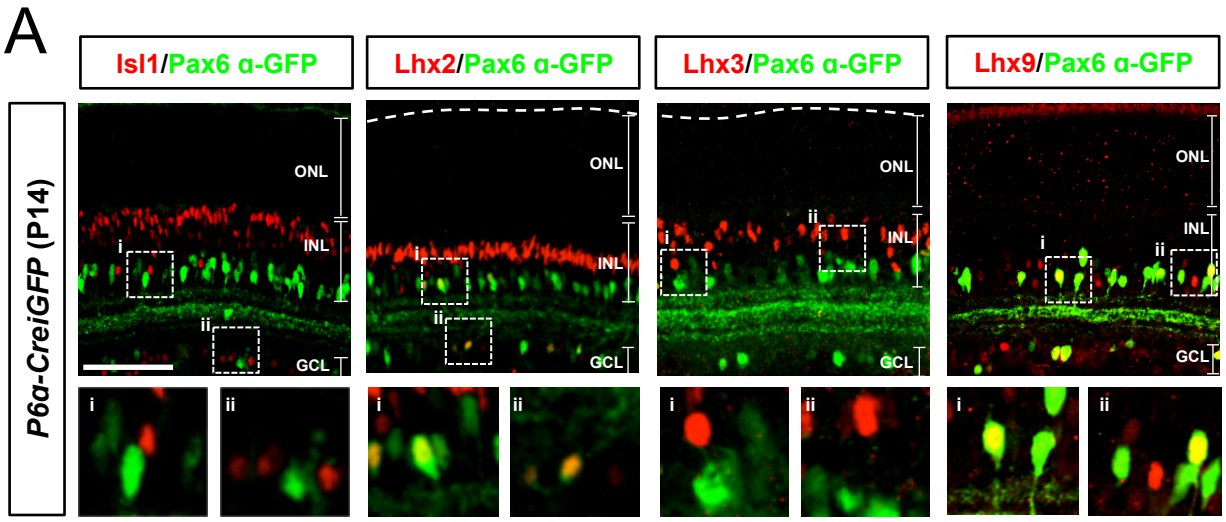
A
Isl1/Pax6 α-GFP
Lhx2/Pax6 α-GFP
Lhx3/Pax6 α-GFP
Lhx9/Pax6 α-GFP
P6α-CreiGFP (P14)
ONL
INL
GCL
i
ii

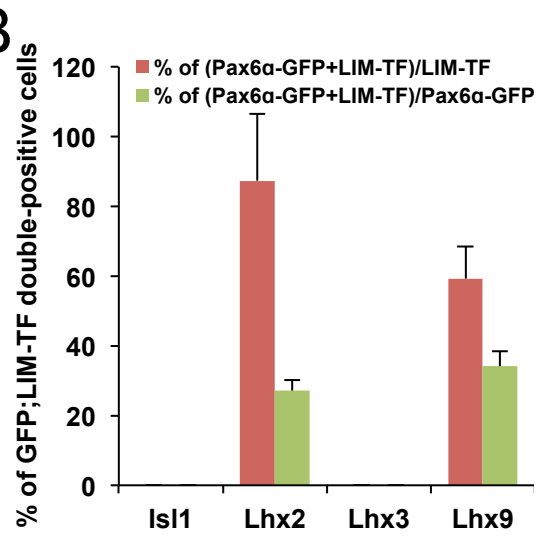
B
% of (Pax6α-GFP+LIM-TF)/LIM-TF
% of (Pax6α-GFP+LIM-TF)/Pax6α-GFP
% of GFP;LIM-TF double-positive cells
120
100
80
60
40
20
0
Isl1
Lhx2
Lhx3
Lhx9

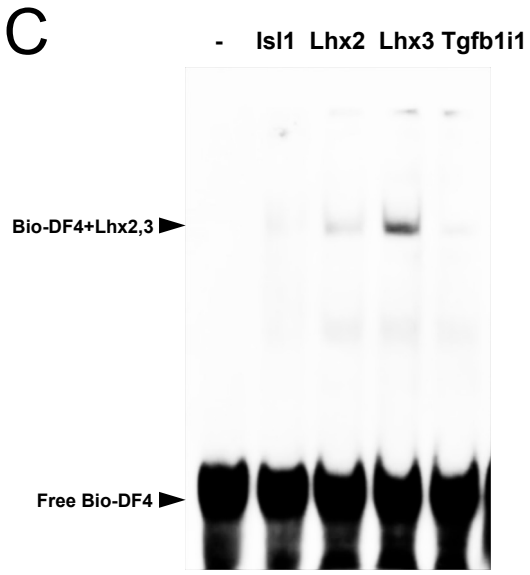
C
- Isl1 Lhx2 Lhx3 Tgfb1i1
Bio-DF4+Lhx2,3
Free Bio-DF4

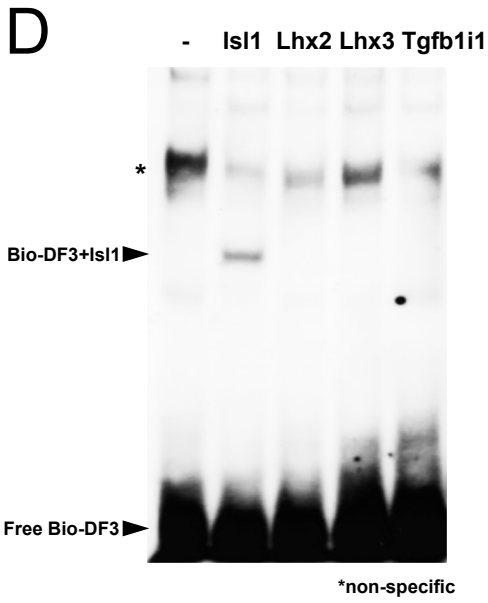
D
- Isl1 Lhx2 Lhx3 Tgfb1i1
*
Bio-DF3+Isl1
Free Bio-DF3
*non-specific

A

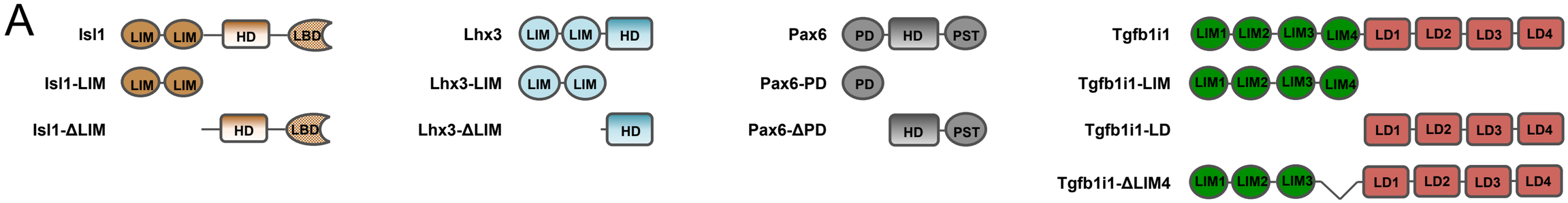
Isl1
LIM
LIM
HD
LBD
Isl1-LIM
Isl1-ΔLIM
Lhx3
Lhx3-LIM
Lhx3-ΔLIM
Pax6
PD
PST
Pax6-PD
Pax6-ΔPD
Tgfb1i1
LIM1
LIM2
LIM3
LIM4
LD1
LD2
LD3
LD4
Tgfb1i1-LIM
Tgfb1i1-LD
Tgfb1i1-ΔLIM4

B

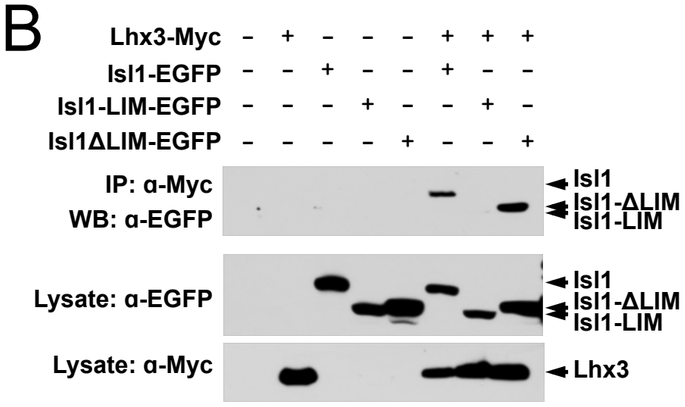
Lhx3-Myc
Isl1-EGFP
Isl1-LIM-EGFP
Isl1ΔLIM-EGFP
IP: α-Myc
WB: α-EGFP
Isl1
Isl1-ΔLIM
Isl1-LIM
Lysate: α-EGFP
Lysate: α-Myc
Lhx3

C

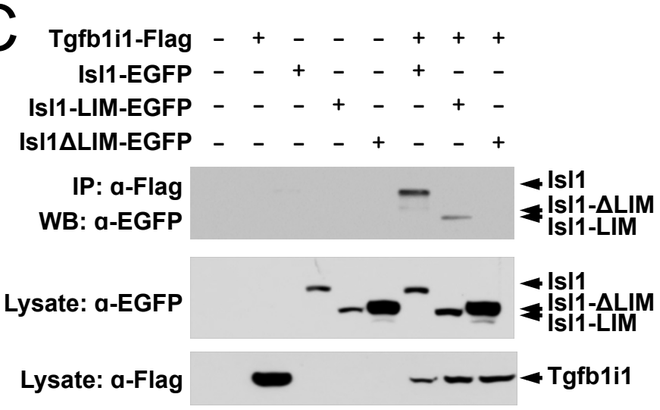
Tgfb1i1-Flag
Isl1-EGFP
Isl1-LIM-EGFP
Isl1ΔLIM-EGFP
IP: α-Flag
WB: α-EGFP
Isl1
Isl1-ΔLIM
Isl1-LIM
Lysate: α-EGFP
Lysate: α-Flag
Tgfb1i1

D

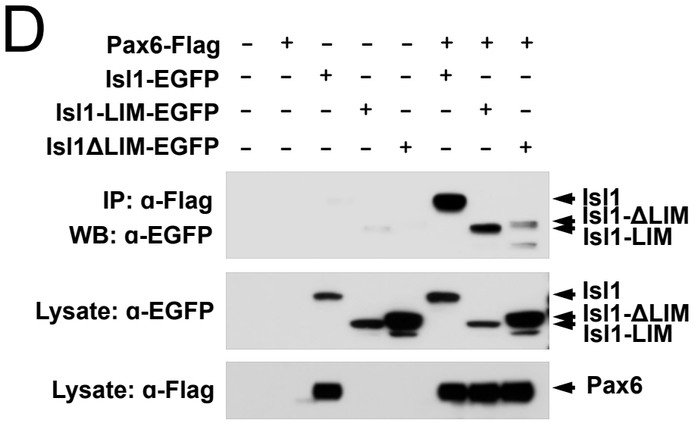
Pax6-Flag
Isl1-EGFP
Isl1-LIM-EGFP
Isl1ΔLIM-EGFP
IP: α-Flag
WB: α-EGFP
Isl1
Isl1-ΔLIM
Isl1-LIM
Lysate: α-EGFP
Lysate: α-Flag
Pax6

E

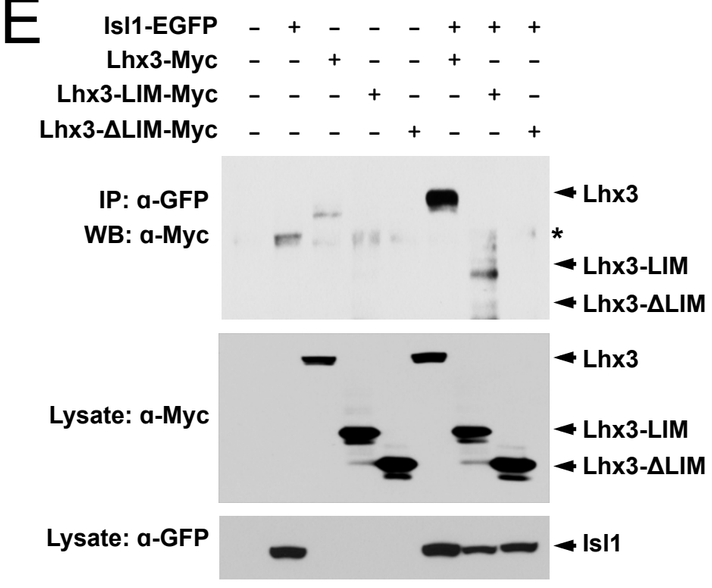
Isl1-EGFP
Lhx3-Myc
Lhx3-LIM-Myc
Lhx3-ΔLIM-Myc
IP: α-GFP
WB: α-Myc
Lhx3
*
Lhx3-LIM
Lhx3-ΔLIM
Lysate: α-Myc
Lysate: α-GFP
Isl1

F

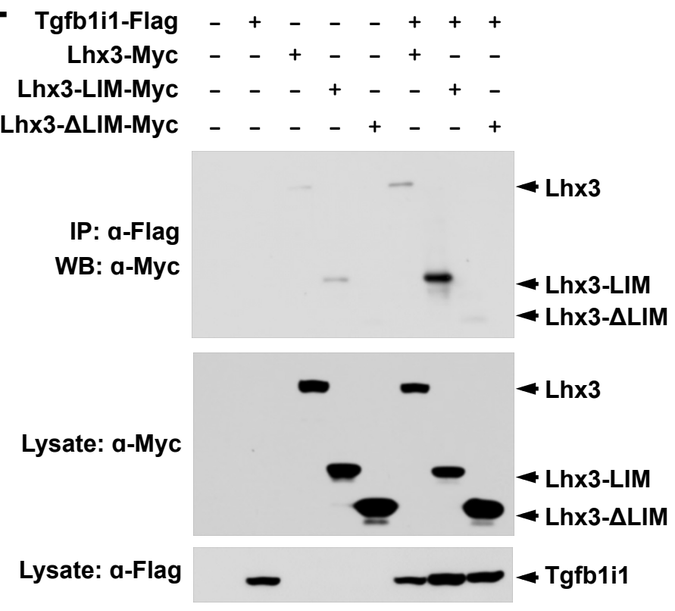
Tgfb1i1-Flag
Lhx3-Myc
Lhx3-LIM-Myc
Lhx3-ΔLIM-Myc
IP: α-Flag
WB: α-Myc
Lhx3
Lhx3-LIM
Lhx3-ΔLIM
Lysate: α-Myc
Lysate: α-Flag
Tgfb1i1

G

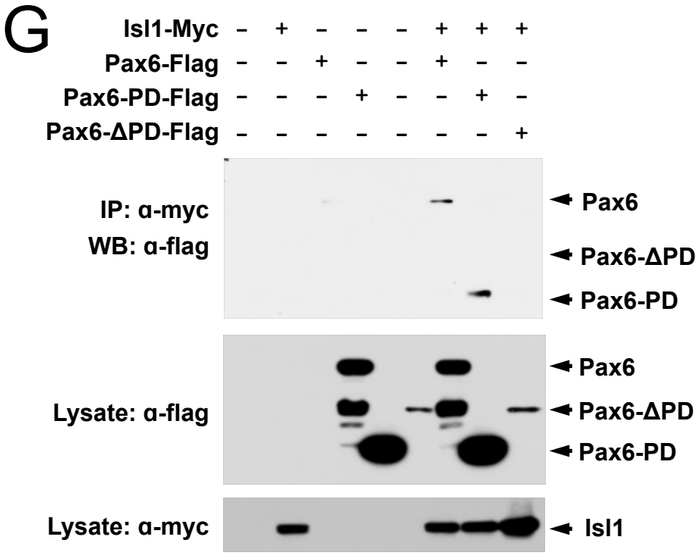
Isl1-Myc
Pax6-Flag
Pax6-PD-Flag
Pax6-ΔPD-Flag
IP: α-myc
WB: α-flag
Pax6
Pax6-ΔPD
Pax6-PD
Lysate: α-flag
Lysate: α-myc
Isl1

H

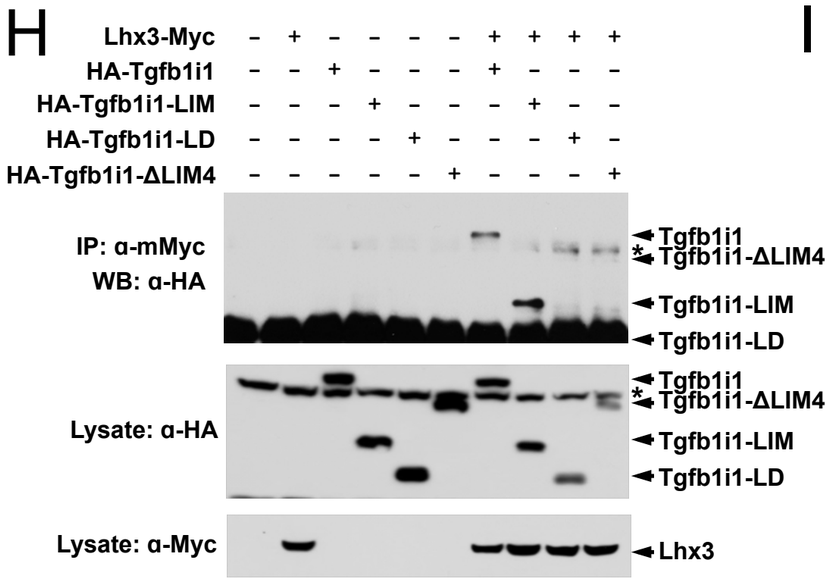
Lhx3-Myc
HA-Tgfb1i1
HA-Tgfb1i1-LIM
HA-Tgfb1i1-LD
HA-Tgfb1i1-ΔLIM4
IP: α-mMyc
WB: α-HA
Tgfb1i1
*
Tgfb1i1-ΔLIM4
Tgfb1i1-LIM
Tgfb1i1-LD
Lysate: α-HA
Lysate: α-Myc
Lhx3

I

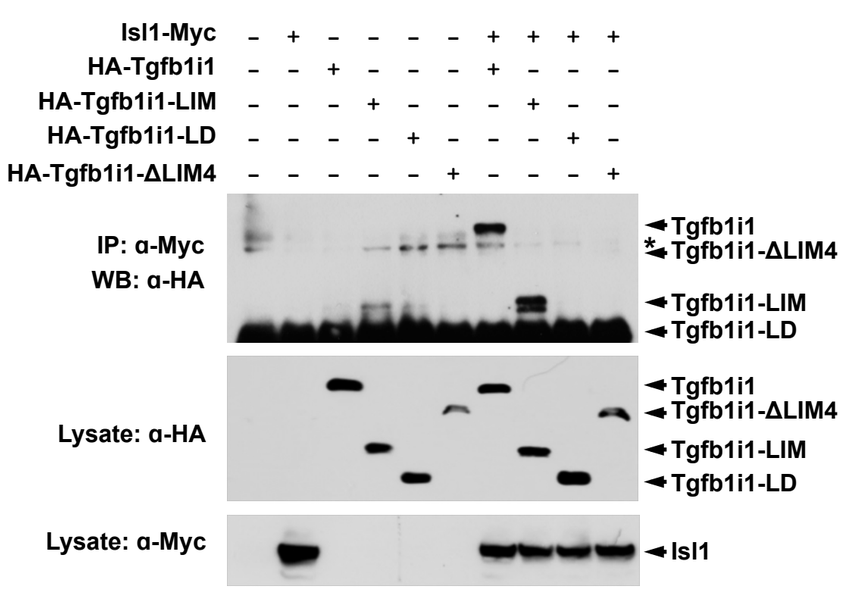
Isl1-Myc
HA-Tgfb1i1
HA-Tgfb1i1-LIM
HA-Tgfb1i1-LD
HA-Tgfb1i1-ΔLIM4
IP: α-Myc
WB: α-HA
Tgfb1i1
*
Tgfb1i1-ΔLIM4
Tgfb1i1-LIM
Tgfb1i1-LD
Lysate: α-HA
Lysate: α-Myc
Isl1

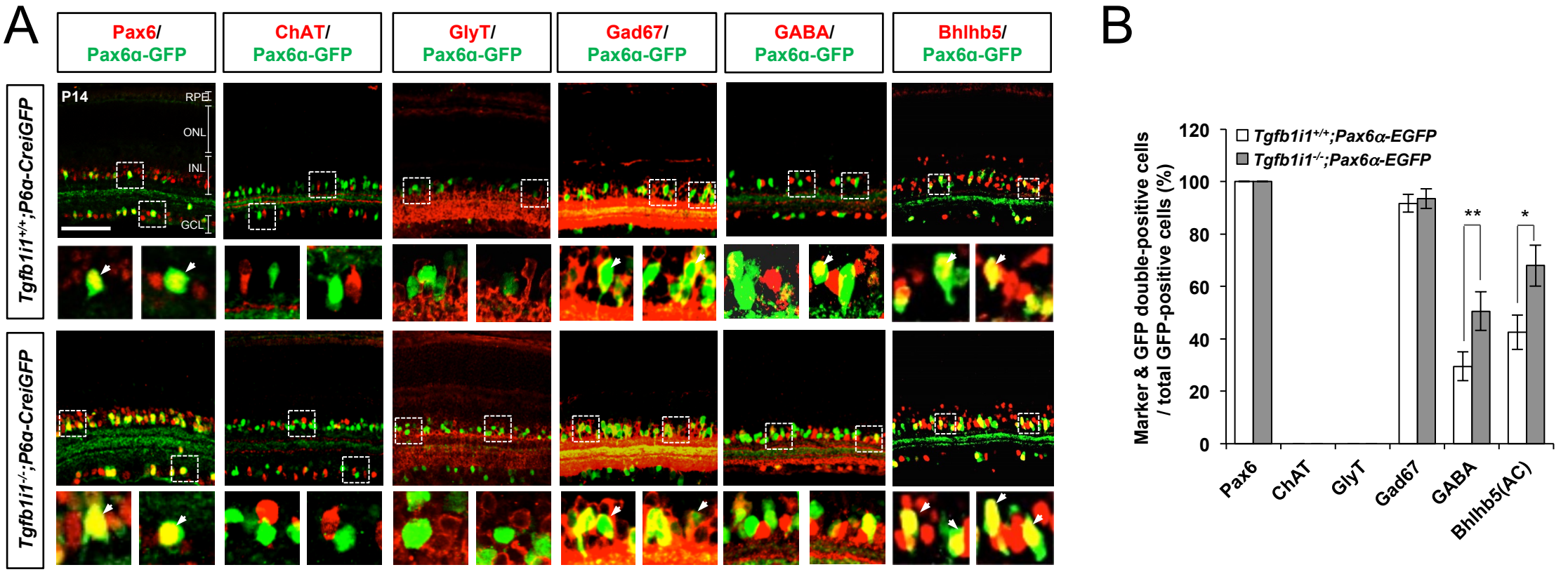
A
Pax6/
Pax6α-GFP
ChAT/
Pax6α-GFP
GlyT/
Pax6α-GFP
Gad67/
Pax6α-GFP
GABA/
Pax6α-GFP
Bhlhb5/
Pax6α-GFP
Tgfb1i1+/+;P6α-CreiGFP
Tgfb1i1-/-;P6α-CreiGFP
P14
RPE
ONL
INL
GCL
B
Tgfb1i1+/+;Pax6α-EGFP
Tgfb1i1-/-;Pax6α-EGFP
Marker & GFP double-positive cells
/ total GFP-positive cells (%)
120
100
80
60
40
20
0
**
*
Pax6
ChAT
GlyT
Gad67
GABA
Bhlhb5(AC)

A

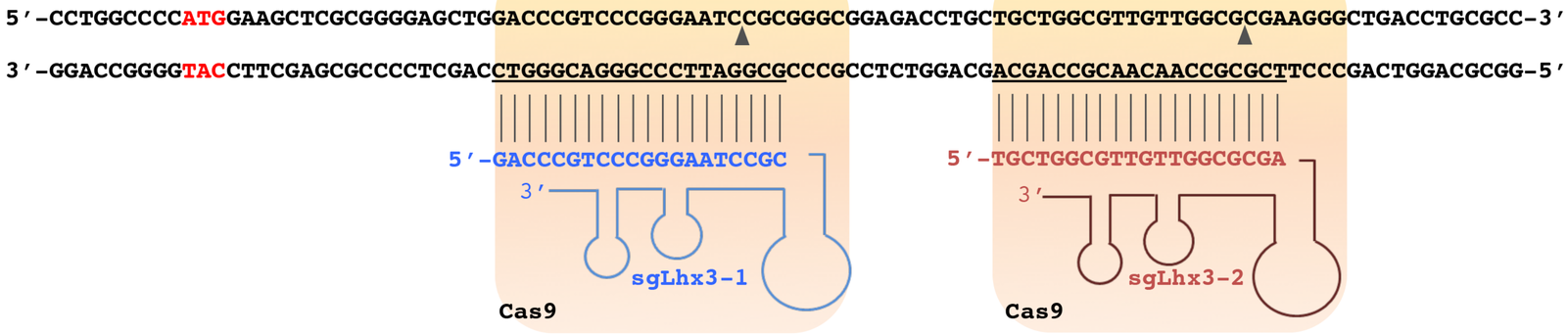
5′-CCTGGCCCCATGGAAGCTCGCGGGGAGCTGGACCCGTCCCGGGAATCCGCGGGCGGAGACCTGCTGCTGGCGTTGTTGGCGCGAAGGGCTGACCTGCGCC-3′
3′-GGACCGGGGTACCTTCGAGCGCCCCTCGACCTGGGCAGGGCCCTTAGGCGCCCGCCTCTGGACGACGACCGCAACAACCGCGCTTCCCGACTGGACGCGG-5′
5′-GACCCGTCCCGGGAATCCGC
3′
sgLhx3-1
Cas9
5′-TGCTGGCGTTGTTGGCGCGA
3′
sgLhx3-2
Cas9

B

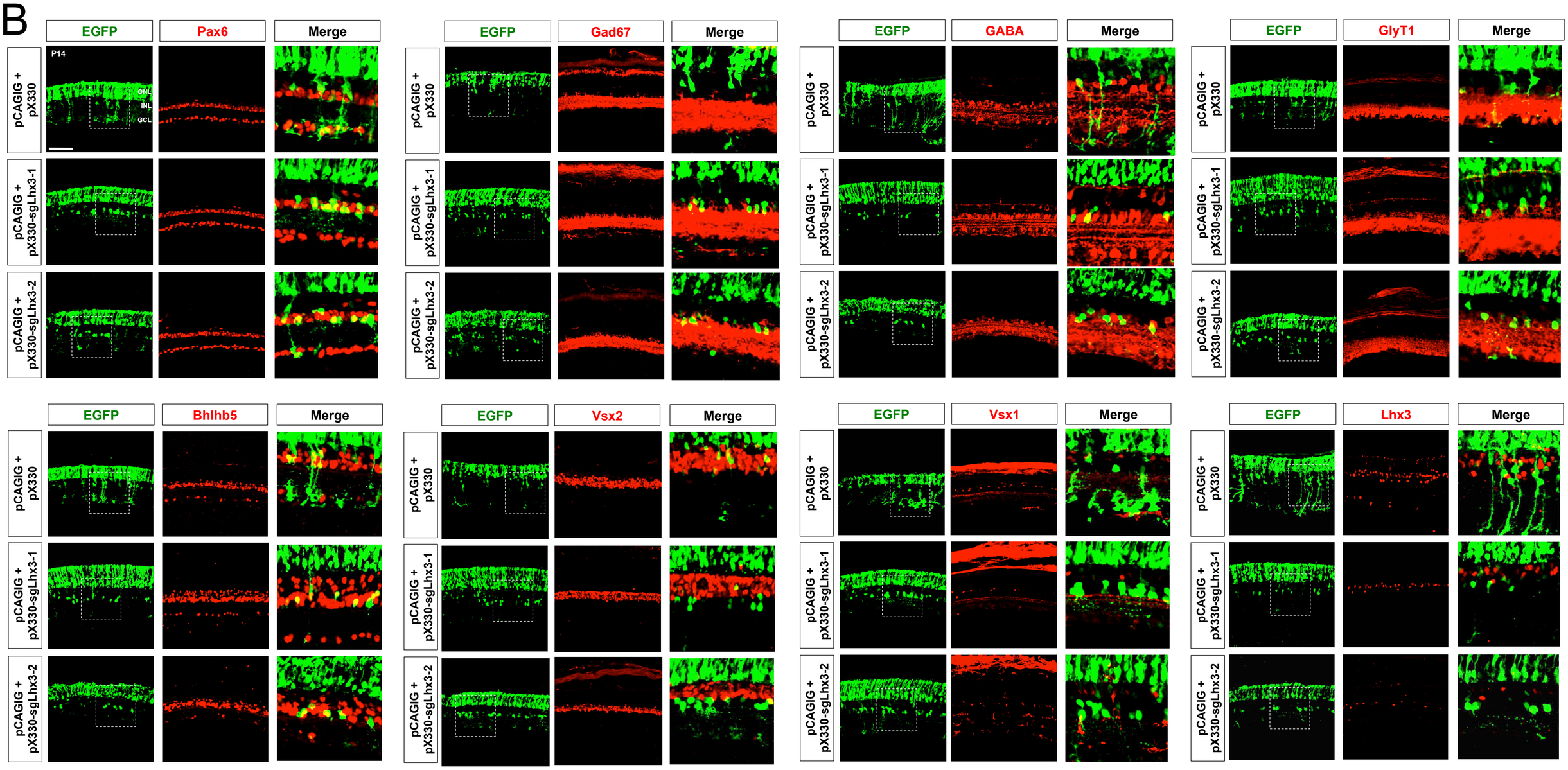
EGFP
Pax6
Merge
Gad67
GABA
GlyT1
Bhlhb5
Vsx2
Vsx1
Lhx3
P14
ONL
INL
GCL
pCAGIG + pX330
pCAGIG + pX330-sgLhx3-1
pCAGIG + pX330-sgLhx3-2

C

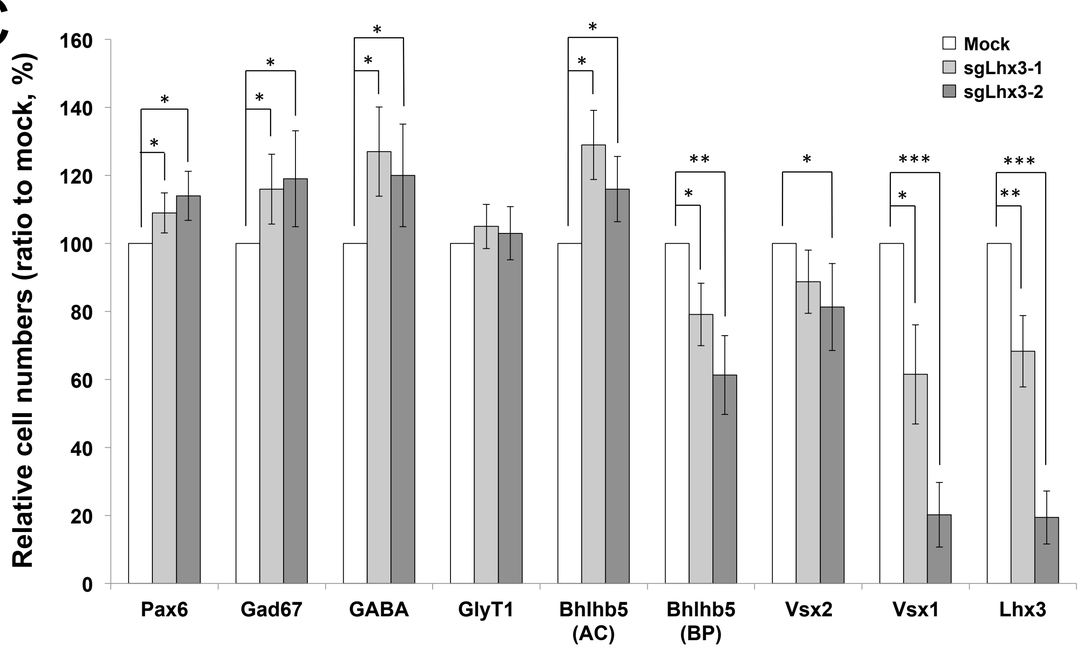
Relative cell numbers (ratio to mock, %)
Mock
sgLhx3-1
sgLhx3-2
Pax6
Gad67
GABA
GlyT1
Bhlhb5 (AC)
Bhlhb5 (BP)
Vsx2
Vsx1
Lhx3

D

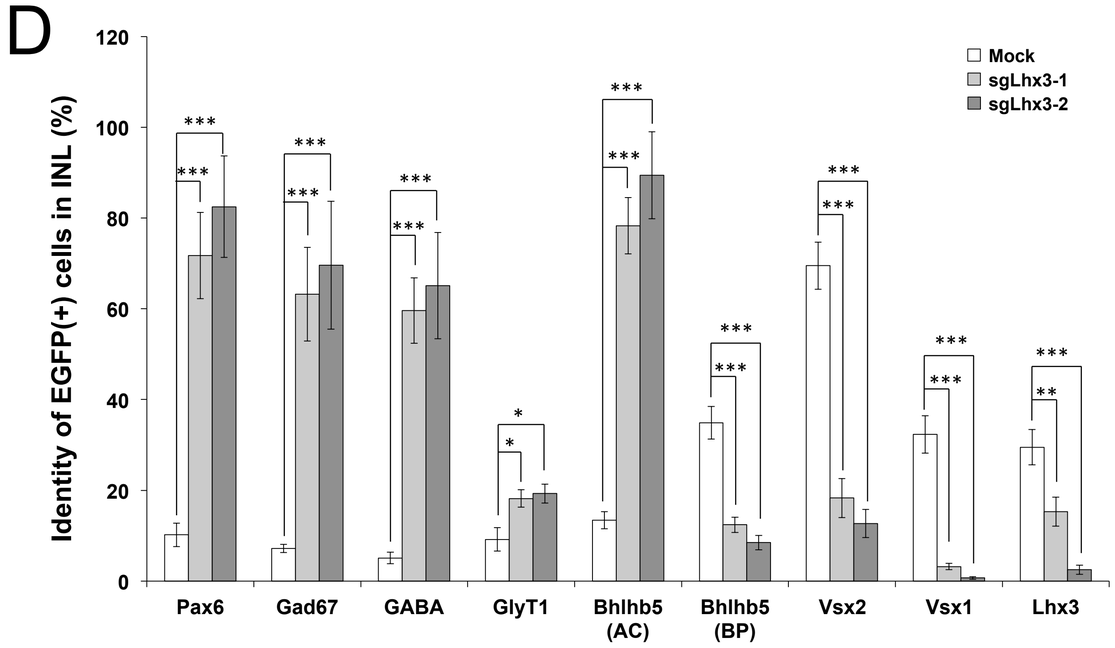
Identity of EGFP(+) cells in INL (%)
Mock
sgLhx3-1
sgLhx3-2
Pax6
Gad67
GABA
GlyT1
Bhlhb5 (AC)
Bhlhb5 (BP)
Vsx2
Vsx1
Lhx3

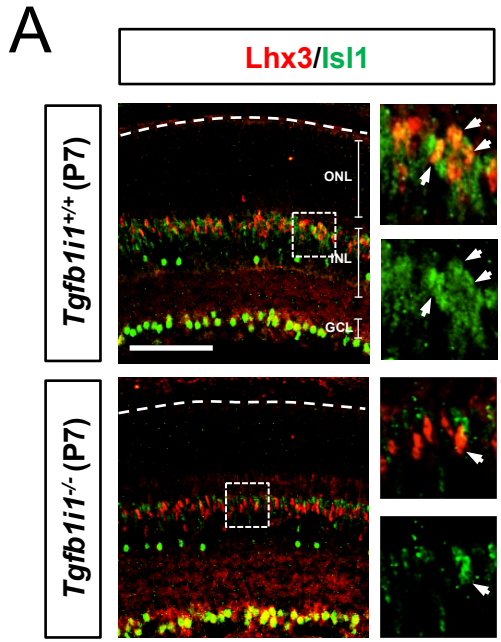
A
Lhx3/Isl1
Tgfb1i1+/+ (P7)
Tgfb1i1-/- (P7)
ONL
INL
GCL

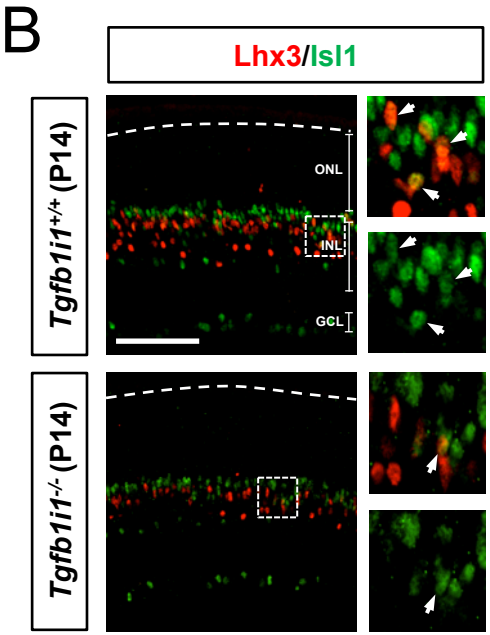
B
Lhx3/Isl1
Tgfb1i1+/+ (P14)
Tgfb1i1-/- (P14)
ONL
INL
GCL

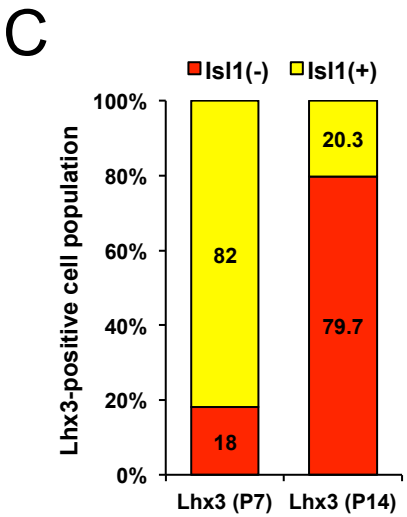
C
Isl1(-)
Isl1(+)
Lhx3-positive cell population
100%
80%
60%
40%
20%
0%
82
18
20.3
79.7
Lhx3 (P7)
Lhx3 (P14)

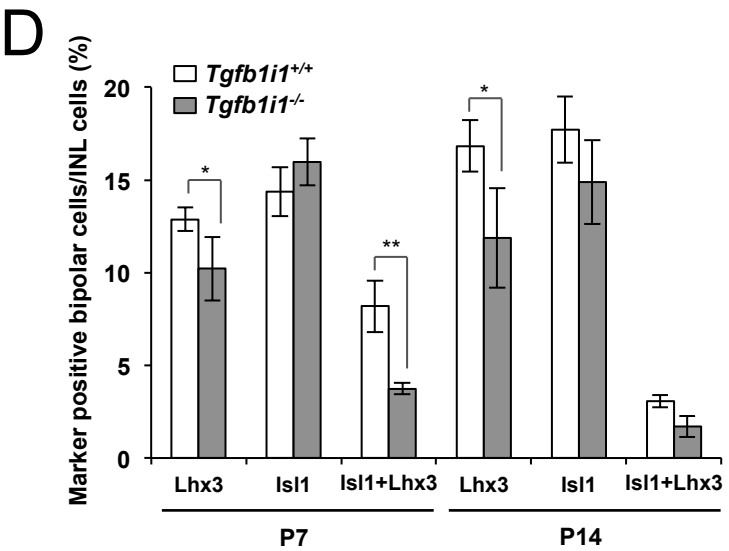
D
Tgfb1i1+/+
Tgfb1i1-/-
Marker positive bipolar cells/INL cells (%)
20
15
10
5
0
*
**
*
Lhx3
Isl1
Isl1+Lhx3
Lhx3
Isl1
Isl1+Lhx3
P7
P14

Kim et al._Fig5_figure supplement 2

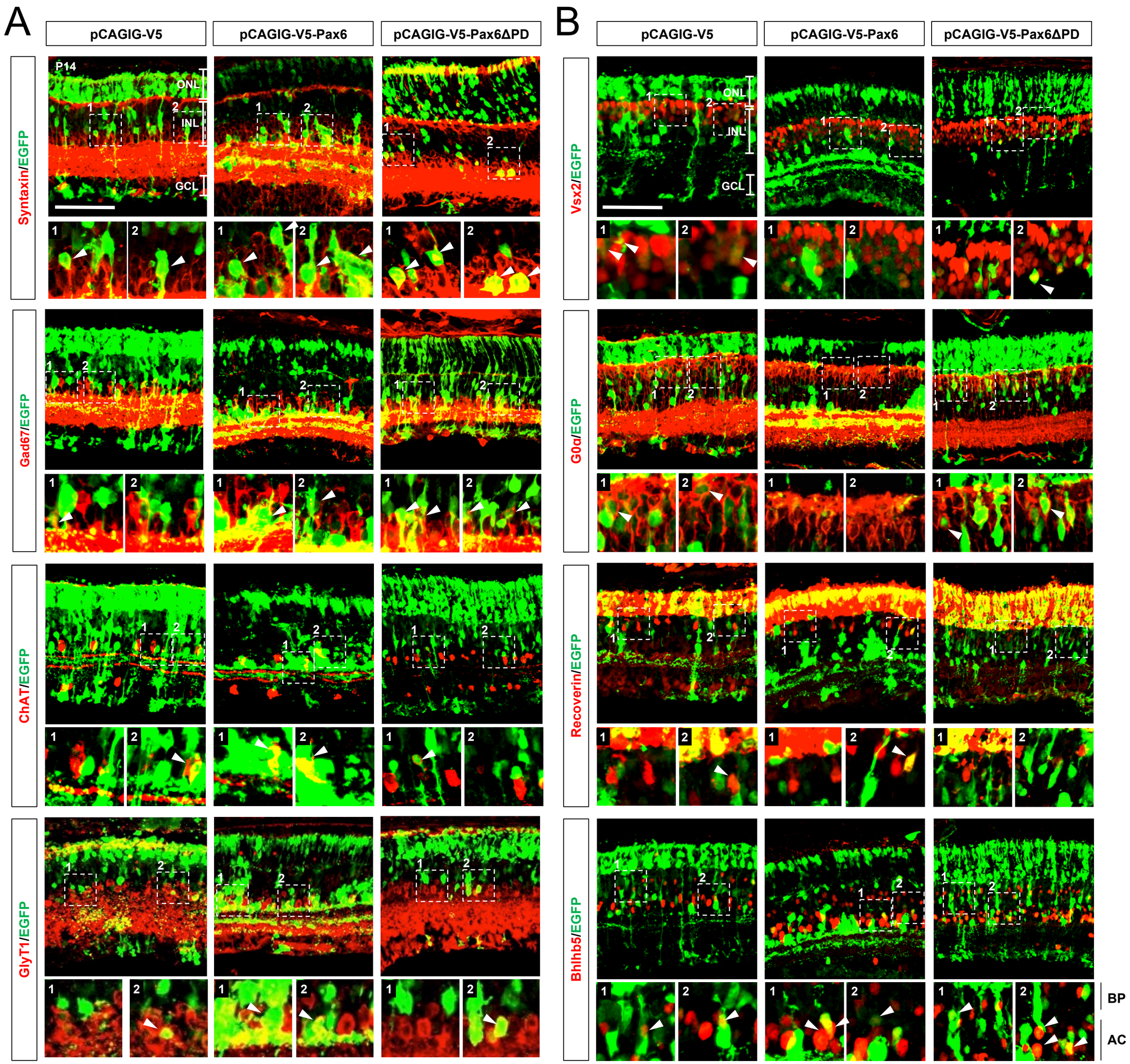

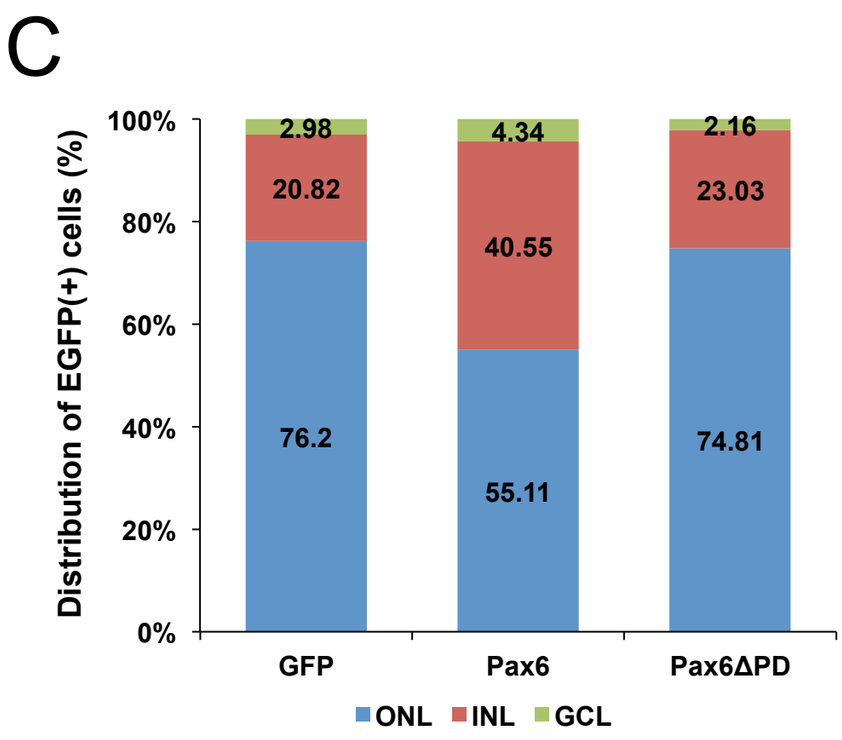

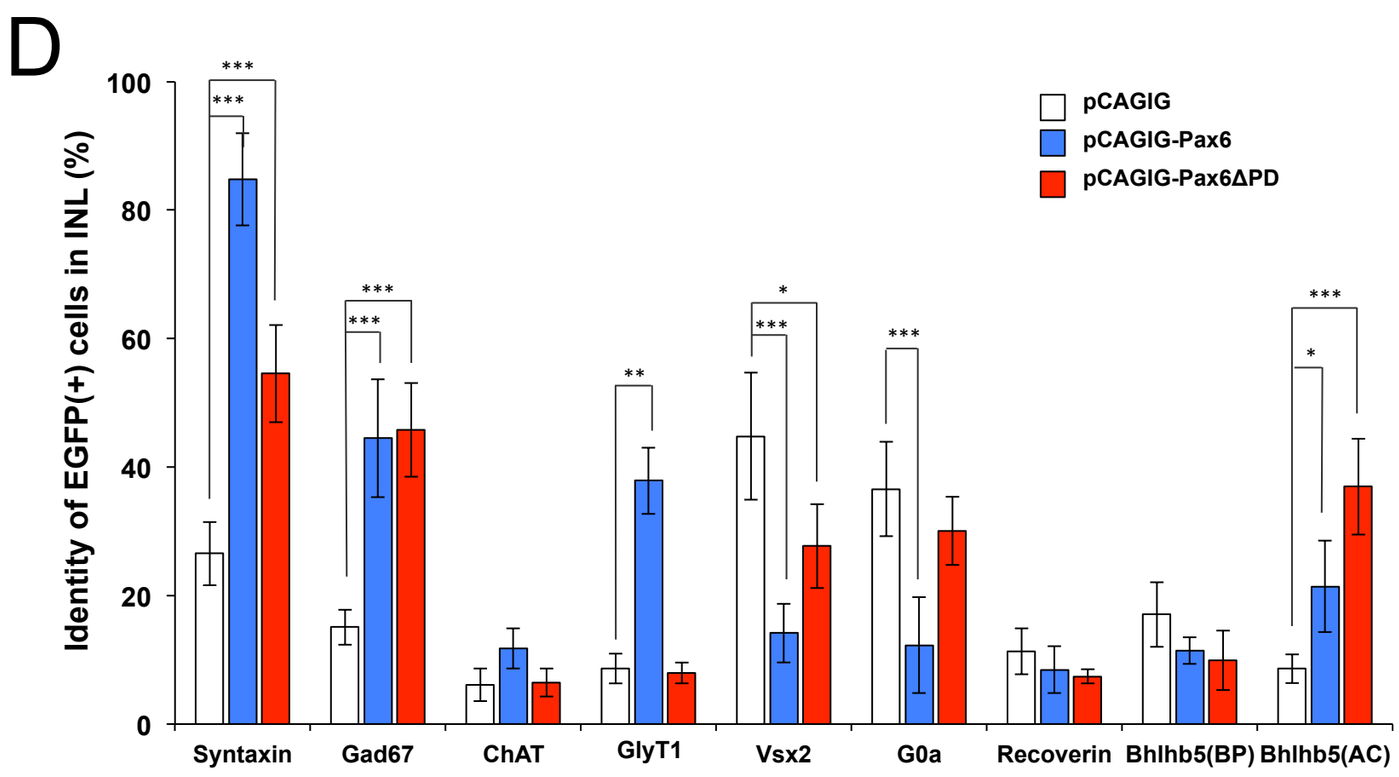

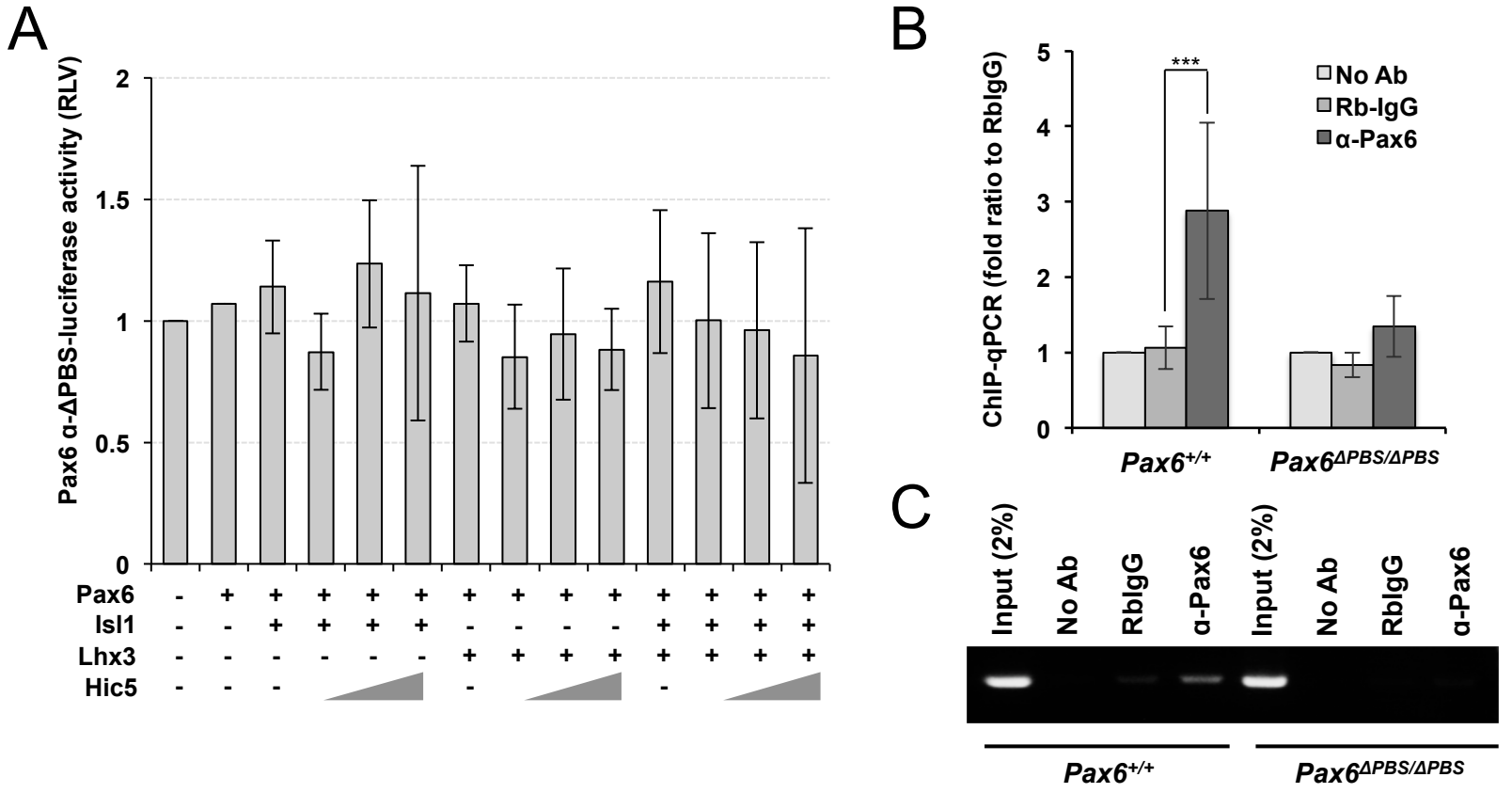
A
Pax6 α-ΔPBS-luciferase activity (RLV)
2
1.5
1
0.5
0
Pax6 - + + + + + + + + + + + + +
Isl1 - - + + + + - - - - + + + +
Lhx3 - - - - - - + + + + + + + +
Hic5 - - -
B
ChIP-qPCR (fold ratio to RbIgG)
5
4
3
2
1
0
***
No Ab
Rb-IgG
α-Pax6
Pax6+/+
Pax6ΔPBS/ΔPBS
C
Input (2%)
No Ab
RbIgG
α-Pax6
Input (2%)
No Ab
RbIgG
α-Pax6
Pax6+/+
Pax6ΔPBS/ΔPBS

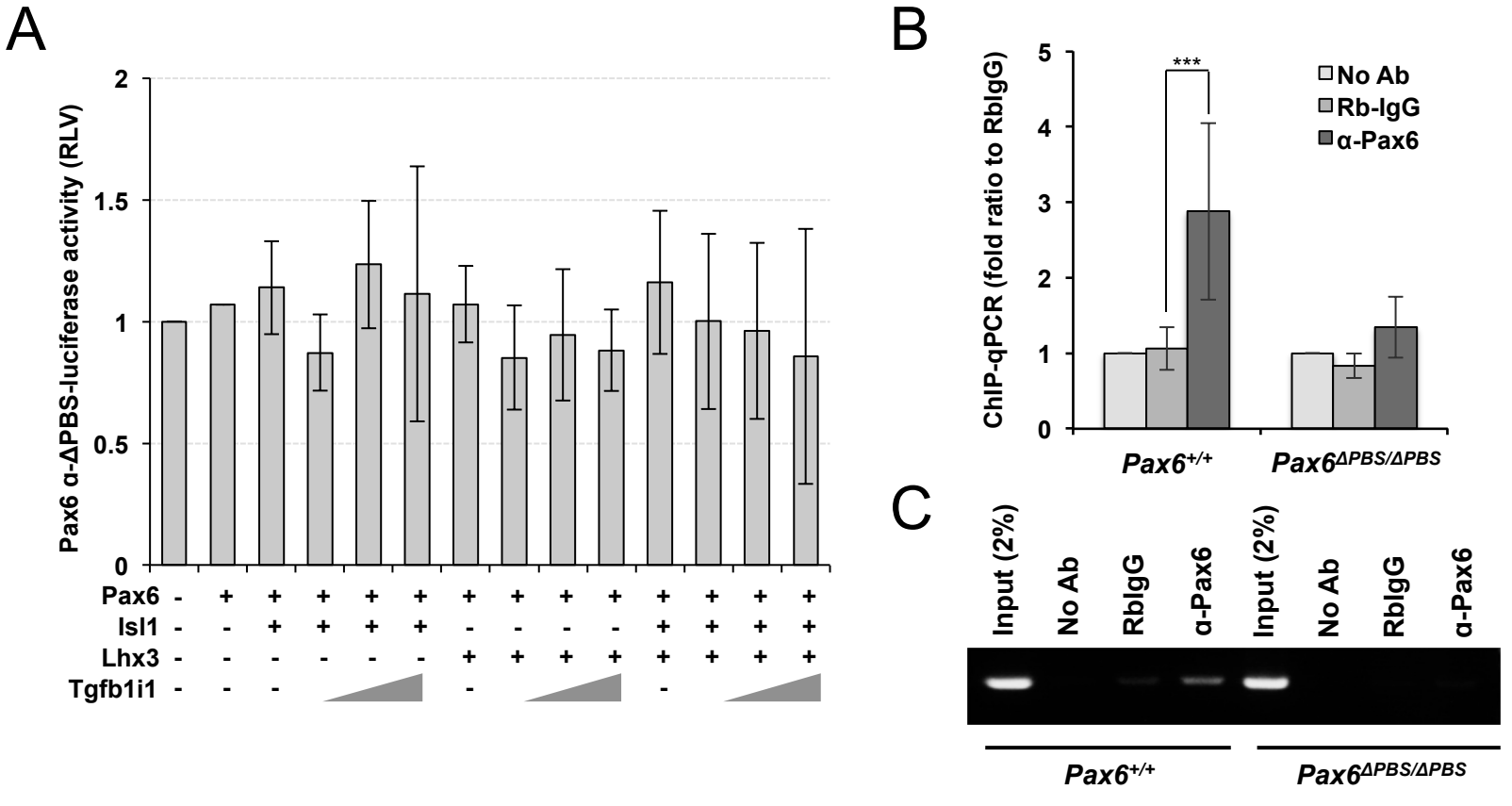
A
Pax6 α-ΔPBS-luciferase activity (RLV)
2
1.5
1
0.5
0
Pax6 - + + + + + + + + + + + + +
Isl1 - - + + + + - - - - + + + +
Lhx3 - - - - - - + + + + + + + +
Tgfb1i1 - - -
B
ChIP-qPCR (fold ratio to RbIgG)
5
4
3
2
1
0
***
No Ab
Rb-IgG
α-Pax6
Pax6+/+
Pax6ΔPBS/ΔPBS
C
Input (2%)
No Ab
RbIgG
α-Pax6
Input (2%)
No Ab
RbIgG
α-Pax6
Pax6+/+
Pax6ΔPBS/ΔPBS

Kim et al._Fig6_figure supplement 2

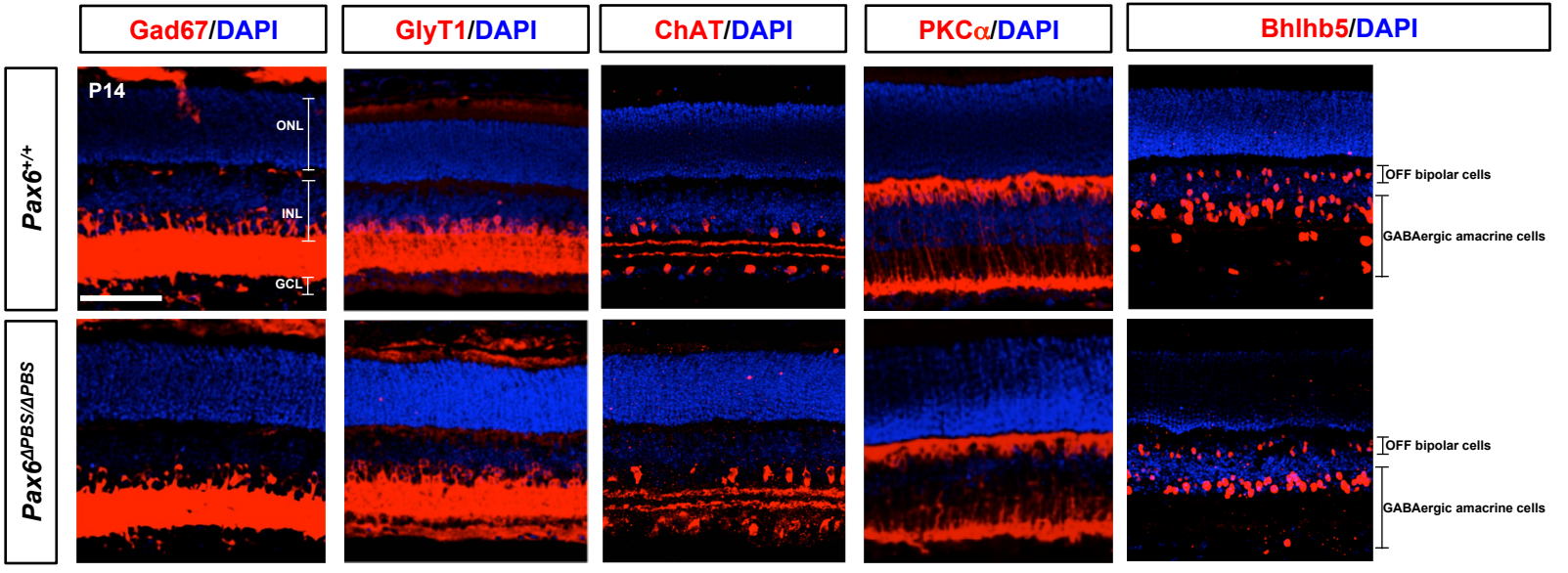

A

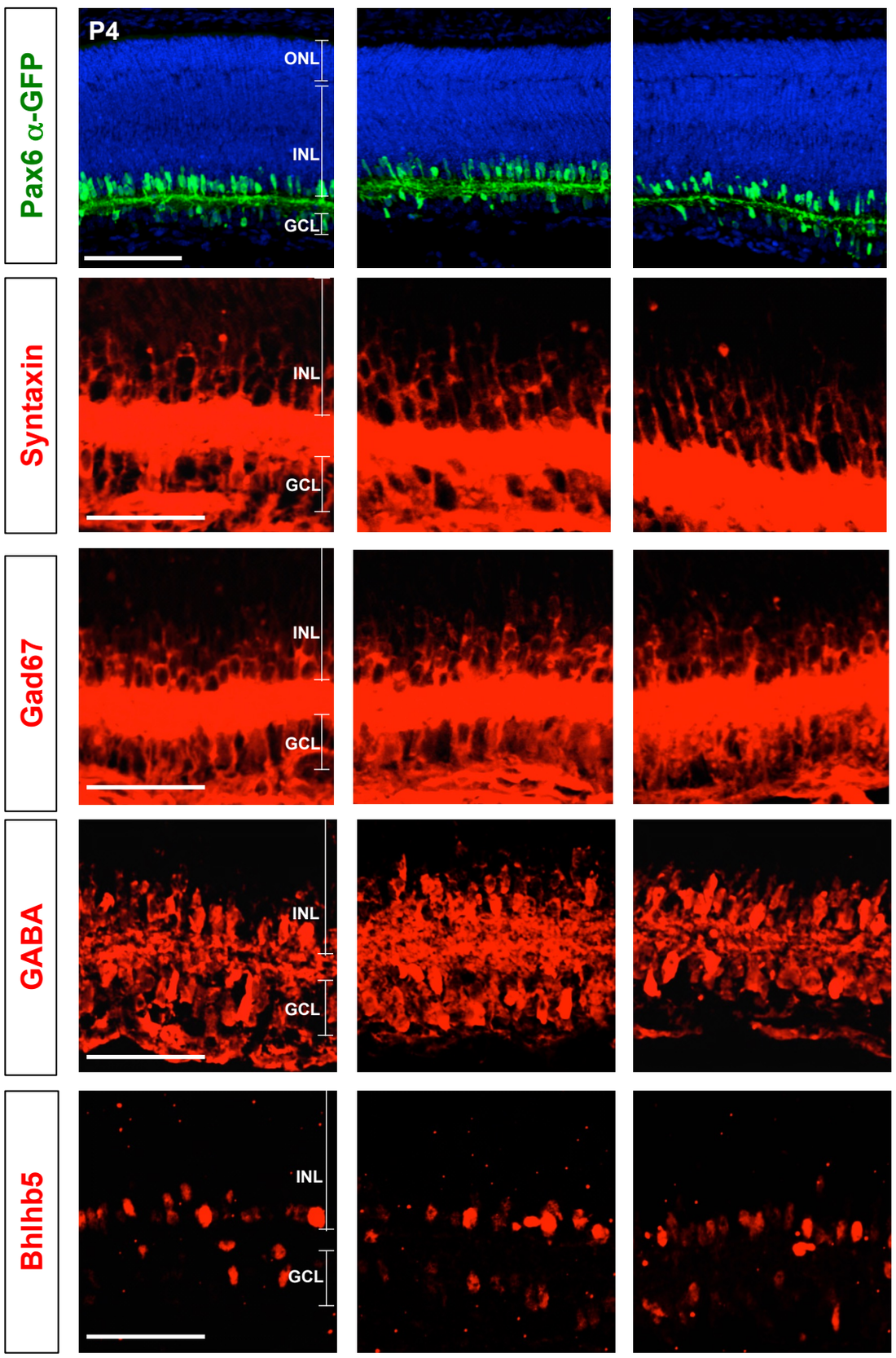
WT; P6a-CreiGFP
Tgfb1i1-/-; P6a-CreiGFP
Pax6ΔPBS/ΔPBS; P6a-CreiGFP
Pax6 α-GFP
Syntaxin
Gad67
GABA
Bhlhb5
P4
ONL
INL
GCL

B

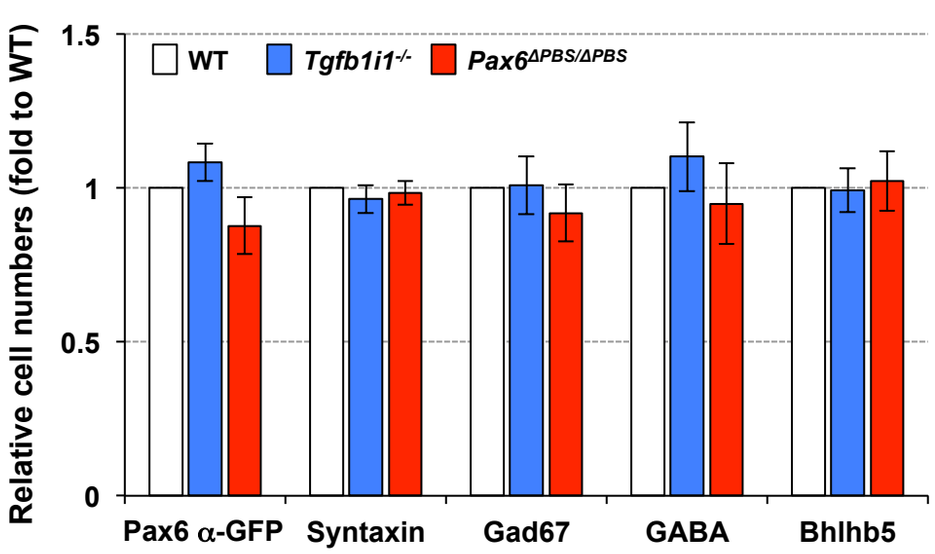
WT
Tgfb1i1-/-
Pax6ΔPBS/ΔPBS
Relative cell numbers (fold to WT)
1.5
1
0.5
0
Pax6 α-GFP
Syntaxin
Gad67
GABA
Bhlhb5

C

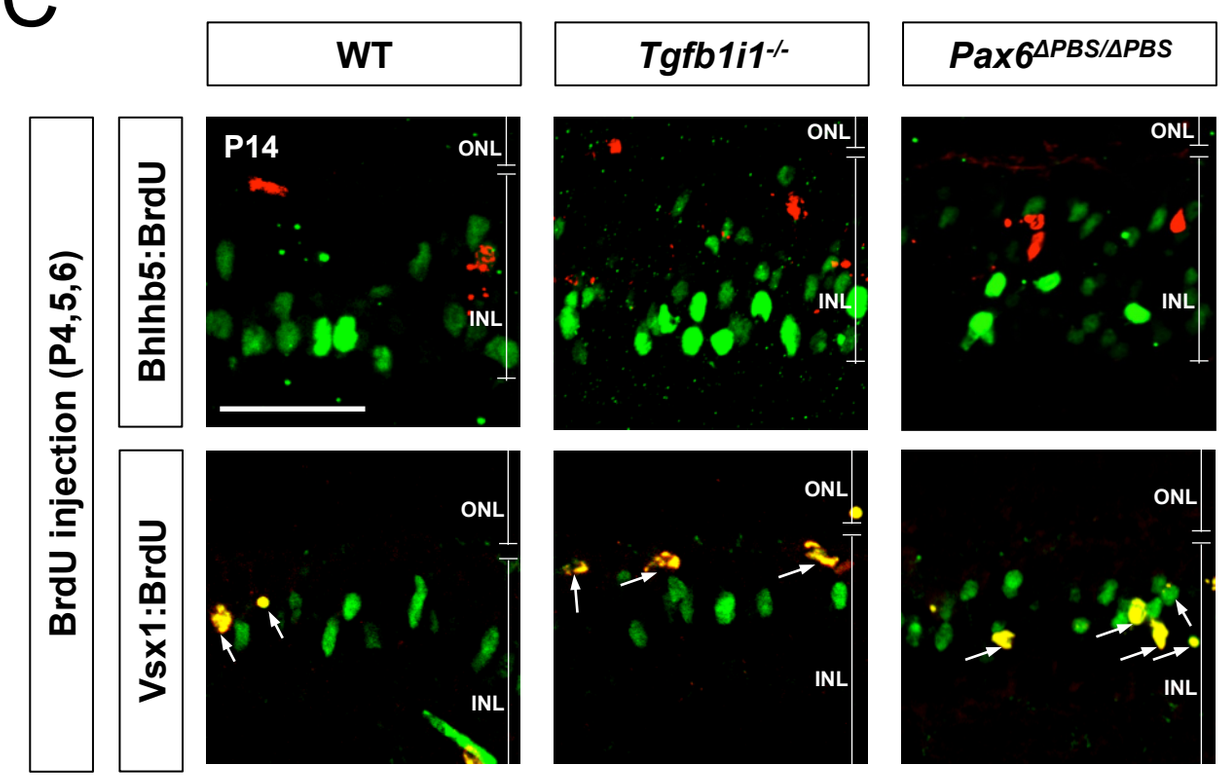
WT
Tgfb1i1-/-
Pax6ΔPBS/ΔPBS
BrdU injection (P4,5,6)
Bhlhb5:BrdU
Vsx1:BrdU
P14
ONL
INL

D

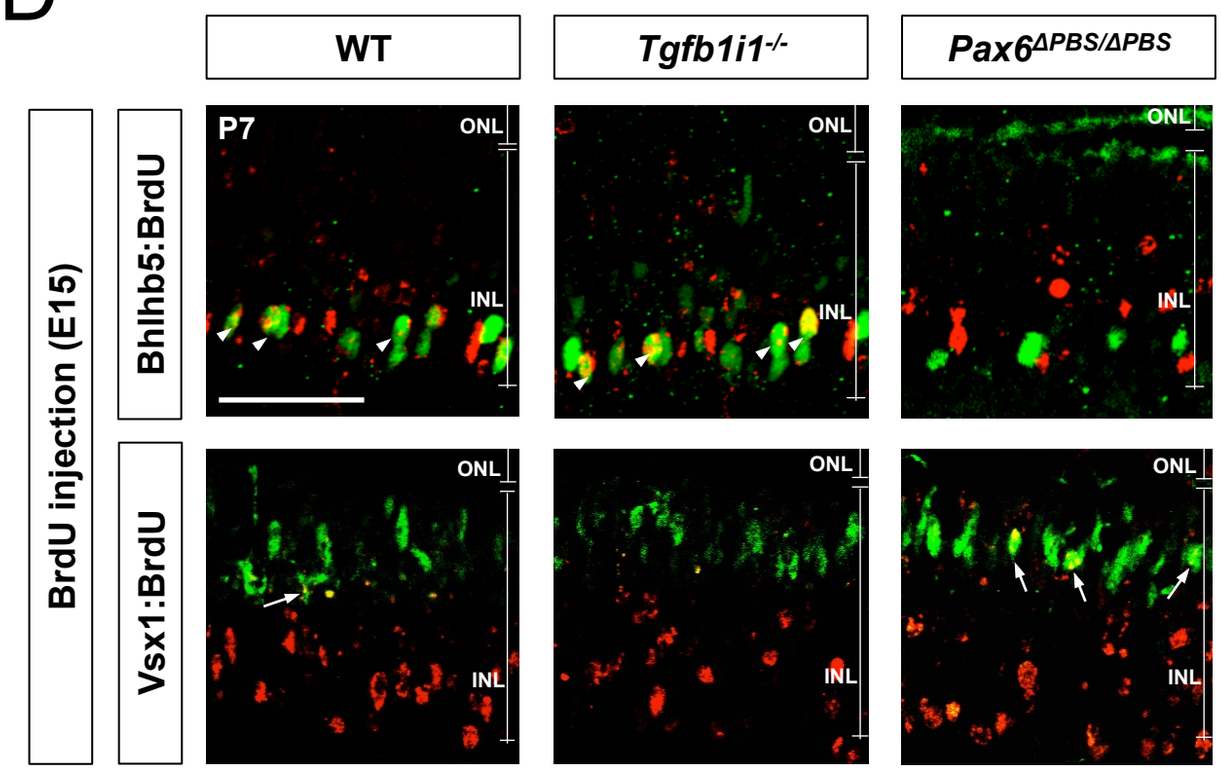
WT
Tgfb1i1-/-
Pax6ΔPBS/ΔPBS
BrdU injection (E15)
Bhlhb5:BrdU
Vsx1:BrdU
P7
ONL
INL

E

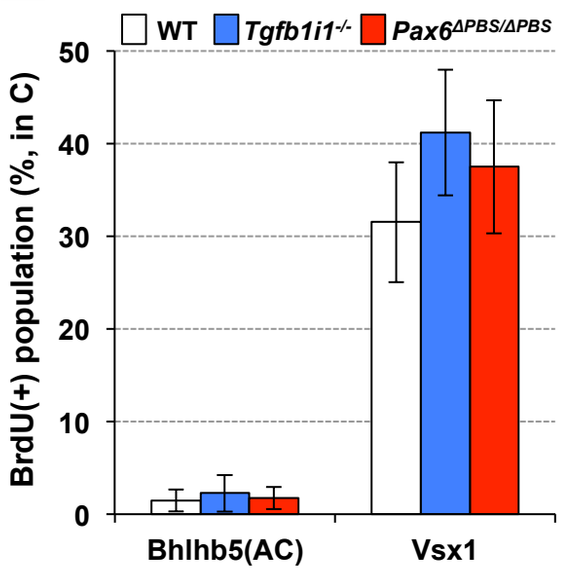
WT
Tgfb1i1-/-
Pax6ΔPBS/ΔPBS
BrdU(+) population (%, in C)
50
40
30
20
10
0
Bhlhb5(AC)
Vsx1

F

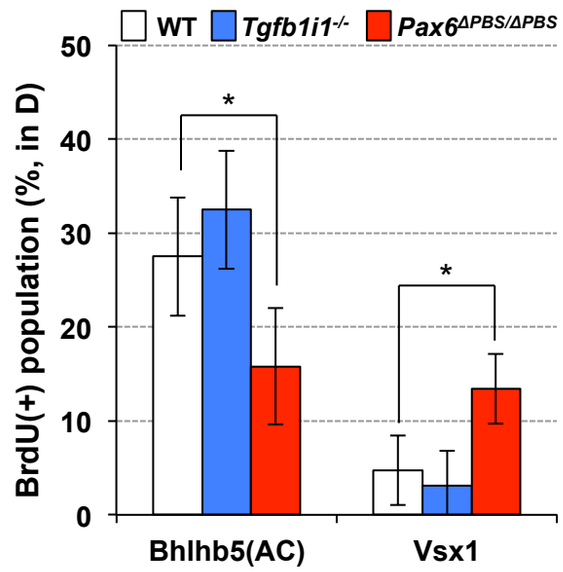
WT
Tgfb1i1-/-
Pax6ΔPBS/ΔPBS
BrdU(+) population (%, in D)
50
40
30
20
10
0
*
*
Bhlhb5(AC)
Vsx1

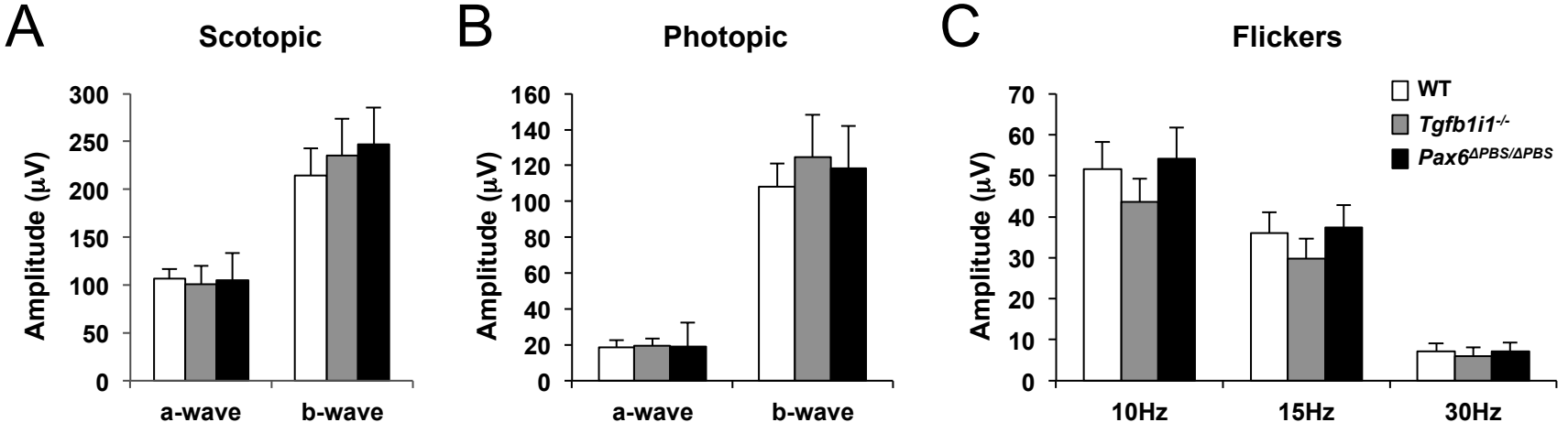
A
Scotopic
Amplitude (μV)
300
250
200
150
100
50
0
a-wave
b-wave
B
Photopic
Amplitude (μV)
160
140
120
100
80
60
40
20
0
a-wave
b-wave
C
Flickers
Amplitude (μV)
70
60
50
40
30
20
10
0
10Hz
15Hz
30Hz
WT
Tgfb1i1-/-
Pax6ΔPBS/ΔPBS

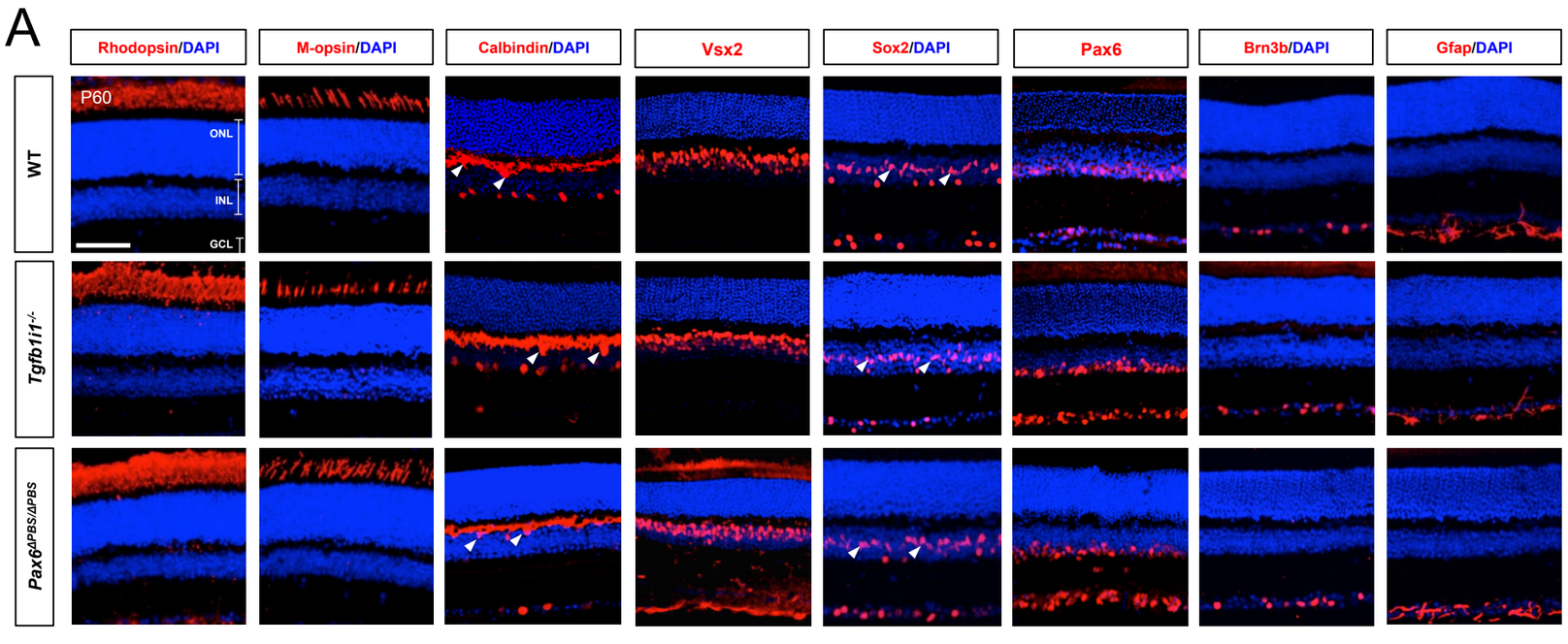
A
Rhodopsin/DAPI
M-opsin/DAPI
Calbindin/DAPI
Vsx2
Sox2/DAPI
Pax6
Brn3b/DAPI
Gfap/DAPI
WT
Tgfb1i1-/-
Pax6ΔPBS/ΔPBS
P60
ONL
INL
GCL

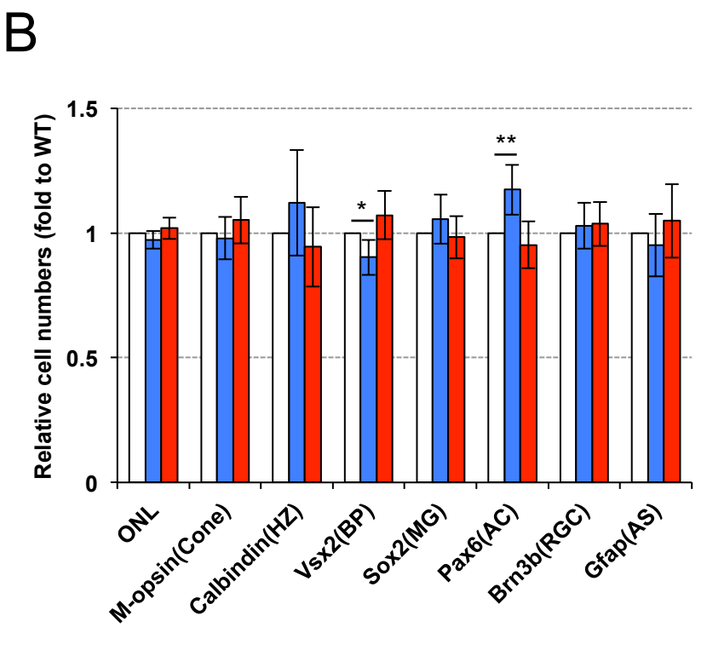
B
Relative cell numbers (fold to WT)
1.5
1
0.5
0
*
**
ONL
M-opsin(Cone)
Calbindin(HZ)
Vsx2(BP)
Sox2(MG)
Pax6(AC)
Brn3b(RGC)
Gfap(AS)

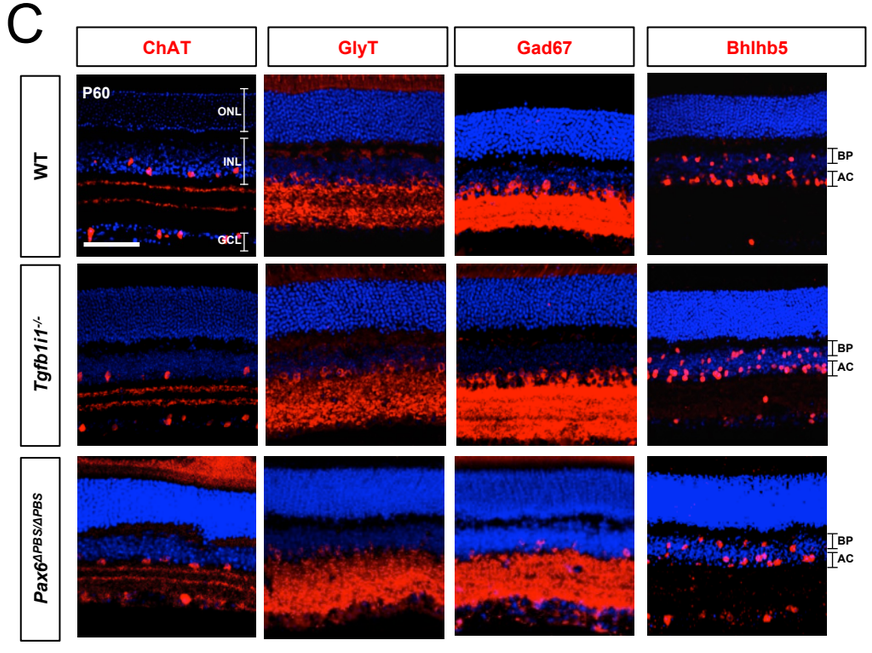
C
ChAT
GlyT
Gad67
Bhlhb5
WT
Tgfb1i1-/-
Pax6ΔPBS/ΔPBS
P60
ONL
INL
GCL
BP
AC

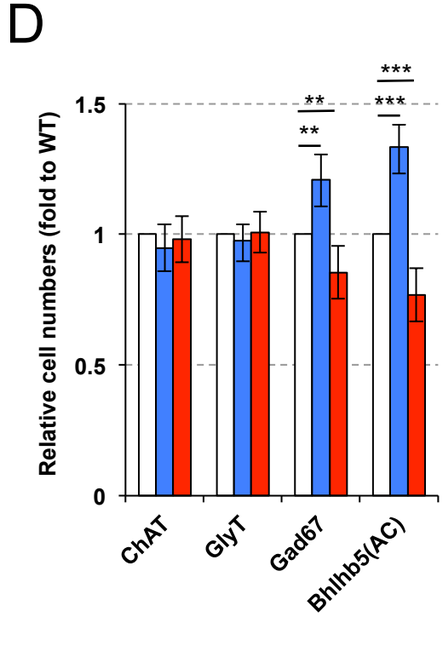
D
Relative cell numbers (fold to WT)
1.5
1
0.5
0
**
**
***
***
ChAT
GlyT
Gad67
Bhlhb5(AC)

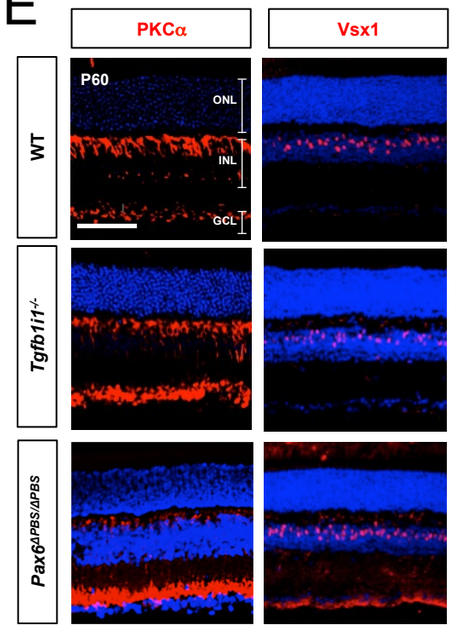
E
PKCα
Vsx1
WT
Tgfb1i1-/-
Pax6ΔPBS/ΔPBS
P60
ONL
INL
GCL

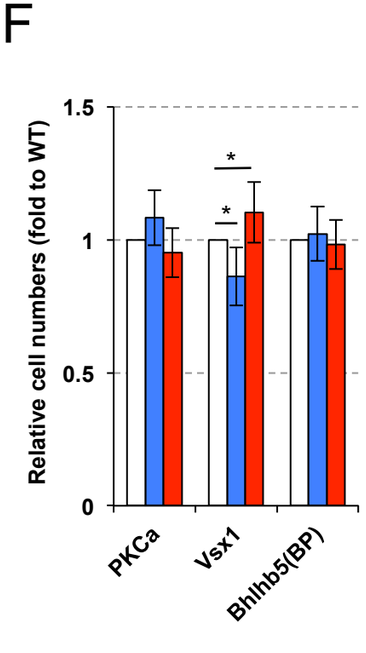
F
Relative cell numbers (fold to WT)
1.5
1
0.5
0
*
*
PKCa
Vsx1
Bhlhb5(BP)

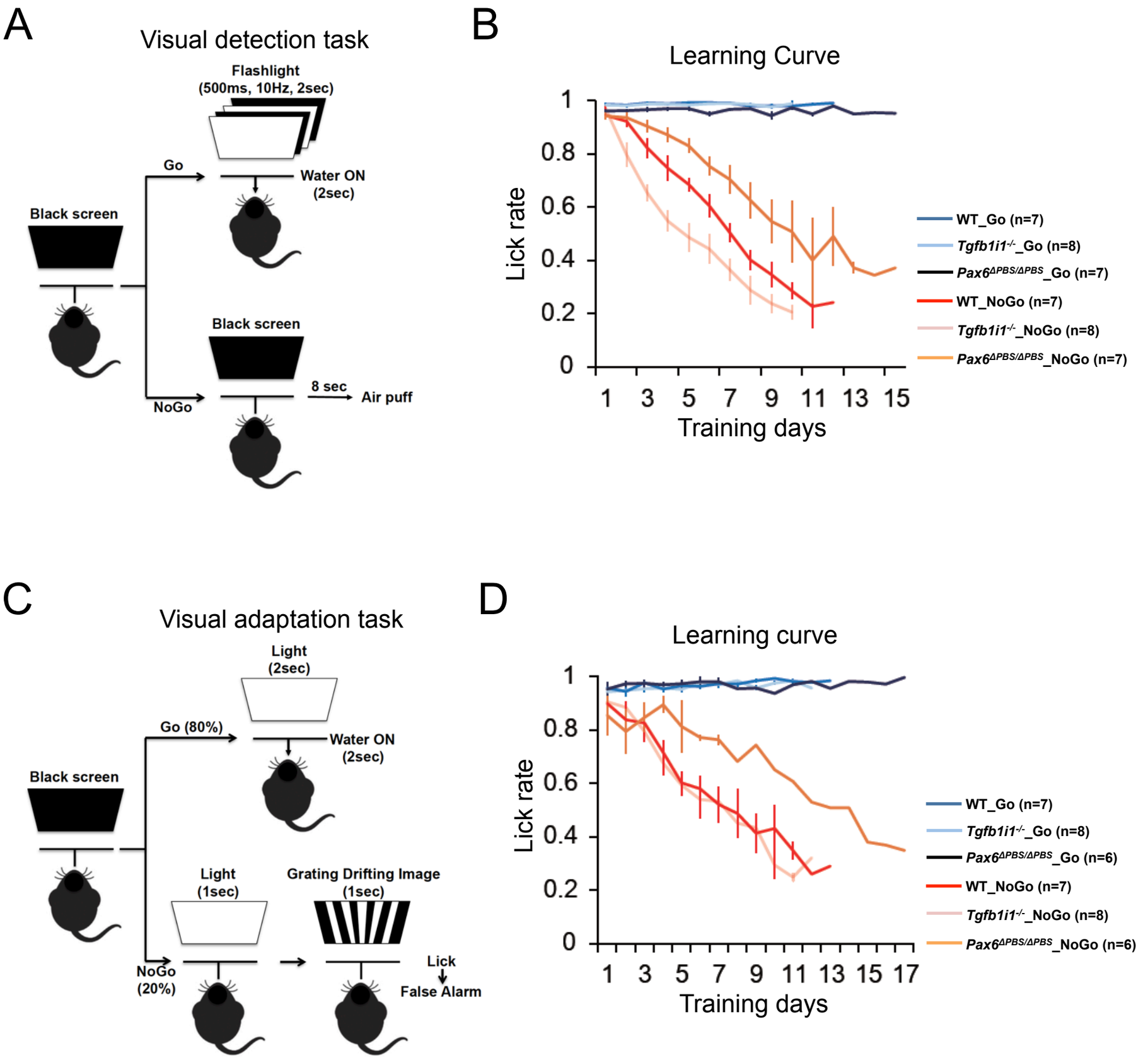
A
Visual detection task
Flashlight
(500ms, 10Hz, 2sec)
Go
Water ON
(2sec)
Black screen
Black screen
8 sec
Air puff
NoGo
B
Learning Curve
Lick rate
Training days
WT_Go (n=7)
Tgfb1i1-/-_Go (n=8)
Pax6ΔPBS/ΔPBS_Go (n=7)
WT_NoGo (n=7)
Tgfb1i1-/-_NoGo (n=8)
Pax6ΔPBS/ΔPBS_NoGo (n=7)
C
Visual adaptation task
Light
(2sec)
Go (80%)
Water ON
(2sec)
Black screen
Light
(1sec)
Grating Drifting Image
(1sec)
NoGo
(20%)
Lick
False Alarm
D
Learning curve
Lick rate
Training days
WT_Go (n=7)
Tgfb1i1-/-_Go (n=8)
Pax6ΔPBS/ΔPBS_Go (n=6)
WT_NoGo (n=7)
Tgfb1i1-/-_NoGo (n=8)
Pax6ΔPBS/ΔPBS_NoGo (n=6)